MODELLING OF DFIG WIND TURBINE WITH CONSIDERATION FOR CONVERTER BEHAVIOUR DURING SUPPLY FAULT CONDITIONS

Yutana Chongjarearn

A thesis submitted for the degree of
Integrated PhD

Newcastle University
School of Electrical and Electronic Engineering

Abstract

The Doubly-Fed Induction Generator (DFIG) is widely used for large grid-connected, variable-speed wind turbines. As the amount of installed wind power increases, it is increasingly important that turbine generators remain connected and support the grid transmission network during transient system disturbances: so-called fault ride-through (FRT), as specified by various grid codes. To study the FRT capability of the DFIG, an accurate model of the system is needed. This must be able to take into account the switching behaviour of the rotor circuit diodes and IGBTs if it is to simulate the converter and the DC-link capacitor current and voltage waveforms during supply fault conditions when vector control is lost, inverter IGBTs are switched off and the inverter appears as a simple 3-phase rectifier.

In this thesis, a Simulink model for a vector controlled DFIG is developed to investigate drive fault through characteristics, allowing for the switching effects of all IGBTs and anti-parallel diodes. The model is used to predict machine and converter current and voltage waveforms during network fault conditions, represented by a 3-phase supply voltage dip, and thus assess the FRT performance of the DFIG in accordance with the transmission system grid codes.

Four case studies during normal conditions and three fault scenarios during fault conditions are investigated and validated by the 7.5kW DFIG Test Rig. The simulation and experimental results are in very close agreement. The simulation shows that transient rotor currents can obviously damage the converter IGBT devices and DC-link capacitor if no protective action (using Crowbar and DC chopper) is taken.

Moreover, the developed model can be used to investigate the transient behaviour of the DFIG drive system during supply fault conditions when the drive IGBTs are switched off and the rotor converter appears to be a simple diode bridge rectifier. Also, the developed model including both FRT devices (Crowbar and DC-brake chopper) will be employed to investigate the DFIGs FRT performance and design the minimum value of crowbar resistance.

Acknowledgements

Firstly I would like to thank my sponsor, Dhurakij Pundit University (DPU) especially DPU's Scholarship Committee, for sponsoring a scholarship to study on this IntPhD programme.

I would like express my deepest appreciation and thanks to my supervisors, Dr. David Atkinson and Dr. Bashar Zahawi, for their professional guidance and encouragement throughout this research. Also I would like to thank my examiners, Dr. Milutin Jovanovic and Dr. Mohamed Dahidah, for providing constructive comments on my thesis and viva.

I must acknowledge the support of Dr. Graham Pannell, who provided some experimental results of grid fault ride through for wind turbine DFIGs. Also thanks are due to the fellow researchers who built the wind turbine test rig.

I would like to thank the administrative and IT-support staff, Mechanical and Electronic support team and all the technicians for their help during the course of this work. Moreover, I would like to thank my friends for making a pleasant environment in which to work and share our experiences in the UG lab.

I would like to thank my friend, Dr. Mohammed Elgendy, for being a very kind person and his good company during my study at Newcastle University.

I would like to thank David and Susan for their friendship during study at Newcastle.

I would like to thank my friend, Alex and Denise, for their very good company and help during the period of this research at Newcastle.

Finally, I would like to thank my wife and son, Audy and Win, for their patience and great encouragement, and to my parents, my families and all people for their continuous support.

Contents

List of Figures

List of Tables

List of Abbreviations

DFIG	Doubly-Fed Induction Generator
DC-Link	DC connection of the back-to-back DFIG converter arrangement
FRT	Fault Ride Through
GUI	Graphic User Interphase
IGBT	Insulated Gate Bipolar Transistor
PLL	Phase Locked Loop (Estimator)
TSO	Transmission System Operator
PI	Proportional-Integral (Controller)
RSC	Rotor Side Converter
GSC	Gide Side Converter
SFIG	Singly-Fed Induction Generator
pu	per unit
PWM	Pulse Width Modulation
WT	Wind Turbine

Symbol

V_s, V_r	Stator and rotor voltage
I_s, I_r	Stator and rotor current
λ_s, λ_r	Stator and rotor flux linkage
R_s, R_r	Stator and rotor resistance
L_s, L_r	Stator and rotor inductance
L_{ls}, L_{lr}	Stator and rotor leakage inductance
L_m	Mutual inductance
τ_s, τ_r	Stator and rotor time constant
C	DC-link capacitance
T	Torque
P, Q	Active power, Reactive power
V_{dc}	DC-link voltage
J	Inertia
ω	Angular speed
θ	Angle
K_{shaft}	Stiffness coefficient
D	Damping coefficient
σ	Flux linkage factor
F	Frequency
ρ	Mass density of air
R	Rotor radius of the wind turbine
V_w	Wind speed
C_p	Power efficient coefficiency
P_w	Wind power
P_M	Mechanical power
S	Apparent power
s	Slip
a	Turns ratio
ref	Reference value
m	Modulation factor

Subscript

a, b, c	Electrical phases
base	Per-unit base value
dc, ac	Direct current, Alternating current
g	Generator quantity
l	Leakage quantity
m	Magnetising quantity
mech	Mechanical quantity
r, s	Rotor, stator quantity
syn	Synchronous quantity
d,q	d-axis, q-axis quantity
rated	Rated value

ref	Reference value
mea	Measuring value
e	Electrical quantity
e	Electrical quantity
m	Machine quantity
t	Turbine
b	Base value
cb	Crowbar

Superscript

*	Conjugate
r, s, e	Rotor, stator and excitation frame
’	Equivalent value

In general:

Symbols with a top-bar (i.e. s) are space vectors and subscripts describe a machine side.

Symbols without a top-bar (i.e. V_{ds}) are instantaneous values and subscripts describe a component-axis and machine side.

Chapter 1 **Introduction**

1.1 Wind Energy Penetration

To reduce the impact of conventional electricity generation on the environment, many countries have increasingly sought to use alternative environmentally friendly sources, i.e. renewable sources. This can reduce carbon emissions in the process of electricity generation by utilising infinite natural sources. One renewable source that is of world-wide interest is wind power [1], as evident from Fig. 1.1 showing installed world wind energy [2, 3].

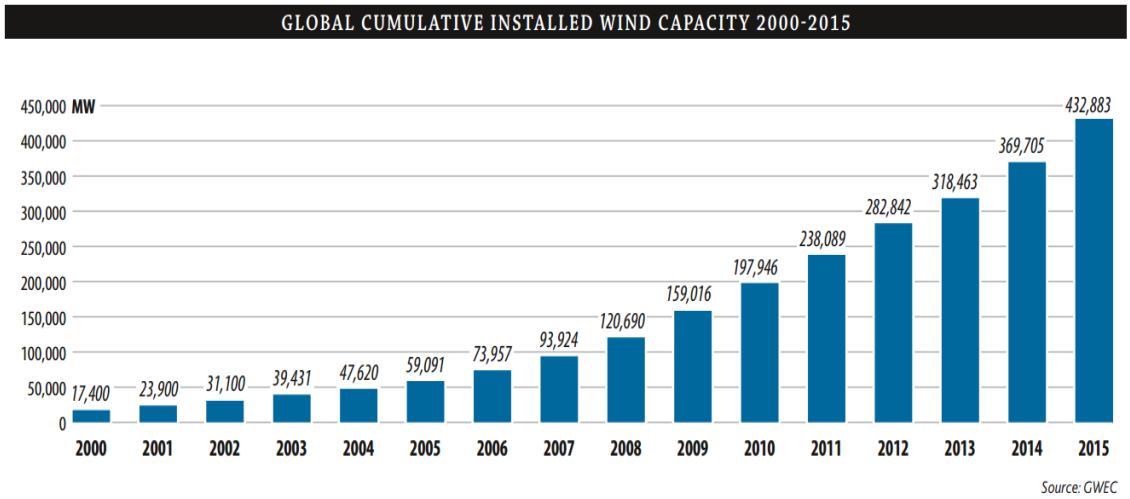

Fig. 1.1 Total world-wide installed wind generation capacity (2000-2015)[2]

According to the global wind report [2], the world has seen a new record in new wind installations. The wind capacity increased by 63.18 GW from the end of 2014, and reached 433 GW within the 2015 for the total wind capacity of the world. Amongst the top 10 markets, China, USA and Germany were the most dynamic countries and saw the strongest growth rates. As shown in Fig 1.2, these three countries shared the global wind market with 33.6%, 17.2% and 10.4%, respectively.

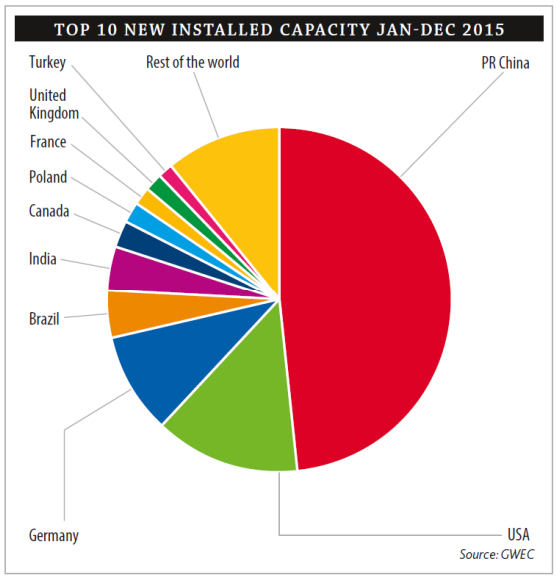

Country	MW	% Share
PR China	145,362	33.6
USA	74,471	17.2
Germany	44,947	10.4
India	25,088	5.8
Spain	23,025	5.3
United Kingdom	13,603	3.1
Canada	11,205	2.6
France	10,358	2.4
Italy	8,958	2.1
Brazil	8,715	2.0
Rest of the world	67,151	15.5
Total TOP 10	**365,731**	**84.5**
World Total	**432,883**	**100**

Source: GWEC

Fig. 1.2 Top 10 countries by total wind installations [2]

Increasing demand for wind power has resulted in many regions or countries developing the technical requirements for the connection of large wind farms with regard to the grid codes issued by Transmission System Operators (TSOs) [4].

These requirements are typically designed to ensure that large wind farms remain connected to the transmission system during disturbances (such as voltage dips), so-called fault ride through (FRT). Grid code requirements have been an important element in the development of wind turbine (WT) technology [5].

1.2 Wind turbine technologies

Wind turbines are generally classified into two main technologies:

1.2.1 Type A: Fixed speed wind turbines

Squirrel cage induction generators directly connected to the grid are usually used for this type, as shown in Fig. 1.3. The rotational speed of the generator is normally fixed with a slip of around 1%. These induction machines consume reactive power from the grid, hence capacitive compensation at the wind turbine grid connection is necessary. Their aerodynamic control is based on stall, active stall or pitch control. A variation of this scheme allows control of the speed of a wound rotor induction generator with external resistors up to 10% above synchronous speed [9].

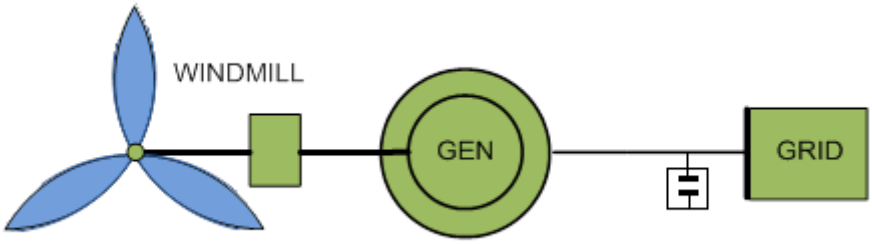

Fig. 1.3 Fixed-speed wind turbine (Type A)

1.2.2 Type B: Variable speed wind turbines

In this type of wind turbine, the rotor speed can be varied in line with prevailing wind conditions. There are two main types in this technology: The first (Type B1) is a synchronous/induction generator the stator of which is connected to the grid via a fully rated power converter, as shown in Fig. 1.4. The second (Type B2) is a Doubly-Fed Induction Generator (DFIG), as shown in Fig. 1.5. Here, the stator is directly connected to the grid while the rotor is connected to the grid via a four-quadrant converter [6-8] or back-to-back converter [9, 10]. The aerodynamic control of variable speed turbines is practically based on blade pitch control.

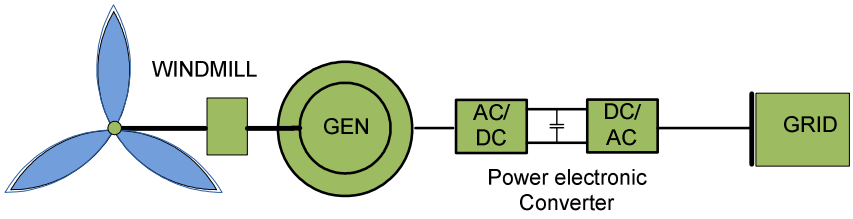

Fig. 1.4 Variable-speed wind turbine with fully-rated converters (Type B1)

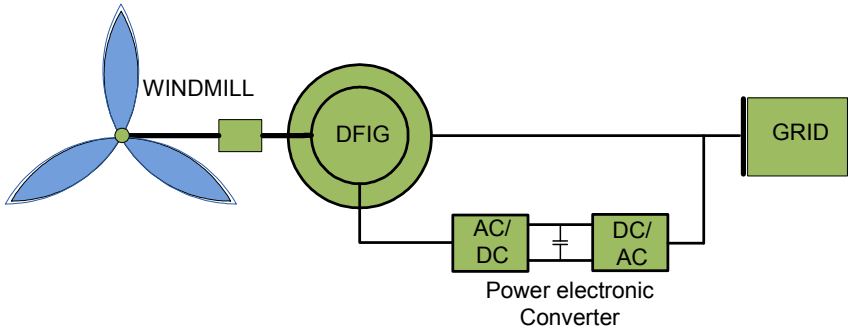

Fig. 1.5 Variable-speed wind turbine with partially-rated converters (Type B2)

Variable speed wind turbines offer a number of advantages [7, 11] when compared with fixed-speed turbines, such as operation over a wider range of wind velocities, independent control of active and reactive power, reduced flicker and lower acoustic noise levels. In the case of variable speed wind turbines, the DFIG converter handles a fraction of the turbine power (about 30% in practice) compared with a fully-rated converter [11, 12]. As a result, the DFIG is more cost-effective and widely used for large grid-connected, variable-speed wind turbines.

1.3 Market Share for Wind Turbine technologies

As mentioned in the above description, Fig. 1.6 shows the share of each manufacturer in the onshore variable-speed wind turbine topologies used globally for the 2013 market [13].

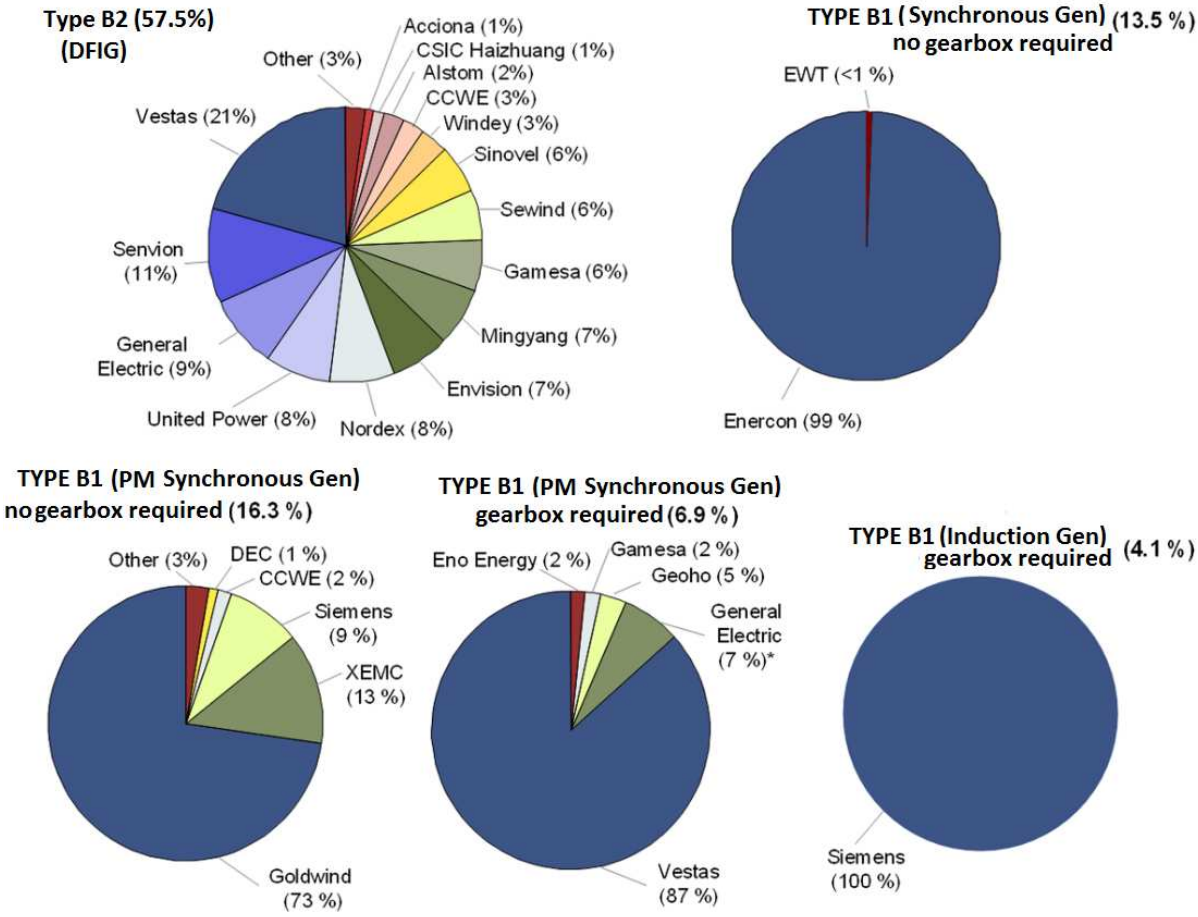

Fig. 1.6 Manufacturers' global market share for each variable-speed wind turbine during 2013 [13]

The global market share of each variable-speed wind turbine type is shown in brackets, while the indicated percentages of each manufacturer are mentioned in each type. The variable-speed wind turbines based on DFIG (TYPE B2) cover 57.5% of the total

installed capacity while others (TYPE B1) are divided into four subsets: First based on electrically excited synchronous generator with no gearbox required, Second based on permanent-magnet synchronous generator with no gearbox required, Third based on permanent-magnet synchronous generator with gearbox required, and the last one based on induction generator with gearbox required. They are involved in 13.5%, 16.3%, 6.9% and 4.1% for their market share, respectively.

1.4 Fault Ride Through (FRT) requirements

As stated in section 1.1, FRT requirements are developed to ensure that large wind farms remain connected to the transmission system during disturbances. Without these requirements, disconnecting large wind farms leads to power system network problems such as voltage collapse which may lead to whole system collapse. Various FRT grid codes [14, 15] from many countries are shown in Fig. 1.7. The German code from E.ON Netz GmbH, the GB code from National Grid Electricity Transmission, the Irish code published by ESB National Grid, the Nordic Grid code from Nordel TSO, the Denmark code of Danish TSO, the grid code for Belgium issued by the Belgian TSO, the grid codes of two Canadian TSOs issued by Hydro-Quebec and Alberta Electric System Operator (AESO), the USA rule for the interconnection of wind generators published by the Federal Energy Regulatory Commission (FERC), and codes from other countries such as Spain, Italy, Sweden and New Zealand.

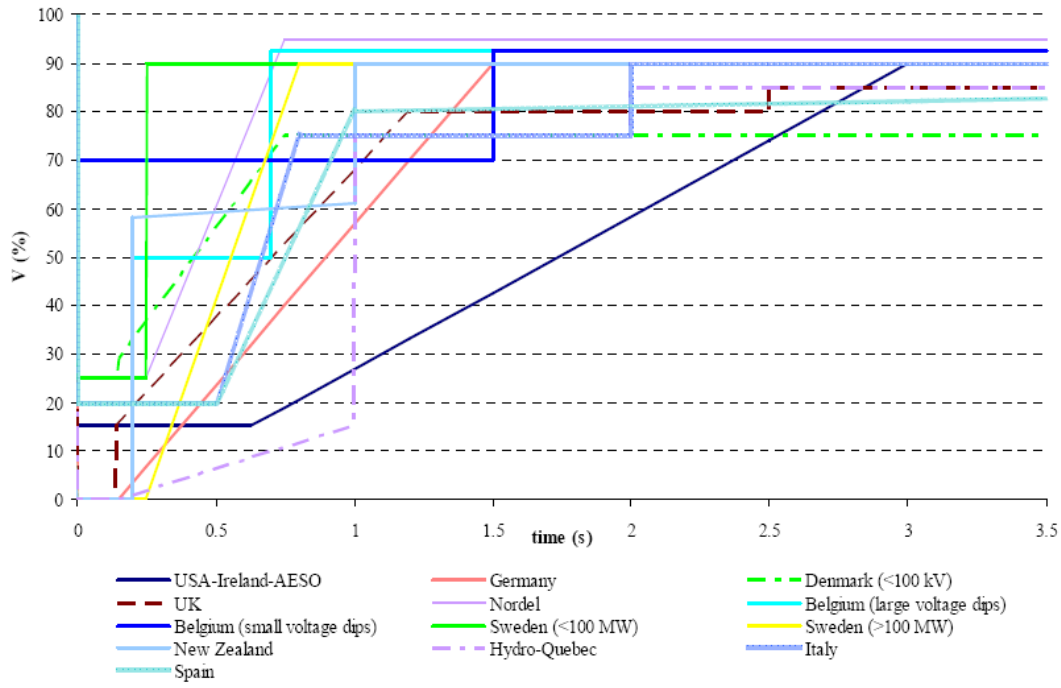

Fig. 1.7 Fault ride through requirements of various grid codes [15]

The Y-axis shows retained voltage (%) which then relates to the time duration (s) of FRT in the X-axis. The FRT requirements depend on the individual characteristics of each grid system. On or above the FRT line, a wind farm must ride through.

Three FRT grid codes will be considered in more detail, namely the Irish, GB and German Grid Codes. The Irish and GB grid represent medium and large isolated power systems, respectively; the German grid represents a high and extra high voltage grid.

- **FRT Irish Grid Code**

Since wind farms need to remain connected to the grid, the Irish Code requires that the wind farm shall provide active power in proportion to the retained voltage and maximum reactive current during the voltage dip (above the heavy black line in Fig. 1.8) and recovers at least 90% of available active power within 1 second of the recovery of transmission system voltage to the normal operating range (nominal ±10%).

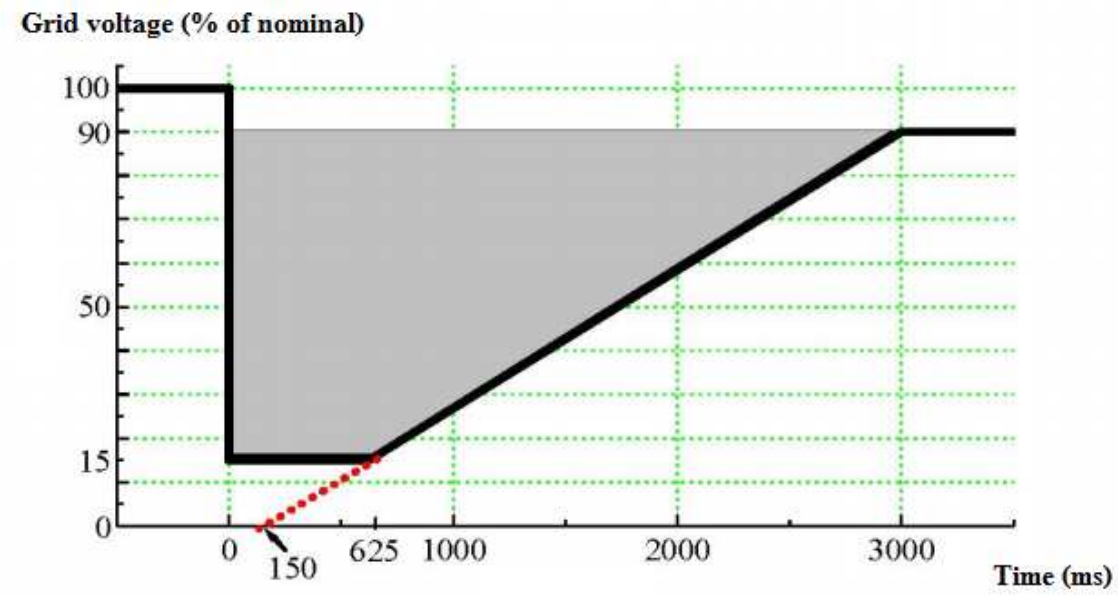

Fig. 1.8 Irish FRT capability for wind farms[16]

- **FRT Great Britain Grid Code**

The Grid Code (issued by National Grid Electricity Transmission (NGET in CC.6.3.15) specifies that each generating unit shall remain transiently stable and connected to the system for two main disturbances.

Balanced voltage dips that last for longer than 140 ms are illustrated in Fig. 1.9 (a) including the two examples shown in Fig. 1.9 (b). Each point on or above the heavy

black line represents a voltage level and an associated time duration for which generating units on the GB network must remain connected. During the voltage dips, the active power output of a generator has to be retained at least in proportion to the retained balanced network voltage. During voltage dips caused by grid faults, wind farms must generate their maximum reactive current to the grid system.

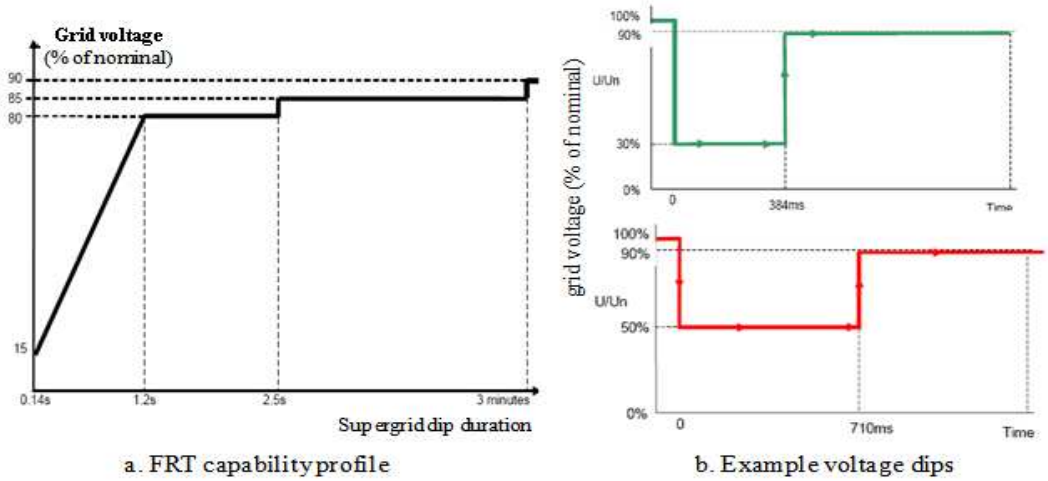

Fig. 1.9 The voltage-duration profile (for longer than 140 ms) and example voltage dips (from Appendix 4 of GB Grid Code)

For short circuit faults that last up to 140 ms, the grid code states that each generating unit shall be designed for the clearance of the fault on the transmission system within 0.5 seconds of the restoration of the voltage at the grid entry point or the voltage at the user system entry point to 90% of nominal or greater. Also the active power output shall be restored to at least 90% of the level available immediately before the faults (mentioned in CC.6.3.15 (a)(ii)[17]). During the period of grid faults, wind farms must generate their maximum reactive current to the grid system.

- **FRT German grid code**

E.ON Netz GmbH, referred to as ENE, is one of the major transmission system operators in Germany. The ENE grid code describes the minimum technical and organizational requirements for setting up and operating grid connections on the high voltage or extra high voltage grid in order to fulfill the regulations of the Union for the Coordination of Transmission of Electricity (UCTE) in Europe and the German transmission system operators. FRT is one of the ENE grid requirements with which wind farms have to comply.

According to the ENE grid code [18] (Fig. 1.10), three-phase short circuits or fault-related symmetrical voltage dips must not lead to instability or to the disconnection of the generating plant from the grid above the Limit Line 1.

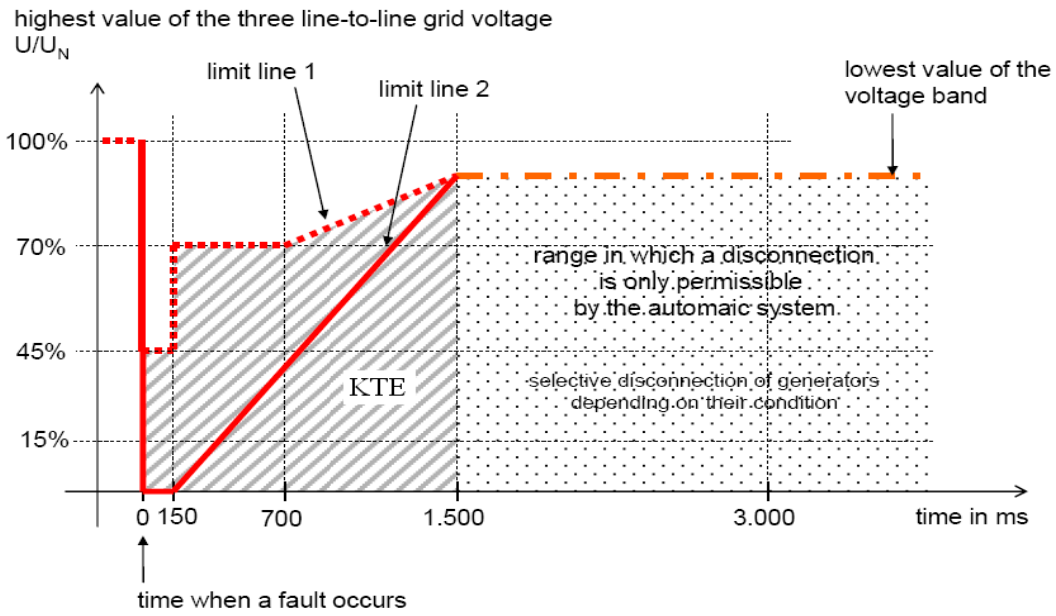

Fig. 1.10 Limit curves for the voltage pattern at the grid connection in the event of a fault in the German grid [18]

For the shaded area above Limit Line 2, all wind farms should experience the fault without disconnection from the grid. For the shaded area below Limit Line 2 (area KTE), a brief disconnection of the generating plant is allowed by agreement with the TSO if during the fault the individual generator becomes unstable, or the generator protection responds. In this KTE area, resynchronization of the generating plant must take place within 2 seconds. The active power in feed must be increased to the original value with a gradient of at least 10% of the rated generator power per second.

For all those wind farms that do not disconnect from the grid during a fault, the active power output must be continued immediately after fault clearance and increased to the original value with a gradient of at least 20 % of the rated power per second. The wind farms must support the grid voltage with additional reactive current during a voltage dip as shown in Fig. 1.11. In the event of a voltage dip of more than 10% of the effective value of the generator voltage, voltage control must take place within 20 ms after fault recognition by providing reactive current on the low voltage side of the generator transformer amounting to at least 2% of the rated current for each percent of the voltage

dip. After the voltage returns within the dead band, the reactive current support still continues to provide the grid voltage for at least 500 ms.

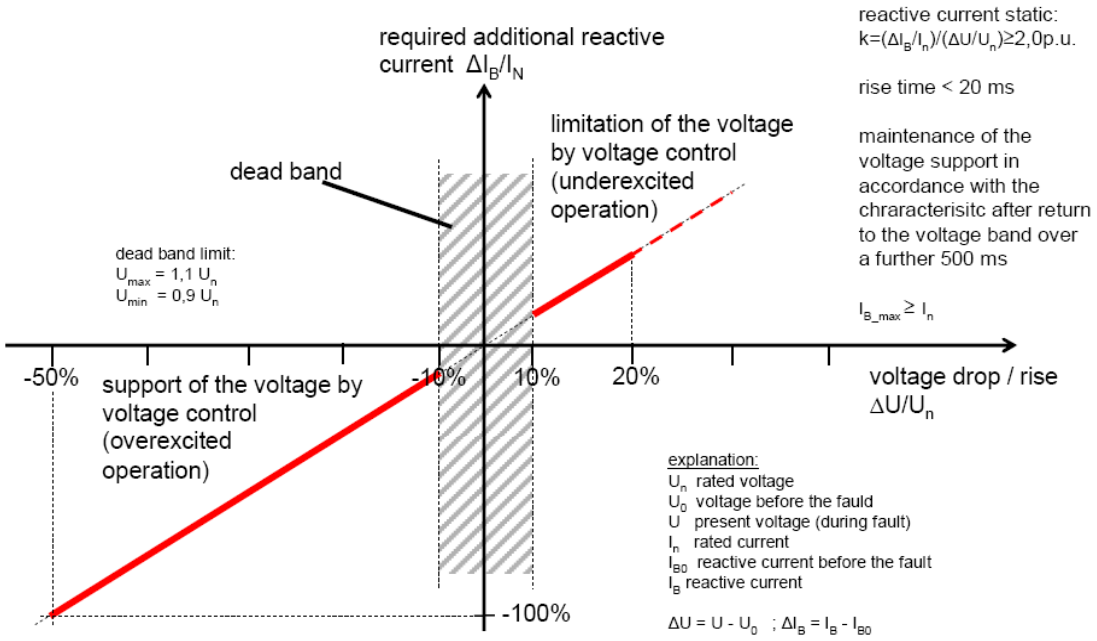

Fig. 1.11 The German grid code requirement for additional reactive current during a voltage dip [18]

1.5 Motivation

Since 2003 a number of authors [86, 88, 89,] have published the essential elements of the combined scheme for FRT capability of a DFIG wind turbine. In [19], the DFIG model with representation of only the rotor converter (RSC) will lead to a higher rotor current than the model with RSC including the GSC and DC-link. Also, as a result of the higher rotor current ***protective devices and converters will need to be enabled or disabled at the value where that current ceases to be appropriate. Therefore, detailed models of RSC, GSC and DC-link (back-to -back converters) are very important in the DFIG system.*** A review of published DFIG wind turbine models [8,19,50,52,72,73] will be described in more detail in Section 2.6.

In addition the combined scheme should be applied in the model for the FRT capability of a DFIG wind turbine. [20, 21] mentioned that both crowbar and DC-brake chopper are necessary for DFIG FRT capability to protect the rotor converter from over-current and overvoltage. [22, 23] also recommended that the combined scheme and control strategy helps to improve the FRT capability of a wind turbine driven DFIG but in connecting to DC-link, a battery energy storage system is used instead of a DC brake

resistor. In 2013, [24] supported the usage of a crowbar and DC brake chopper for DFIG Fault ride through and also proposed the capacitance in a crowbar circuit. While in [25] the authors also used crowbar and DC-link chopper to improve the ride through ability of the DFIG system. As mentioned above, the conclusion is that the crowbar operating alone gives rise to a number of concerns because of an unacceptable increase in the DC-link voltage. Also the most important thing when using only the crowbar circuit is the difficulty in finding the proper removal operation [26]**.** ***In order to overcome this, the combined scheme (using both crowbar and DC-brake chopper) continues to be a requirement.***

Summary

As the penetration of wind power in power systems increases, wind farms are required to remain grid-connected during disturbances in order to keep systems stable. Many grid codes have been revised to ensure wind farms connected to the transmission system during faults – so-called *fault ride through*. Fault scenarios corresponding to three grid codes (Irish, GB and German) are chosen to investigate FRT capability of the DFIG wind turbine. The Irish and GB codes are used to represent island systems, especially GB which has a high potential for off-shore wind farms, while the German code is used to represent a regional system which is connected to a European transmission system which is important for the wind farm market.

Irish and GB FRT requirements focus on active power restoration which needs at least 90% of available active power within 1 second of the recovery of transmission system voltage to the normal operating voltage, while the German code requires only that the active power restoration must be continued and increased by at least 20% of the rated power per second after fault clearance. During grid faults, both Irish and GB FRT grid codes require wind farms to supply maximum reactive current to the grid. The German code specifies the required reactive current support in more detail, i.e. at least 2% of the rated current for each percent of the voltage dip.

To study FRT capability, an accurate model of the DFIG system is needed. DFIG modelling is a contemporary research area being pursued by many scholars and institutions [27]. They have studied control schemes in more detail, rather than power electronic devices. The assumed ideal converter model (the switching devices are modelled as ideal switches, with no attempt to simulate the turn-on, turn-off

characteristics of devices) has been used in many publications [28-31]. The main problem of this is its inability to deal with the situation where switching off the IGBT device leaves the rotor circuit connected to a diode bridge rectifier. ***Therefore, it is necessary take into account the switching behaviour of rotor converter diodes and IGBTs if we are to complete the picture in a way that has not, as yet, been covered in contemporary literature.***

Finally, the combined scheme should be applied in the DFIG system for the FRT capability of DFIG wind turbines, as many authors have expressed concerns about protecting the converter and DC-link during fault conditions. ***Hence, the proposed DFIG system model with converter extension (the switching behaviour of rotor converter diodes and IGBTs) is essential to investigating the DFIG FRT, especially a combined scheme which is the subject of on-going research, and also protection techniques which are interesting and deserve further examination.***

1.6 Research Aims

The main aims of the research lead to developing and experimentally validating a model of a wind turbine doubly fed induction generator during grid faults, allowing for switching off IGBT devices and leaving the rotor circuit connected to a diode bridge rectifier. This study is mainly focused on:

- Studying the behaviour of the DFIG during faults
- Modelling of DFIG operating under grid fault conditions
- Validation of the model with experimental test data
- Using the model to investigate the FRT performance of the DFIG in accordance with the Irish transmission system grid code (because it is more onerous at minimum retained voltage when compared with other codes, such as the GB and German grid codes)
- Using the model to study the FRT capability of the DFIG with a combined scheme (having both a crowbar and DC-brake chopper)

1.7 The contribution of this work

A Simulink model for a stator-voltage vector controlled DFIG with experimental verification is developed to investigate fault drive through characteristics, allowing for the switching effects of IGBT and anti-parallel diode devices. The developed model can be used to predict machine and converter current and voltage waveforms during

network fault conditions, represented by a 3-phase supply voltage dip, and to investigate the FRT performance of the DFIG wind turbine. By taking into account the switching behaviour of the rotor converter diodes and IGBTs the model can be used to predict a fault scenario when switching off the IGBT devices, leaving the rotor circuit connected to a diode bridge rectifier. Also, the model can be useful in designing the minimum crowbar resistance value for a DFIG system with a combined protection scheme which is concerned with the FRT capability of the DFIG.

1.8 Structure of Thesis

Chapter 2 of the thesis reviews DFIG concepts and existing models published in contemporary literature. Chapter 3 describes the developed model of a DFIG used to investigate its operating characteristics under normal and fault conditions. Chapter 4 presents an experimental verification of the model during normal operating conditions and fault conditions. Chapter 5 provides an investigation of DFIG Fault-Ride-Through capability. Chapter 6 concludes the research work carried out in this thesis and presents recommendations for future work.

Appendices A, B, C and D describe in detail the per unit system used in this investigation, basic vector control, the DFIG Test Rig data and the detailed Simulink diagrams of the DFIG System Model, respectively.

1.9 Publication

Publications related to this Ph.D. thesis:

"**New Method of Setting the Maximum Crowbar Resistance for Doubly-Fed Induction Generators under Grid Faults**"

Yutana Chongjarearn, 11th International Conference on Electrical Engineering/Electronics, Computer, Telecommunications and Information Technology, 2014.

"**Doubly-Fed Induction Generator Wind Turbine Model for Fault Ride-Through Investigation**"

Yutana Chongjarearn, 9th International Conference on Electrical Engineering/Electronics, Computer, Telecommunications and Information Technology, 2012.

Chapter 2 **Wind Turbine DFIGs and their Models**

As introduced in Chapter 1, the DFIG wind turbine is increasingly used for large grid-connected, variable speed wind turbines. This chapter provides a general description of the DFIG wind turbine and a review of published wind turbine models.

2.1 Wind turbine model

Generally, there are two main parts to a wind turbine model: an aerodynamic model and a drive train model.

2.1.1 Aerodynamic Model

The characteristics of a wind turbine rotor can be described by the relationships between the total available wind power and the mechanical power extracted by the wind turbine. The power transferred to a wind turbine (P_w) is described by

$$P_W = \frac{1}{2}\rho\pi R^2 V_W^3 \qquad (2\text{-}1)$$

where ρ is mass density of air (kg/m^3), R is the rotor radius of the wind turbine (m**)** and V_W is the wind speed (m/s).

Not all the kinetic energy of the wind can be captured by a wind turbine. Only a fraction of the wind power is transferred to rotational power in the turbine. This proportion is given by the power efficiency coefficient (C_P) of the wind turbine. The mechanical power (P_M) of a wind turbine measured at the hub of the turbine is a fraction of P_W as expressed in the following equation:

$$P_M = \frac{1}{2}C_p\rho\pi R^2 V_W{}^3 \qquad (2\text{-}2)$$

C_p is a function of λ and β ($C_p = C_p(\lambda, \beta)$ given by the manufacturers) where β is the rotor blades pitch angle (deg) and λ is the ratio between the blade tip speed (V_t) and the incoming wind speed (V_w) (m/s) given by

$$\lambda = V_t/V_w = \omega_r R/ V_w \quad (2\text{-}3)$$

Hence, V_w can be expressed as a function of λ, ω_r and R

$$V_w = (R/\lambda)\omega_r$$

where ω_r is turbine speed (rad/sec).

For optimal tracking, the maximum generated power ($P_{max)}$ can be expressed as

$$P_{\max} = \frac{1}{2} C_{popt} \rho \pi R^2 (R/\lambda_{opt})^3 \omega_r^3 \quad (2\text{-}4)$$

where ω_r is the turbine speed referred to the generator side of the gearbox (rad/sec), λ_{opt} is the optimum tip speed ratio and C_{popt} is the optimum power coefficient.

For wind speeds higher than rated, while the P_{max} is greater than the generator rated power (P_{rated}), pitch control is applied by changing the pitch angle of the blades to limit the power to the rated value. For wind speeds lower than rated, optimal tracking to generate maximum power is given [32], [10] by:

$$P_{\max} = K_{opt} \omega_r^3 \quad ; \quad K_{opt} = \frac{1}{2} C_{popt} \rho \pi R^5 / \lambda_{opt}^3 \quad (2\text{-}5)$$

where K_{opt} is a constant determined by the density of the air, the radius of the wind turbine, the optimum power coefficient with constant pitch angle and the optimal tip speed ratio which is varied by the turbine speed at the generator side. This turbine speed is demanded by a speed controller in order to provide the reference mechanical torque for the generator.

This power can be used as the electrical power reference for controlling the electrical output of the generator [33] or for the stator side active power reference [34]. In general, the mechanical torque, T_{mech}, applied instead of the mechanical power can be calculated as [35], [10]:

$$T_{mech} = \frac{P_{\max}}{\omega_r} = K_{opt} \omega^2_r \quad (2\text{-}6)$$

For studying the behaviour of the system during short transients such as FRT and fault conditions [36-40], the variation in wind speed can be ignored; as a result, wind speed

can be considered constant. Hence controlling the generated power or torque is based on turbine speed (rpm) according to (2-6) and the optimum torque-speed curve.

2.1.2 Drive train Model

Two main representations of the mechanical drive train of variable wind turbines, namely single-mass and two-mass models, are used in the literature [41-45], according to the application. The actual drive train consists of a low-speed shaft, gearbox, high-speed shaft and generator rotor, as shown in Fig. 2.1 (a).

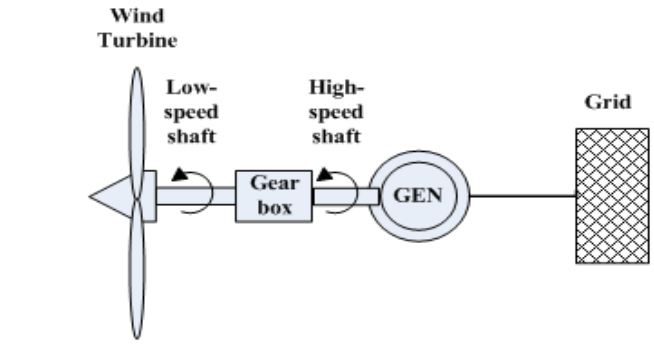

(a)

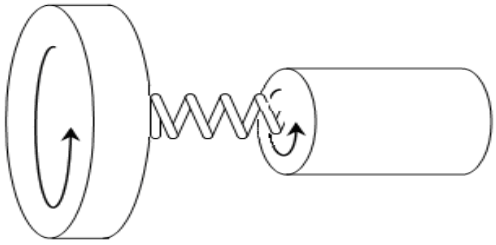

Wind turbine rotor +
Low-speed shaft + Gearbox

Generator
Rotor

(b)

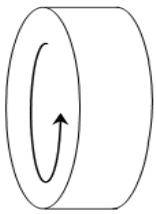

Wind turbine rotor + Low-speed shaft + Gearbox +
High-speed shaft + Generator rotor

(c)

Fig. 2.1 a) The actual drive train b) The two-mass model c) The single-mass model

A single-mass shaft model is usually sufficient for the normal operation of variable speed wind turbines, because shaft oscillations of generators do not affect the electrical

grid because of the fast active power control [46]. For stability analysis related to heavy fault conditions, the two-mass model is strongly recommended by many authors to represent the drive train system in order to obtain accurate results [19, 27, 42, 47]. More complex models can be found in some examples [48].

2.2 Doubly-fed induction generator (DFIG) characteristics

A DFIG is composed of a three-phase stator winding connected to the grid, and a three-phase rotor winding which is fed through PWM converters via slip rings. There are two voltage source converters in a DFIG power circuit, a rotor side converter (RSC) and grid side converter (GSC) which are connected back-to-back via a dc link and controlled using vector control methods, as shown in Fig. 2.2. The purpose of the GSC is to keep the dc link voltage constant while the RSC independently controls the active and reactive power to the grid utilising a vector control technique. An over-current "crowbar" circuit is needed to protect the machine and converters during disturbances in the network: for instance, operating when the rotor current is greater than twice the rated value [49].

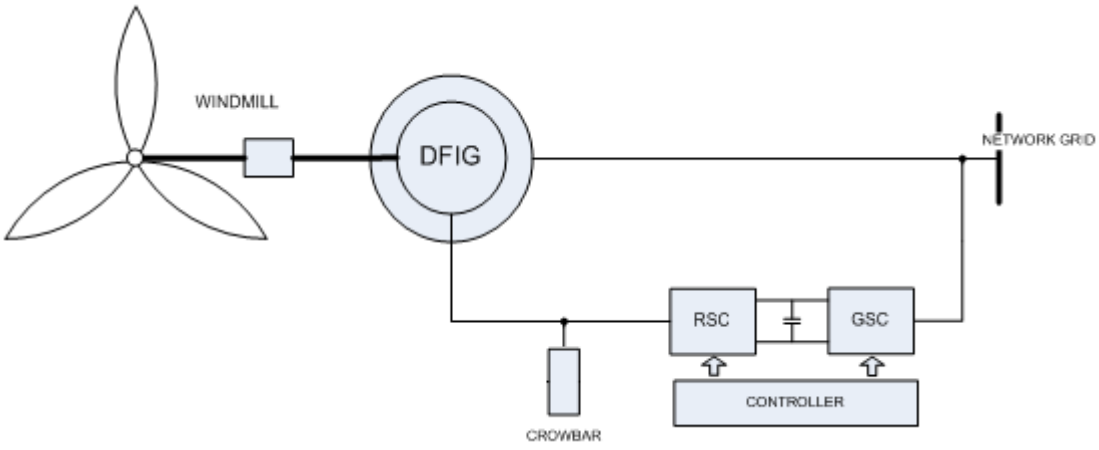

Fig. 2.2 Schematic diagram of the DFIG wind turbine system

Because the DFIG system allows a variable speed range within ±30% of synchronous speed, the converter rating can be designed to handle approximately 30% of the generator rated power. As a result, the converter rating does not depend on the generator power directly but instead on the slip power related to the selected speed range around synchronous speed.

Therefore, if the allowed speed range increases, the cost of the converter will increase [50, 51]. It has been recommended by [51] that a practical speed range could be between 0.7 and 1.1 pu because of mechanical restrictions.

Since the speed range is limited, the induced rotor voltage (V_r) is a fraction of the stator voltage (V_s):

$$V_r = s.V_s/a \tag{2-7}$$

where s is the slip and a is the turns ratio.

The DFIG can operate at both sub-synchronous (s>0) and super-synchronous (s<0) speeds. Power flows into the rotor in sub-synchronous operating mode but out of the rotor in over-synchronous operating mode, and out of the stator in both cases. Therefore a back-to-back or bi-directional power converter is needed for the DFIG wind turbine.

2.3 Control system for a variable speed DFIG wind turbine

The DFIG wind turbine has two main control parameters (P and Q) for active and reactive power control. P is the active power generated by the DFIG in order to provide power optimisation below the rated wind speed, or the rated power above the rated wind speed (see Fig. 2.3). Q is the reactive power generated by the DFIG in order to operate at the required power factor.

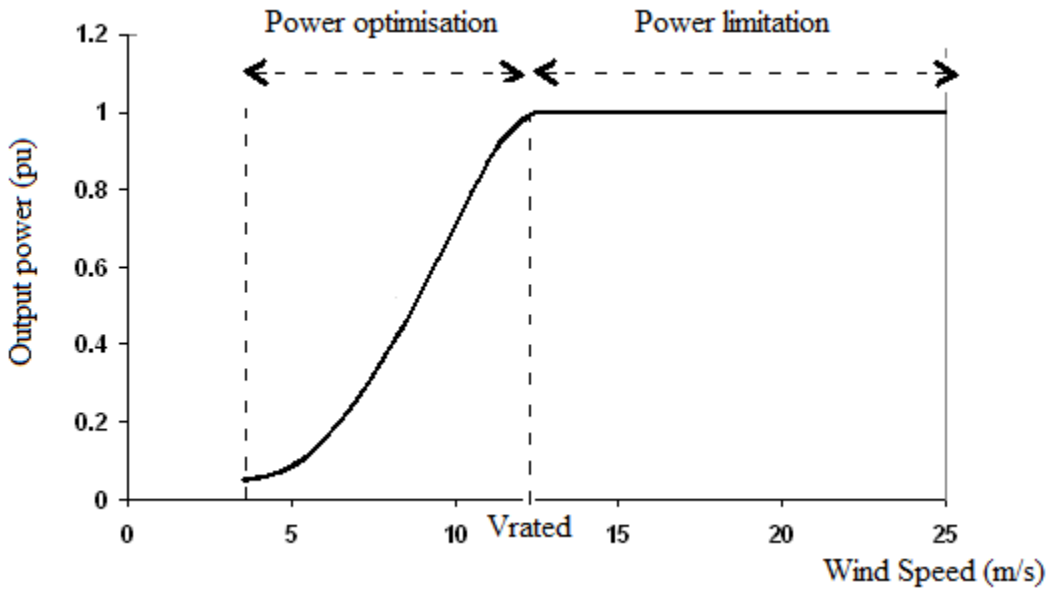

Fig. 2.3 A typical curve of output power and wind speed

Normally, a wind turbine system consists of the aerodynamical, mechanical and electrical parts all operating with different time constants, with the electrical dynamics being typically much faster than the mechanical changes. Given the presence of the power electronics converter in the DFIG wind turbine, the difference in time constants becomes bigger in the case of a variable speed wind turbine [50].

Two main control systems are essential for controlling a DFIG wind turbine, as shown in Fig. 2.4. These two control systems are significantly connected to each other, i.e. generator and wind turbine controls, of which the generator control operates much faster.

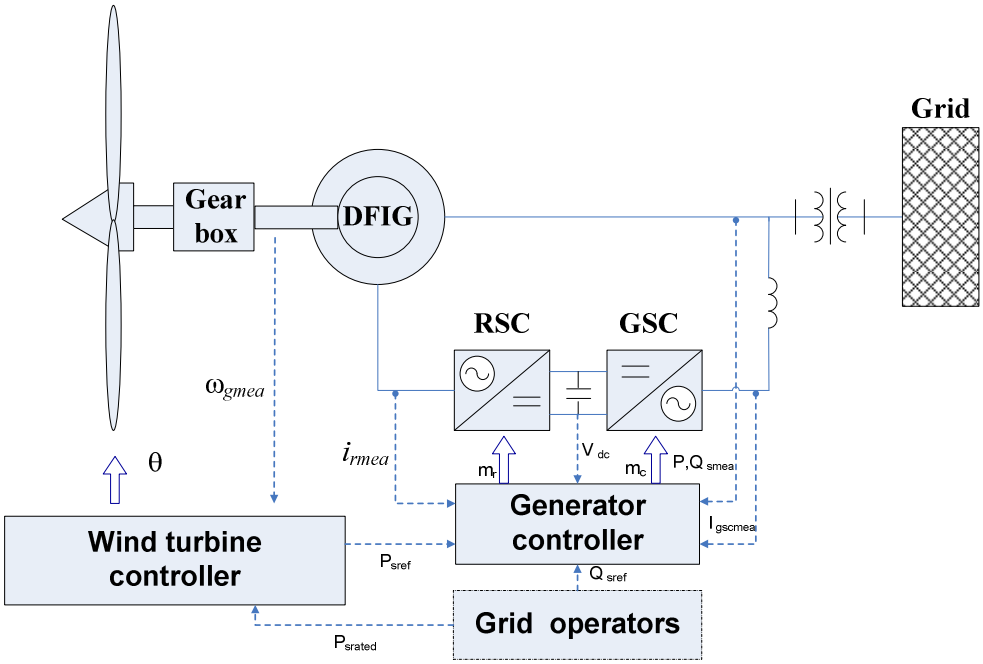

Fig. 2.4 Schematic diagram of the control system of a DFIG wind turbine

2.3.1 Generator controllers

The generator control is composed of two independently decoupled control schemes: one for the rotor side converter (RSC) and the other for the grid side converter (GSC) (see Fig. 2.4). Pulse width modulation (PWM) technique is used to control the RSC and GSC; the PWM modulation factor can be given by [52]:

$$m = K*V_{ac}/V_{dc} \qquad (2\text{-}8)$$

where K = $(2\sqrt{2})/\sqrt{3}$, V_{ac} is the demanded line-to-line ac voltage and V_{dc} is the defined dc voltage.

In each voltage source converter, classical PI controllers are used to obtain the modulation factor for power electronics switching in order to produce the demanded line-to-line ac voltage according to (2-8). The PI controllers in the RSC are used to control the stator active and reactive power, while controllers in the GSC are used to control the dc link voltage of the capacitor connected between the RSC and GSC and the reactive power between the GSC and the grid.

2.3.2 Wind turbine controllers

The wind turbine control normally has slower dynamics compared with the generator control. The wind turbine control is comprised of two different controllers: a speed controller, and a power limitation or pitch angle controller. These controllers can provide the reference pitch angle for the pitch actuator and also a power converter reference for the DFIG control.

In summary, there are two main controls for the DFIG wind turbine:

1. DFIG control with three reference inputs:
   - The reference active power (P_{sref}) provided by the wind turbine characteristic for RSC control as shown in Fig. 2.4.
   - The reference reactive power (Q_{sref}) defined by the grid operators for RSC and GSC control. For instance, during fault conditions the DFIG is required to generate reactive power to support the grid system.
   - The reference dc-link voltage (V_{dcref}) defined by the size of the converter, the stator-rotor voltage ratio and the modulation factor of the power converter for GSC control.
2. Wind turbine control with two reference inputs (see Fig. 2.4):
   - The reference active power (P_{sref}) for the generator control generated by the speed controller within the wind turbine controller as seen in Fig. 2.4, when the wind speed is less than the rated speed (V_{rated}) (see Fig. 2.3). The speed controller operates to keep the generator speed at the minimum limit, as well as maintaining the generator speed for tracking maximum wind power [50].
   - The pitch angle (θ) of the wind turbine blades is controlled by the pitch controller within the wind turbine controller, as seen in Fig. 2.4, when the wind speed is higher than the rated speed. The pitch controller is in operation

to limit the wind power capture at the rated turbine power (P_{rated}) [53] and [54].

Hence, while the reference active power (P_{sref}) is less than the rated turbine power (P_{rated}) (at power optimisation zone in Fig. 2.3), the wind turbine control keeps the pitch angle in an optimal value and provides the reference active power (P_{sref}) to the generator controller. However, when wind speeds are higher than the rated wind speed (at the power limitation zone in Fig. 2.3), the pitch controller operates in order to keep the reference active power (P_{sref}) within the limits of the rated power (P_{rated}). The generator controller is also used to control the generator speed within a specific range.

2.4 Doubly-fed induction generator (DFIG) control

The operating principle of the DFIG can be analysed by space vector theory and the popular direct (d) and quadrature (q) axis model, as well as both 3-to-2 and 2-to-3 axes transformations. In order to deal with the machine dynamic behaviour both stator and rotor variables are referred to the excitation frame in the developed model, i.e. the stator and rotor components such as current, voltage or flux linkage are referred to a synchronous reference frame. Variables in each reference frame can be transferred to another reference frame or vice versa, as explained in Appendix B.

In the DFIG, the three-phase stator windings are usually distributed so that the magnetomotive force may be assumed to be sinusoidally distributed in space around the air gap [55]. Therefore, in representing the dynamic model of DFIG and its control, space vector concepts are useful and used in many publications [8, 56-59]. The basic principle of space vector theory can be found in Appendix B.

In general, the space vector representation of the dynamic model of the DFIG is given by equations (2-9)–(2-12) for the stator and rotor side voltage, flux linkage and electrical torque.

$$\bar{v}_S = R_S \bar{i}_S + \frac{d\bar{\lambda}_S}{dt} + j\omega_e \bar{\lambda}_S \tag{2-9}$$

$$\bar{v}_r = R_r \bar{i}_r + \frac{d\bar{\lambda}_r}{dt} + j(\omega_e - \omega_r)\bar{\lambda}_r \tag{2-10}$$

$$\bar{\lambda_s} = L_m \bar{i_r} + L_s \bar{i_s} \tag{2-11}$$

$$\bar{\lambda_r} = L_m \bar{i_s} + L_r \bar{i_r} \tag{2-12}$$

Stator and rotor voltages in the d-q frame of reference are given by

$$V_{ds} = R_s i_{ds} + \frac{d\lambda_{ds}}{dt} - \omega_e \lambda_{qs} \tag{2-13}$$

$$V_{qs} = R_s i_{qs} + \frac{d\lambda_{qs}}{dt} + \omega_e \lambda_{ds} \tag{2-14}$$

Similarly,

$$V_{dr} = R_r i_{dr} + \frac{d\lambda_{dr}}{dt} - (\omega_e - \omega_r)\lambda_{qr} \tag{2-15}$$

$$V_{qr} = R_r i_{qr} + \frac{d\lambda_{qr}}{dt} + (\omega_e - \omega_r)\lambda_{dr} \tag{2-16}$$

Stator and rotor flux linkages in the d-q frame of reference are given by

$$\lambda_{ds} = L_m i_{dr} + L_s i_{ds} \tag{2-17}$$

$$\lambda_{qs} = L_m i_{qr} + L_s i_{qs} \tag{2-18}$$

Similarly,

$$\lambda_{dr} = L_m i_{ds} + L_r i_{dr} \tag{2-19}$$

$$\lambda_{qr} = L_m i_{qs} + L_r i_{qr} \tag{2-20}$$

Where $L_s = L_m + L_{ls}$ and $L_r = L_m + L_{lr}$.

Finally, the electromagnetic torque generated by a machine is given by

$$T_e = \bar{\lambda}_s \times \bar{i}_s \tag{2-21}$$

By substituting the rotor and stator flux linkages in the d-q frame, the torque is written as

$$T_e = \lambda_{ds} i_{qs} - \lambda_{qs} i_{ds} \tag{2-22}$$

or

$$T_e = \lambda_{qr} i_{dr} - \lambda_{dr} i_{qr} \tag{2-23}$$

The dynamic model of the DFIG can be represented by the equivalent circuits as shown in Fig. 2.5. While the machine is operating in steady-state, the equivalent circuit model will perform similarly to the equivalent circuit in Fig. 2.6.

Various vector control methods have been described in the DFIG literature. Stator-flux vector control is the most commonly used for controlling the active and reactive power generated by the DFIG [8, 10, 34, 60-62] while [7, 63, 64] use a stator voltage-oriented control method. The stator voltage-oriented or stator-voltage vector control can be accomplished because the stator winding of the DFIG is usually connected to the mains network which has a constant frequency, so its reactance is more dominant than the resistance in the winding, especially for a large wind turbine. As a result, the voltage drop across the stator resistance can be ignored [64, 65].

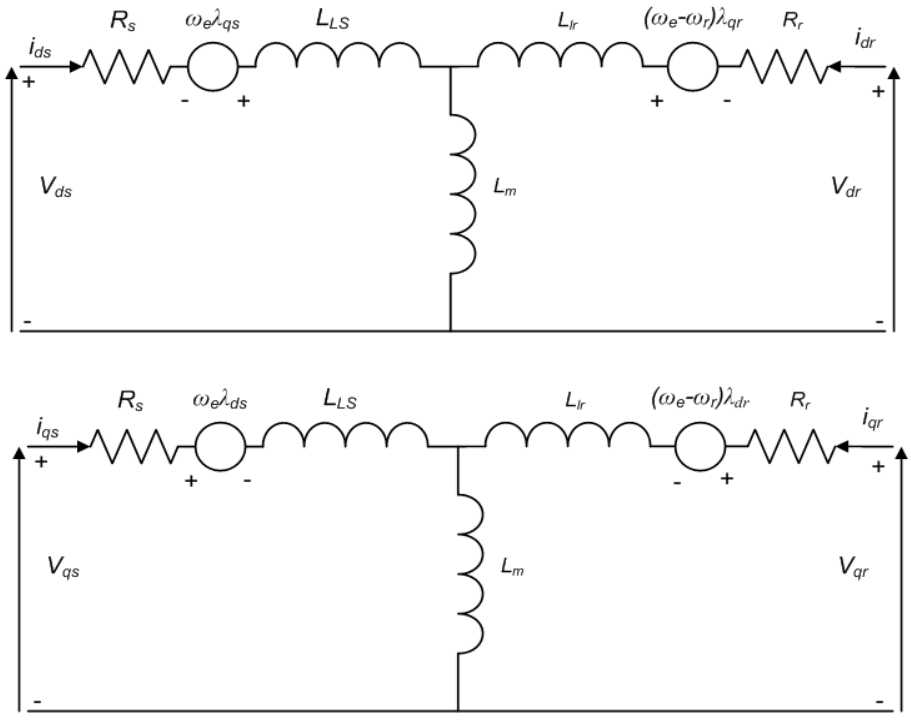

Fig. 2.5 The equivalent circuit of the DFIG in d-q components

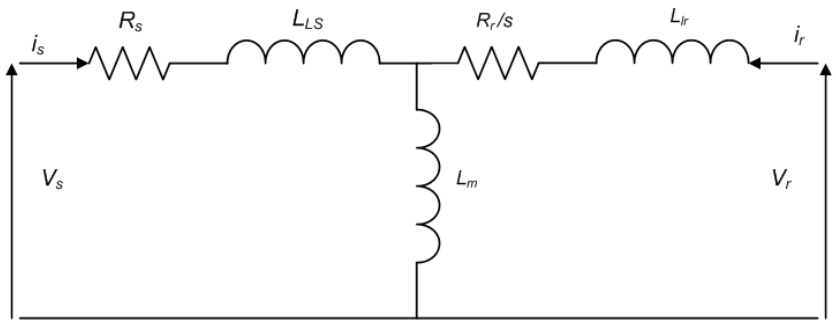

Fig. 2.6 Equivalent circuit diagram of an induction machine

2.4.1 Rotor side converter (RSC) control

The concept of stator flux-vector control is generally used for decoupled control of stator active and reactive power. As a result, both stator and rotor quantities are transformed to the synchronous reference frame of which the d-axis is aligned to the stator flux position as shown in Fig. 2.7.

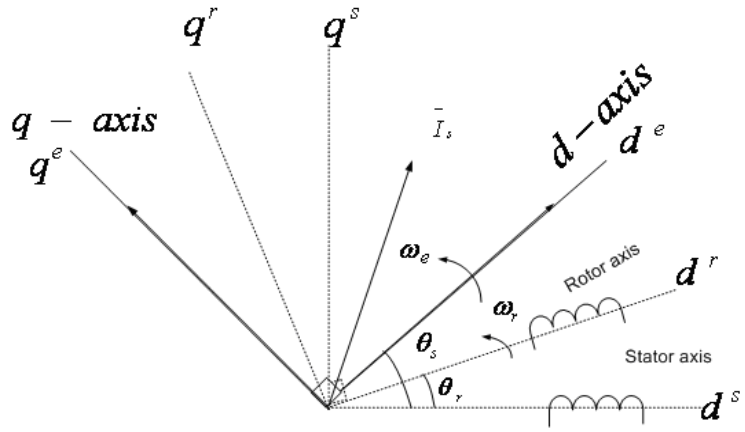

Fig. 2.7 Stator, rotor and synchronous reference frame

The stator active and reactive powers in per-unit three-phase system are as follows.

$$P_S = \mathrm{Re}(\bar{V}_s \cdot \bar{i}_s^*) = V_{ds}.i_{ds} + V_{qs}.i_{qs} \tag{2-24}$$

$$\text{and } Q_S = \mathrm{Im}(\bar{V}_s \cdot \bar{i}_s^*) = V_{qs}.i_{ds} - V_{ds}.i_{qs} \tag{2-25}$$

Referring to the stator-flux vector frame, the d-q voltages are given by

$$V_{ds} = 0, V_{qs} = \overline{|V_s|} \tag{2-26}$$

while stator and rotor flux linkages in the d-q frame are given by

$$\lambda_{ds} = L_m i_{dr} + L_m i_{ds} + L_{ls} i_{ds} = L_m i_{dr} + L_s i_{ds} \tag{2-27}$$

$$\lambda_{qs} = 0 \tag{2-28}$$

Thus,

$$P_s = v_{qs} i_{qs} = v_{qs}\left(-\frac{L_m i_{qr}}{L_s}\right) \tag{2-29}$$

and

$$Q_s = v_{qs} i_{ds} = v_{qs}\left(\frac{\lambda_{ds}}{L_s} - \frac{L_m i_{dr}}{L_s}\right) \tag{2-30}$$

Therefore, the stator active and reactive powers are independently regulated by the rotor currents in the stator flux vector reference frame as (2-29) and (2-30).

2.4.2 Grid side converter (GSC) control

Stator–voltage vector control is employed for the decoupled control of real and reactive power, i.e. both real and reactive power are interchanged with the grid using a control of stator current in the d-q axis in the stator voltage reference frame [9], [37], [66]. The current in the d-axis is used to control DC link voltage via real power, while the q-axis current is used to regulate the power factor via reactive power. All voltage and current quantities are transformed to the stator voltage reference frame of which the d-axis is aligned to the stator voltage vector.

2.5 Wind turbine control

The dynamic response of the wind turbine control is normally slower when compared with that of the generator control. Variable wind turbine control designs are based on two typical curves: (1) Mechanical power and wind speed and (2) Electrical power and generator speed.

2.5.1 Mechanical power and wind speed curve

As given in (2-1), the available energy in the wind depends on the cube of the wind speed as previously shown in Fig. 2.3. The power curve of a wind turbine follows the relationship between cut-in wind speed (the speed to start the wind turbine operating is approximately 4-5 m/s) and the rated capacity which is between approximately 12-16 m/s [67], depending on the design of each wind turbine**.** At wind speeds above rated, the output power production is limited by controlling the blades with so-called ‘pitch control’ or ‘stall control’ before the wind turbine is stopped at the cut-out wind speed, typically 25 m/s.

2.5.2 Electrical power and generator speed curve

DFIG operating characteristics depend on the characteristics of each wind turbine, as previously explained, and also on the size and efficiency of the generator and converter. The limited generator speed takes into account that the electrical power in (2.5) is generated within the operational range between minimum (ω_{min}) and maximum (ω_{max}) generator speed. The electrical power curve is shown in Fig. 2.8.

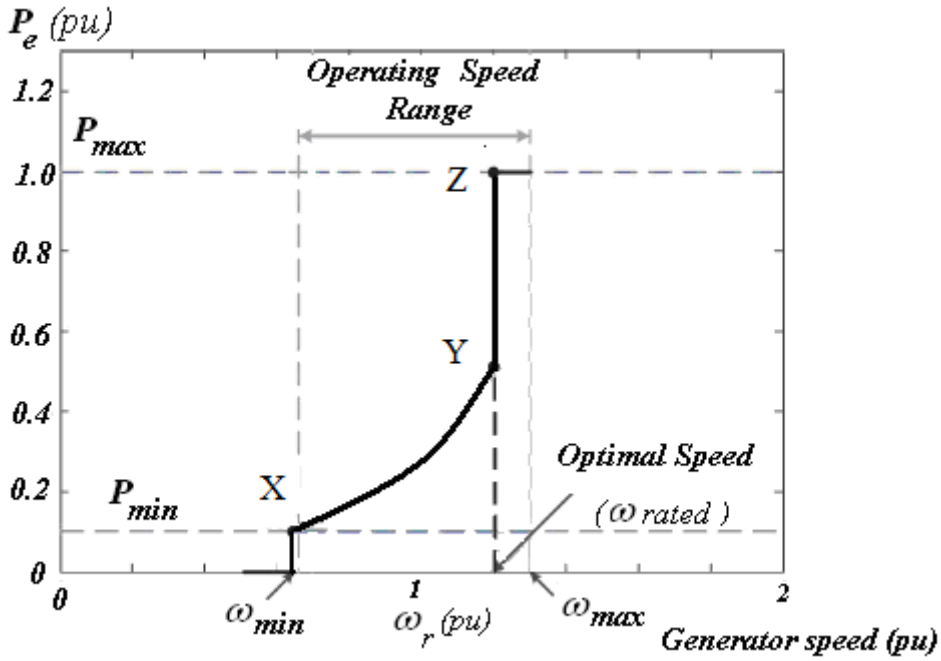

Fig. 2.8 A typical curve of electrical generator power and generator speed

Two control schemes are used for the variable-speed wind turbine: the speed controller and the pitch controller, or power limitation control [50]. These control schemes can be found in [50].

2.5.2.1 Speed controller

In power optimisation mode, the speed controller is active (as explained in Section 2.3.2 for wind turbine control) and also keeps the generator control at the minimum limit (X) for generator power (P_{min}) and speed (ω_{min}) as shown in Fig. 2.8. At low wind speeds, where the power does not exceed the rated value, the generator speed is varied to track maximum power at optimal C_p operation (curve X-Y). In higher winds, the speed is limited to its maximum value and the blades' stall properties are used to limit the power below the design values (curve Y-Z) [48].

2.5.2.2 Pitch or power limitation controller

For wind speeds higher than rated, the pitch or power limitation controller is activated and limits the wind power capture in order to track the rated generator power in the range from Z to the maximum generator speed (ω_{max}) as shown in Fig. 2.8.

For variable wind turbines, pitch control or active control is the most common method of controlling the aerodynamic power generated by a turbine rotor. Below rated wind speed the turbine should produce maximum power using a speed control.

Above the rated wind speed the pitch angle is controlled to limit the aerodynamic power at the rated turbine power [53] and [54].

2.6 A review of published wind turbine models

Research on the modelling of wind turbines has been undertaken during three decades of increasing use of wind power. For example, the dynamic modelling of synchronous generators was published by [68-71] between 1930 and 1981. A detailed d-q model was presented by [72] for a doubly-fed induction generator connected to a rotor side bridge rectifier and dc-link converter in 1985. Since 1985 most authors have represented the machine using Park's equations or the T-form of linear equivalent circuit [55, 73] and subsequently the well-known Space vector concept has been used to represent the machine model [8, 56-59, 74].

In this section, a brief overview of the development of wind turbine models will be presented. Because this thesis mainly focuses on large wind turbines connected to the grid, the modelling of large wind turbines (multi-megawatt size) is studied, especially the modelling of DFIG variable wind turbines published over the last decade. Third and fifth order models have been used by many authors to model the operation of a doubly-fed induction generator. A 3rd order model, presented by [75] and [38] represents the doubly-fed induction machine by a system of three differential equations, i.e. real, imaginary parts of the rotor flux and generator speed. Stator transients were neglected and the rotor voltage was assumed to have only the fundamental frequency while the third order model was used to study a DFIG under steady state operating conditions in order to increase the computational speed [76]. It has been showed that the third order model does not give sufficiently accurate results for disturbance conditions [19]. While a comparison between the 3rd and 5th order machine models has been examined by [77],

the fifth order model which includes the stator and rotor transients provided better results [78-81].

In [80, 81], the fifth-order model predicted better responses, especially the initial current occurring under transient and fault conditions. In a practical DFIG system, the converter voltage and current ratings as well as the size of the dc link capacitor are important to ensure good performance during grid disturbances. Therefore the 5^{th} order machine model, including detailed modelling of the converter, is necessary to give more accurate results.

The conventional drive for double-output induction generator (DOG) wind turbines consist of a rectifier and inverter based on diode and thyristor bridges (based on the static Kramer drive) but this technology has become obsolete for variable wind turbines [1, 82, 83]. Nowadays back-to-back converters based on six-IGBTs parallel with anti-diodes are used, because they make possible the independent control of active and reactive power [7]. Both conventional and back-to-back converters are shown in Fig. 2.9.

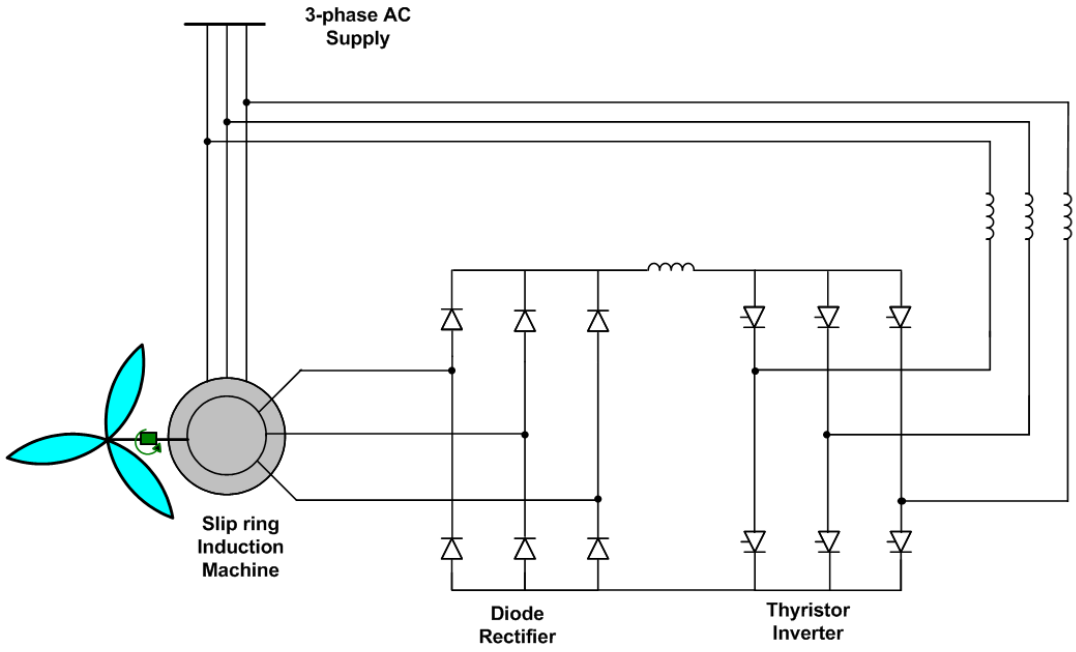

a) Conventional Drive

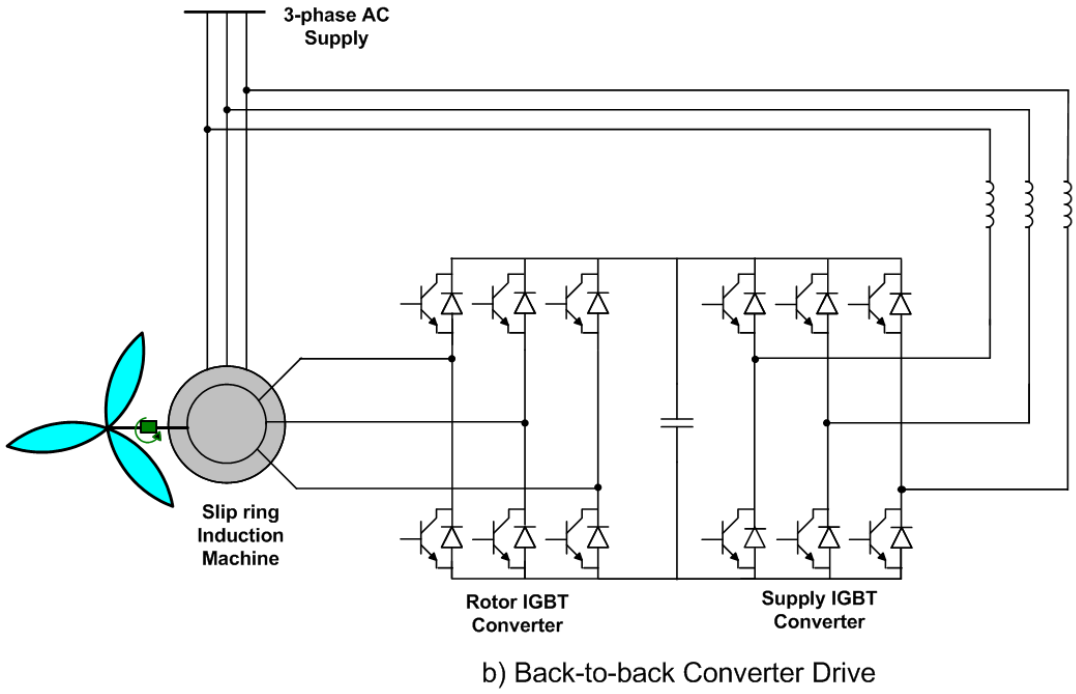

Fig. 2.9 The converter drive for DOG wind turbines

Many authors [10, 30, 61, 63, 81, 84-86] have concentrated on the effects of various control schemes on machine behaviour by assuming a converter as an ideal switch. Because they do not include power electronic devices (IGBTs and Diodes) for modelling the converter, the model cannot be used to simulate DFIG behaviour when the IGBT is switched off leaving only a diode rectifier circuit. For example, [30] proposed a model of DFIG using algebraic equations and current control loops for transient stability studies, but the converter model was not taken into account. [63] used only the active power balance before and after the converters to find voltages and currents in a DFIG, and focused on control systems in more detail. [10] and [61] studied DFIG behaviour only in normal operation on different control schemes. [85] proposed an extension to the 3th order model of DFIG with operating modes of a rotor side converter for simulation studies, but has not experimentally verified the system model. Moreover, in [19], the DFIG model with representation of the rotor converter (RSC) only will lead to a higher rotor current than the model with RSC including the GSC and DC-link. As a result of the higher rotor current, the operation of protective devices and converters will be enabled in an inappropriate condition. The details of RSC, GSC and DC-link (back-to-back converters) are thus very important in the DFIG model.

Similarly, mechanical models of DFIG wind turbines have been reported [19, 37, 87-89]. A two-mass model of the mechanical drive train is needed, especially for FRT studies.

The two-mass model is characterised by a first mass for the turbine rotor and a second mass for the generator rotor [19]. The two masses are connected to each other with a shaft that has a specific stiffness and damping constant value, as described in [19, 37, 87, 88]. During a grid fault, the electrical torque of the generator is significantly decreased; the drive train of the wind turbine behaves as an untwisted torsion spring. Because of the torsion spring characteristic of the turbine drive train, the generator speed starts to oscillate [90] with a so-called free-free frequency [37] or natural frequency [19]. This frequency is in the range of 0.5 to 2 Hz.

2.7 Summary

Generally, modelling of DFIG wind turbines consists of two main parts, i.e. wind turbine and generator models. A wind turbine model is comprised of an aerodynamic model and a drive train model, while a generator model is represented by the equation of the space vector of stator and rotor voltages, flux linkage and electrical torque. The basic concepts of the DFIG wind turbine were described, including generator and wind turbine controllers. A review of wind turbine models was introduced identifying some omissions in the published research.

In order to investigate the FRT capability of DFIG wind turbines, a proposed model of the DFIG wind turbine suitable for studying FRT performance will be developed in Chapter 3 and verified in Chapters 4 and 5.

Chapter 3 Modelling of the DFIG system

A three-phase wound rotor induction machine is the main part of the DFIG wind turbine system in which mechanical power is converted to electrical power. As mentioned in chapter 2, for the dynamic model of a doubly-fed induction generator, the use of a fifth order machine model as well as detailed modelling of the converter is very important when modelling the DFIG system under transient fault conditions. In this chapter, a stator-voltage-vector control DFIG model will be developed using Matlab/Simulink. The model is composed of a drive train and wind turbine with the DFIG connected to a three-phase supply. Further RSC and GSC converters, a crowbar, a dc link and brake chopper, line side filter and grid connections will be investigated in more detail using SimPowerSystems. A DFIG diagram is shown in Fig. 3.1.

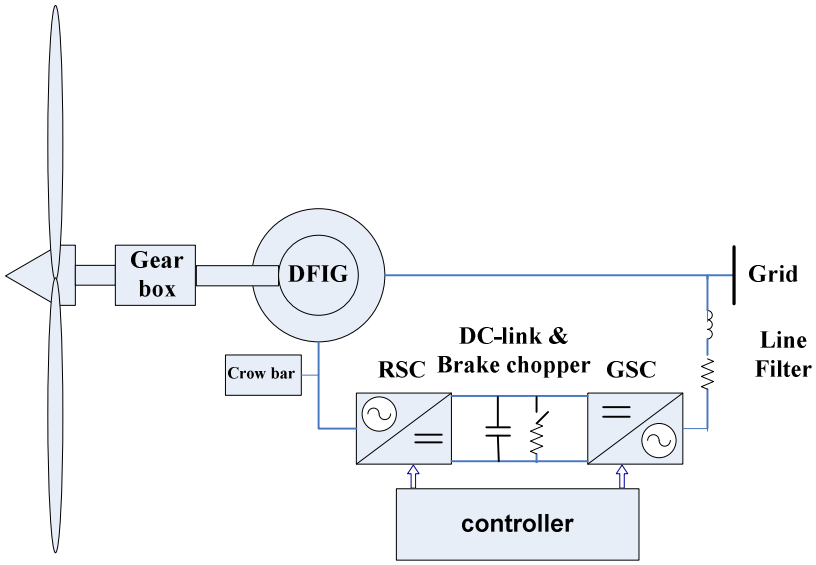

Fig. 3.1 A diagram of the DFIG model

3.1 Wind turbine and drive train model

As reviewed in chapter 2, the wind turbine speed can be assumed to be constant in the fault simulations. Typically, wind speed is averaged over ten minute periods [91] while FRT capacities are generally required for less than 5 seconds [39]. Therefore, the

modelled wind speed and the active stator power demand are held constant. Fig. 3.2 shows the per unit power output of a range of wind turbines for a given wind speed.

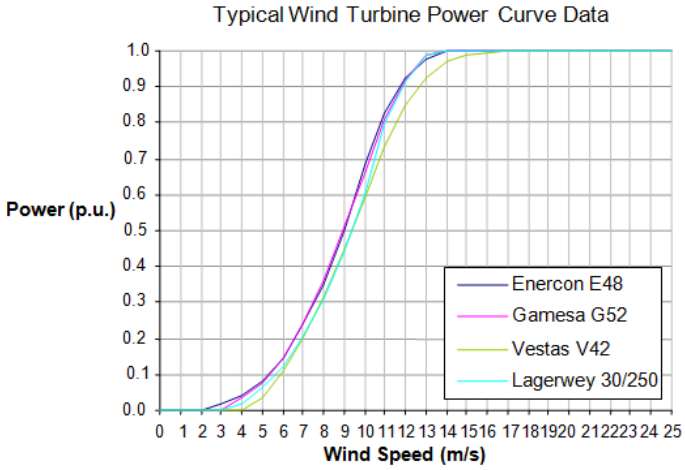

Fig. 3.2 Typical wind turbine power curves (taken from [39])

For the purposes of investigating the FRT capability of a DFIG wind turbine, a single operating point is chosen to represent a typical normal operating condition: at a typical wind speed of 10 m/s, the DFIG generates 0.67 pu power output.

The drive train consists of the turbine, gearbox, shafts and other mechanical components, represented by a two-mass model as shown in Fig. 3.3.

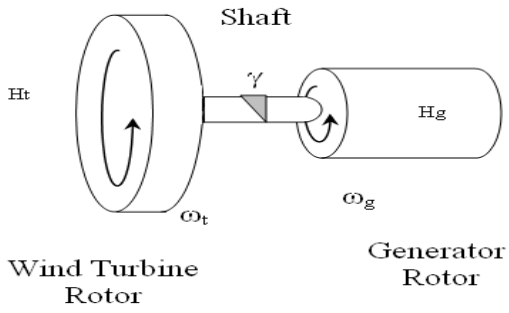

Fig. 3.3 A two-mass model of wind turbine DFIG

The mechanical dynamics of the wind turbine can be represented by:

$$\frac{d\omega_t}{dt} = \frac{\omega_b}{2H_t}\left(T_t - T_{shaft}\right) \tag{3-1}$$

where T_t is the mechanical torque produced by the wind turbine, T_{shaft} is the torque from the shaft connecting the induction generator with the wind turbine and H_t is the inertia

constant of the turbine, while ω_t ,ω_b are the wind turbine and base angular velocity. All quantities are given in pu.

The mechanical dynamics of the induction generator can be represented as

$$\frac{d\omega_g}{dt} = \frac{\omega_b}{2H_g}\left(T_{shaft} - T_g\right) \tag{3-2}$$

where T_g is the electromagnetic torque produced by the induction generator, H_g is the inertia constant of the induction generator and ω_g is the generator speed.

The incoming torque from the shaft (T_{shaft}) to the DFIG is composed of two terms: $T_{torsion}$ and $T_{damping}$.

$$T_{shaft} = T_{torsion} + T_{damping} \tag{3-3}$$

(3-1)-(3-3) represent a two-mass model of a drive train system in which $T_{torsion}$ represents the elasticity of the shaft and $T_{damping}$ represents the damping torque of the shaft in both wind turbine and generator [11, 38].

Torsion is described as a function of the angular displacement (rad) between the two ends of the shaft.

$$T_{torsion} = K_{shaft}\gamma = K_{shaft}\left(\theta_t - \theta_g\right) \tag{3-4}$$

where K_{shaft} is the shaft stiffness coefficient (pu. torque/rad), and γ is the angular displacement (rad) between the turbine and the generator.

Damping is related to the speed of wind turbine and generator.

$$T_{damping} = D(\omega_t - \omega_g) \tag{3-5}$$

where D is the shaft damping constant (pu. torque/(rad/sec)) and represents the damping torque in both wind turbine and induction generator.

For the drive train model there are two methods of controlling the mechanical torque into the generator, i.e. current-mode or speed-mode control [10].

In this thesis the speed controller is applied to obtain the turbine torque reference value ($T_{e,ref}$) at the generator speed reference value ($\omega_{e,ref}$), representing the mechanical power into the generator, from the maximum power characteristics of a wind turbine as illustrated in Fig. 3.4.

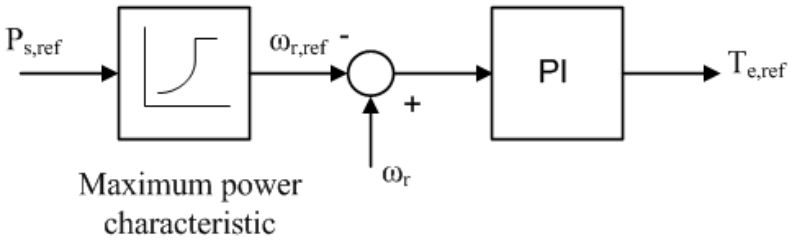

Fig. 3.4 Speed control for a wind turbine

To respond to the torque demand, a generator will produce more electrical torque until a balance is achieved between turbine torque and generator torque. As a result, the generator speed will increase until the required speed is attained. For a wind speed above rated, the speed controller will still provide the torque demand but maximum power is limited to the DFIG rated power. As mentioned above, the wind speed is assumed constant in fault conditions, so detailed interactions between pitch and torque controllers are not studied in this thesis. However, the model will be experimentally verified using a 10-kW dc motor and its drive to provide a torque demand to the DFIG. The blade-pitch control action of the turbine, a simulated mechanical two-mass shaft model and blade-pitch control model can be represented by the following torque equations [92]:

$$2H_t \frac{d\theta_t^2}{dt^2} + B_t \frac{d\theta_t}{dt} + D(\omega_t - \omega_g) + K_{shaft}(\theta_t - \theta_g) = T_t \tag{3-6}$$

$$2H_g \frac{d\theta_g^2}{dt^2} + B_g \frac{d\theta_g}{dt} + D(\omega_g - \omega_t) + K_{shaft}(\theta_g - \theta_t) = T_g \tag{3-7}$$

All mechanical parts' data can be found in an appendix A.

In transient modelling, the speed controller can be adjusted to emulate the dynamics of pitch control. Accordingly realistic speed increase and oscillations can be represented during and after grid disturbances, as illustrated in Fig. 3.5.

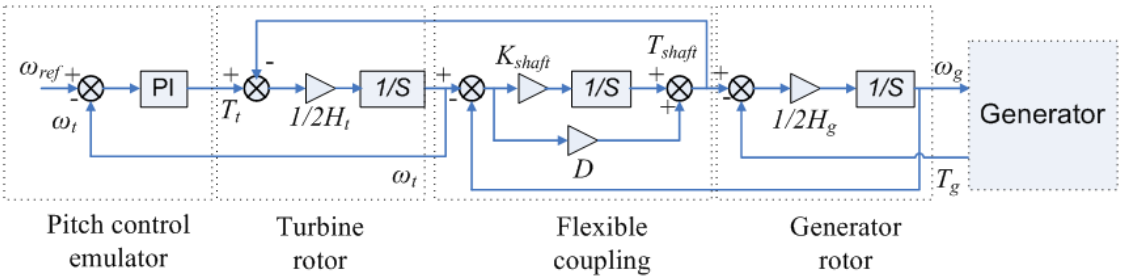

Fig. 3.5 Block model of mechanical drive train and pitch control mechanism

3.2 Power converters

Both the rotor side and grid side converters are modelled with six IGBTs and anti-parallel diodes connected back to back. The diodes and IGBTs are simulated by a resistor, inductor and DC voltage source connected in series with a switch. The diode switching operation is controlled by the anode-cathode voltage and current while IGBTs switching operation is controlled by the gate signal, the collector-emitter voltage and current. Switching these IGBTs is operated with the PWM techniques shown in the vector control scheme (see Fig. 3.6 and Fig. 3.7). In this control scheme the task of the RSC is decoupled control of the stator active and reactive power of the DFIG, while the GSC has to keep the DC-link voltage constant at a reference demand regardless of the magnitude and direction of rotor power. Both converters are normally set to control the DFIG operating at unity power factor, using stator voltage-oriented vector control as explained in more detail in section 3.5. The RSC and GSC are controlled independently with a switching frequency of 5 kHz.

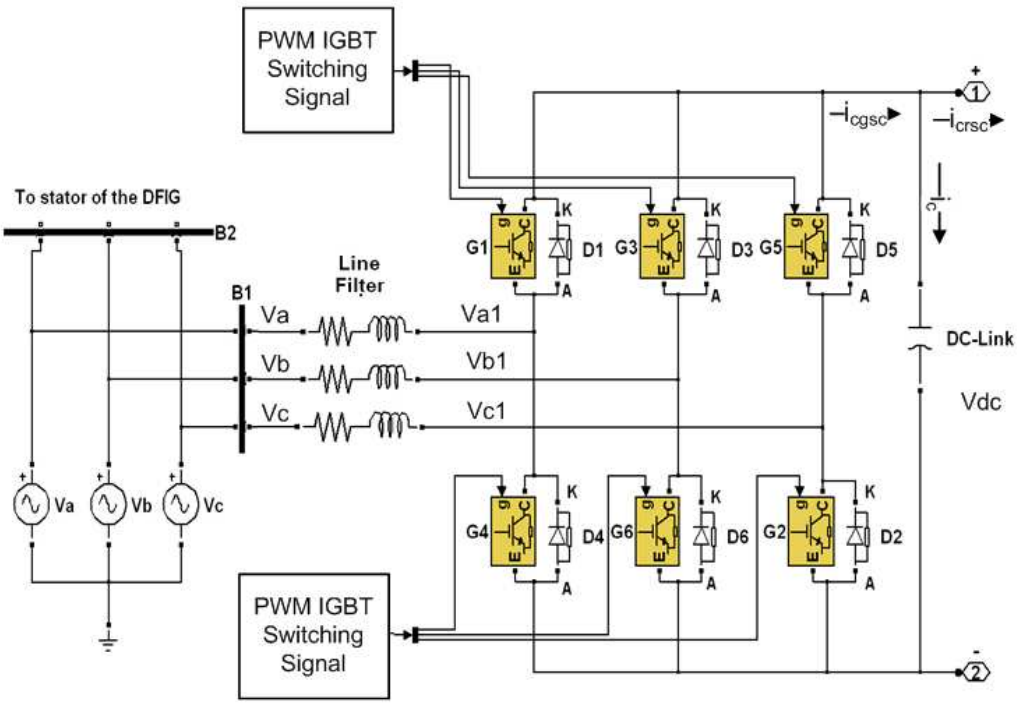

Fig. 3.6 Grid-side converter (GSC) schematic diagram

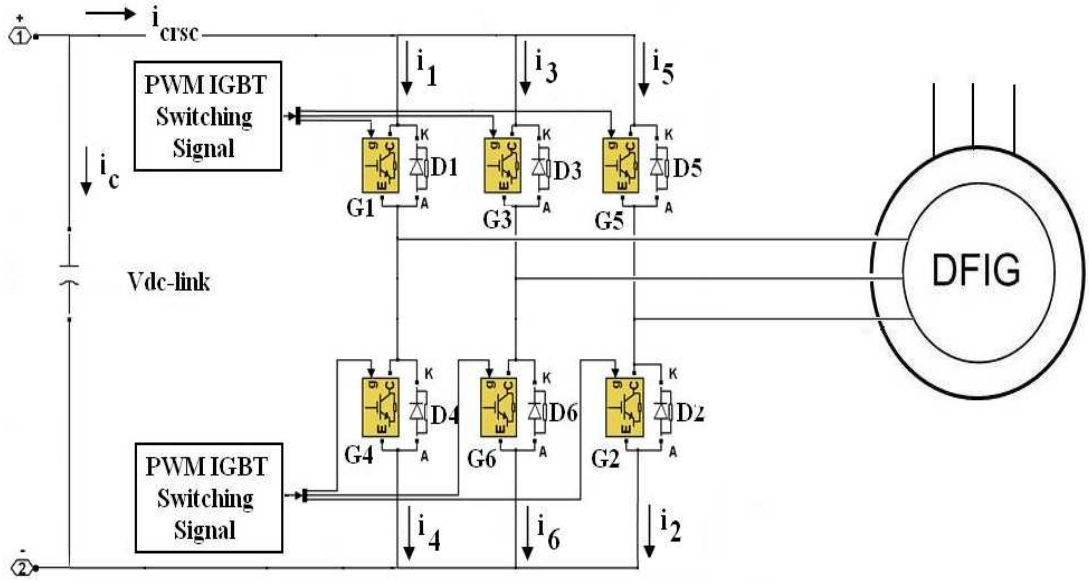

Fig. 3.7 Rotor-side converter (RSC) schematic diagram

In converter modelling, with consideration given to converter behaviour during fault, rotor currents are fed to the separated back-to back converters (RSC and GSC with DC-Link) modelled using SimPowerSystems as shown in Fig. 3.8.

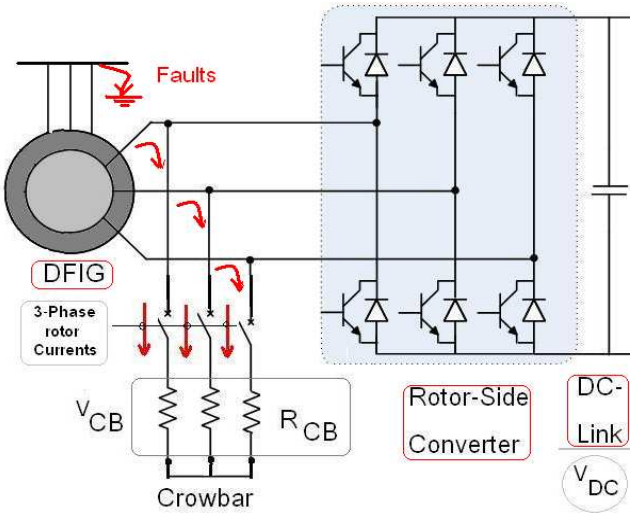

Fig. 3.8 Schemetic diagram of a DFIG with a crowbar connected to the rotor circuit

3.3 Stator-to-rotor turns ratio

The high current flowing into the converter can incur losses in the power converter. In order to reduce the rotor current, having the stator-to-rotor turns ratio can help to minimise the current. As a result the cost of the converter can be reduced. For example if the stator-to-rotor turns ratio, ns/nr, is 0.3, the rotor current is approximately 0.3 times smaller than the stator current. When the machine is operating at a max slip (s) of 30%, the rotor voltage is approximately $V_r = s.V_s/(ns/nr) = 0.3.V_s/0.3 = V_s$. In the DFIG model, the stator-to-rotor turns ratio is 0.32 according to the designed DFIG test rig.

3.4 DFIG vector control scheme

The dynamic modelling is used to perform both conventional equivalent circuit and transient behaviour of the DFIG. The model is based on the space vector representation of electrical quantities in per unit represented by state equations (3-8), (3-9), (3-10), (3-11) and (3-12) [56].

Stator flux linkage: $$\bar{\lambda}_s = L_m \bar{i}_r + L_s \bar{i}_s \quad (3\text{-}8)$$

Rotor flux linkage: $$\bar{\lambda}_r = L_m \bar{i}_s + L_r \bar{i}_r \quad (3\text{-}9)$$

Stator side voltage: $$\bar{V}_S = R_s \bar{i}_s + \frac{1}{\omega_b}\frac{d\bar{\lambda}_s}{dt} + \omega_e M \bar{\lambda}_s \quad (3\text{-}10)$$

Rotor side voltage:

$$\bar{V}_r = R_r \bar{i}_r + \frac{1}{\omega_b}\frac{d\bar{\lambda}_r}{dt} + (\omega_e - \omega_r) M \bar{\lambda}_r \qquad (3\text{-}11)$$

where M represents a 90^o space rotator, namely M = [0 -1; 1 0]], ω_b, ω_e and ω_r are base, synchronous and rotor angular speeds, R_s, R_r are stator and rotor resistances, and i_s, i_r are stator and rotor currents, respectively. The machine torque is given by:

$$T_e = \bar{\lambda}_s \times \bar{i}_s \qquad (3\text{-}12)$$

A schematic diagram of the model is shown in Fig. 3.8. Also, the above equations from (3-8)-(3-12) can be represented as the equivalent circuit in Fig. 3.9.

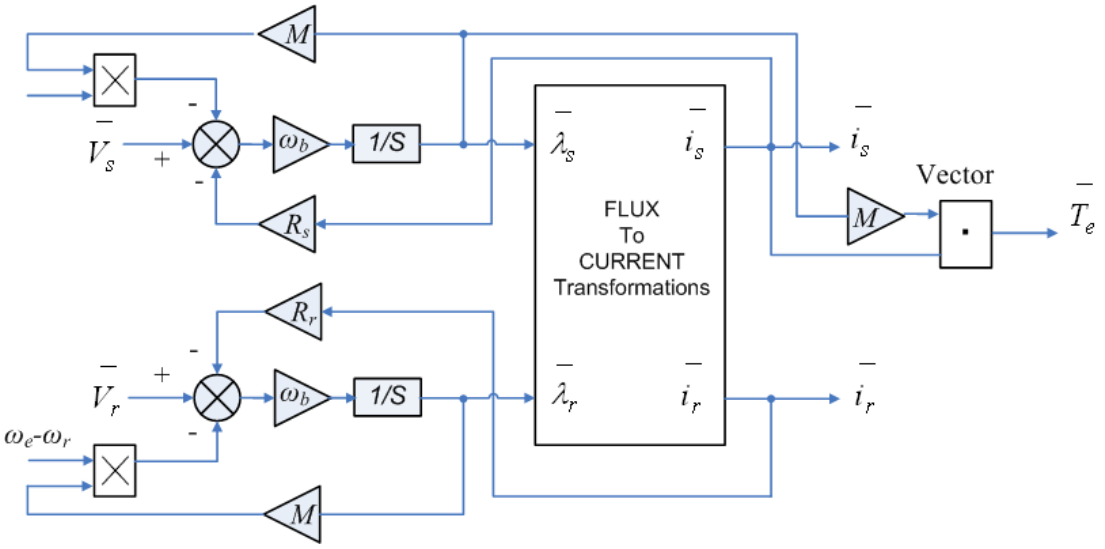

Fig. 3.8 Block model of an induction generator

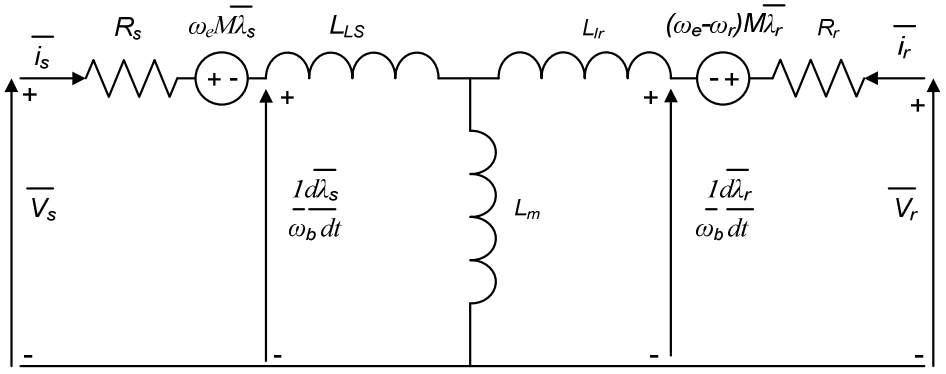

Fig. 3.9 The equivalent circuit of an induction generator

All quantities in equations are decomposed into the d-q reference frame using stator-voltage vector control method. The stator voltage in the d-q frame is expressed as

$$V_{ds} = R_s i_{ds} + \frac{1}{\omega_b}\frac{d\lambda_{ds}}{dt} - \omega_e \lambda_{qs} \tag{3-13}$$

$$V_{qs} = R_s i_{qs} + \frac{1}{\omega_b}\frac{d\lambda_{qs}}{dt} + \omega_e \lambda_{ds} \tag{3-14}$$

Similarly, the rotor voltage in the d-q frame is expressed as

$$V_{dr} = R_r i_{dr} + \frac{1}{\omega_b}\frac{d\lambda_{dr}}{dt} - \left(\omega_e - \omega_r\right)\lambda_{qr} \tag{3-15}$$

$$V_{qr} = R_r i_{qr} + \frac{1}{\omega_b}\frac{d\lambda_{qr}}{dt} + \left(\omega_e - \omega_r\right)\lambda_{dr} \tag{3-16}$$

The per unit electromagnetic torque (T_e) produced by the induction generator can be expressed as

$$T_e = \lambda_{ds} i_{qs} - \lambda_{qs} i_{ds} \tag{3-17}$$

The per unit flux linkage equations can be written in the d-q frame as

Stator flux linkage:

$$\lambda_{ds} = L_m i_{dr} + L_s i_{ds} \tag{3-18}$$

$$\lambda_{qs} = L_m i_{qr} + L_s i_{qs} \tag{3-19}$$

Rotor flux linkage:

$$\lambda_{dr} = L_m i_{ds} + L_r i_{dr} \tag{3-20}$$

$$\lambda_{qr} = L_m i_{qs} + L_r i_{qr} \tag{3-21}$$

where L_m is mutual inductance and L_s, L_r are stator and rotor self inductances.

3.5 DFIG power and current control

Stator Power-flow of DFIG is represented by

$$\bar{S}_S = P_S + jQ_S = \bar{V}_S \bar{i}_S^* \tag{3-22}$$

where $\bar{i}_s^*$ is conjugate of $\bar{i}_S$

The active and reactive powers generated by DFIG in per unit system can be written in terms of stator currents as

$$P_S = V_{ds} i_{ds} + V_{qs} i_{qs} \tag{3-23}$$

$$Q_S = V_{qs} i_{ds} - V_{ds} i_{qs} \tag{3-24}$$

Since stator-voltage vector control is used for both rotor side and grid side converters, the excitation or stator voltage-vector angle (θ_e) is obtained by using a Phase-Locked Loop (PLL) estimator as in Fig. 3.10. The PLL estimator can be used to find the angle and frequency of a voltage signal i.e. θ_e and ω_e. All voltage and current quantities are transformed to the stator voltage reference frame of which the d-axis is aligned to the stator voltage vector, as shown in Fig. 3.11.

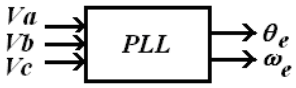

Fig. 3.10 The PLL estimator

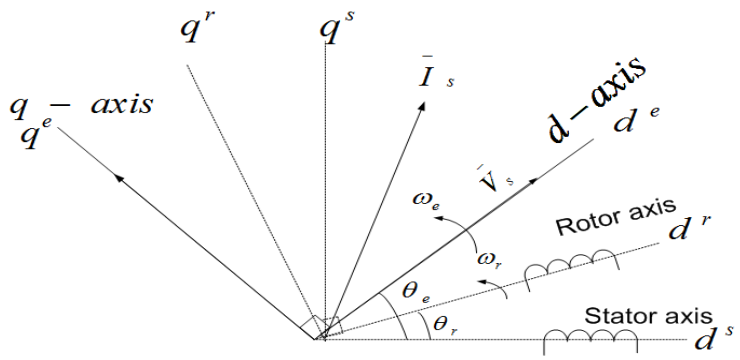

Fig. 3.11 Stator, rotor and excitation reference frame

3.5.1 Rotor side converter (RSC) control

Control on the rotor side converter is used to regulate the active and reactive power generated by the DFIG. Stator-voltage vector control is applied to decouple the active and reactive power. For the active and reactive powers in (3.25) and (3.26), stator currents will be given in terms of rotor quantities derived from (3.20) and (3.21) as

$$P_s = V_{ds}\left(\frac{\lambda_{ds}}{L_s} - \frac{L_m i_{dr}}{L_s}\right) + V_{qs}\left(\frac{\lambda_{qs}}{L_s} - \frac{L_m i_{qr}}{L_s}\right) \tag{3-25}$$

$$Q_s = V_{qs}\left(\frac{\lambda_{ds}}{L_s} - \frac{L_m i_{dr}}{L_s}\right) - V_{ds}\left(\frac{\lambda_{qs}}{L_s} - \frac{L_m i_{qr}}{L_s}\right) \tag{3-26}$$

Because the stator-voltage vector is aligned with the d-axis of the reference frame, the d-axis component of stator voltage is equal to the magnitude of stator-voltage vector; V_{ds} = V_s and V_{qs} = 0. Moreover, due to the large DFIG connected to a constant frequency grid network the voltage drop across the stator resistance can be neglected. Hence, the flux-linkage vector leads the stator-voltage by 90^{θ}, as a result the q-axis component of flux-linkage is equal to the magnitude of flux-linkage vector; λ_{ds} =0 and $\lambda_{qs} = \lambda_s$.

Substituting $V_{qs}, \lambda_{ds} = 0$ in the above power equation, the active (P_s) and reactive (Q_s) power equations can be shown as

$$P_s = V_{ds}\left(-\frac{L_m i_{dr}}{L_s}\right) \tag{3-27}$$

$$Q_s = -V_{ds}\left(\frac{\lambda_{qs}}{L_s} - \frac{L_m i_{qr}}{L_s}\right) \tag{3-28}$$

As seen in the active power generated by the DFIG in (3-27), the magnitude of the d-axis stator current (i_{ds}) is directly proportional to the d-axis rotor current (i_{dr}) used to control the active power generated by the DFIG. Similarly, in (3-28), a positive input of the q-axis rotor current (i_{qr}) will produce a lower value of the q-axis stator current resulting in controlling the reactive power drawn from the power supply. Therefore, the reference rotor currents ($i_{rdref,}$ i_{rqref}) for active and reactive power control are given by

$$i_{rdref} = PI\,(P_s - P_{sref}) \tag{3-29}$$

$$i_{rqref} = PI\,(Q_{sref} - Q_s) \tag{3-30}$$

where PI is the proportional and integral gain and $P_{sref,}$ Q_{sref} are the demand values of active and reactive powers of the DFIG supplied to the grid .

From the rotor voltage in (3-11), it can be rewritten as

$$\bar{v_r} = (R_r + \frac{1}{\omega_b}\sigma L_r \frac{d}{dt} + (\omega_e - \omega_r)\sigma L_r M)\bar{i_r} + ((\omega_e - \omega_r)\frac{L_m}{L_s}M + \frac{1}{\omega_b}\frac{L_m}{L_s}\frac{d}{dt})\bar{\lambda_s} \tag{3-31}$$

The d-axis and q-axis components of rotor voltages in (3-31) are obtained as

$$v_{dr} = R_r i_{dr} - (\omega_e - \omega_r)\sigma L_r i_{qr} - (\omega_e - \omega_r)\frac{L_m}{L_s}\lambda_{qs} + \frac{1}{\omega_b}\sigma L_r \frac{di_{dr}}{dt} \tag{3-32}$$

$$v_{qr} = R_r i_{qr} + (\omega_e - \omega_r)\sigma L_r i_{dr} + \frac{1}{\omega_b}\left(\sigma L_r \frac{di_{qr}}{dt} + \frac{L_m}{L_s}\frac{d\lambda_{qs}}{dt}\right) \tag{3-33}$$

where σ (flux linkage factor) $= 1 - \frac{L_m^2}{L_r L_s}$.

In (3-32) and (3-33), there are rotational-emf and transformer-emf terms. Because the operating slip range of a DFIG is limited, as mentioned in chapter 2, the effect of the former term is very small. Moreover, the stator flux is constant so the latter term can be ignored.

Therefore, in rotor currents control, the d-axis and q-axis components of reference rotor voltages for active and reactive powers control can be written as

$$v_{rdref} = PI(i_{rdref} - i_{dr}) \tag{3-34}$$

$$v_{rqref} = PI(i_{rqref} - i_{qr}) \tag{3-35}$$

where *PI* is the proportional and integral gain and i_{rdref}, i_{rqref} are the d-q-axis components of reference rotor currents. Finally, these d-q axis reference voltages will be converted to a 3-phase frame to generate modulation indices for the RSC PWM converter. Fig. 3.12 shows the RSC control block diagram.

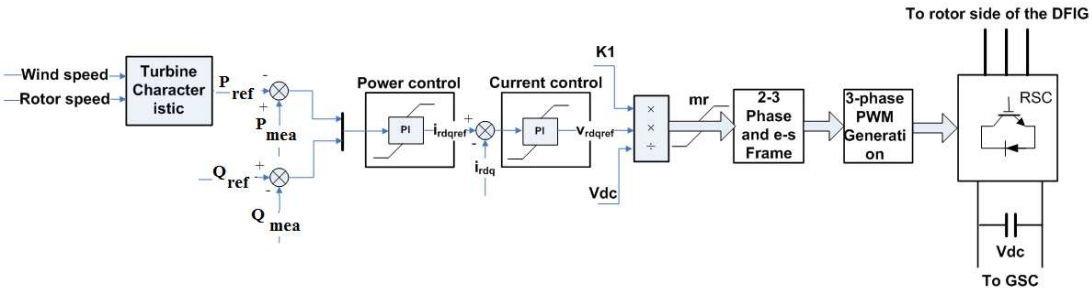

Fig. 3.12 RSC control block diagram

The RSC connected to the rotor circuit allows for fast control of the machine by modifying the line voltage on the rotor side. This voltage can be adjusted by the modulation index PWM. To generate 3-phase PWM signals to drive the six-IGBTs converter, the voltage demand needs to be scaled by using the factor (K_1) and DC-link voltage (V_{dc}). So the modulation index (m_r) for RSC can be written as:

$$m_r = K_1 * V_{rdq,ref} / V_{dc} \tag{3-36}$$

where $K_1 = ((2\sqrt{2}) * V_{rac} / \sqrt{3})$.

The ratio between DC (V_{dc})and AC (V_{rac}) voltage of the rotor side of the DFIG as seen in Fig. 3.7 is controlled by the modulation factor given in (3-36).

3.5.2 Grid side converter (GSC) control

A stator-voltage vector control is also used for the decoupled control of active and reactive powers of GSC, i.e. both active and reactive powers are interchanged with the grid using control of the d-q axis components of GSC currents. The d-axis current is used to control the DC-link voltage via active power, while the q-axis current is used to regulate the power factor via reactive power. The GSC is connected to the grid through a filter inductance (L) and resistance (R) as shown in Fig. 3.13.

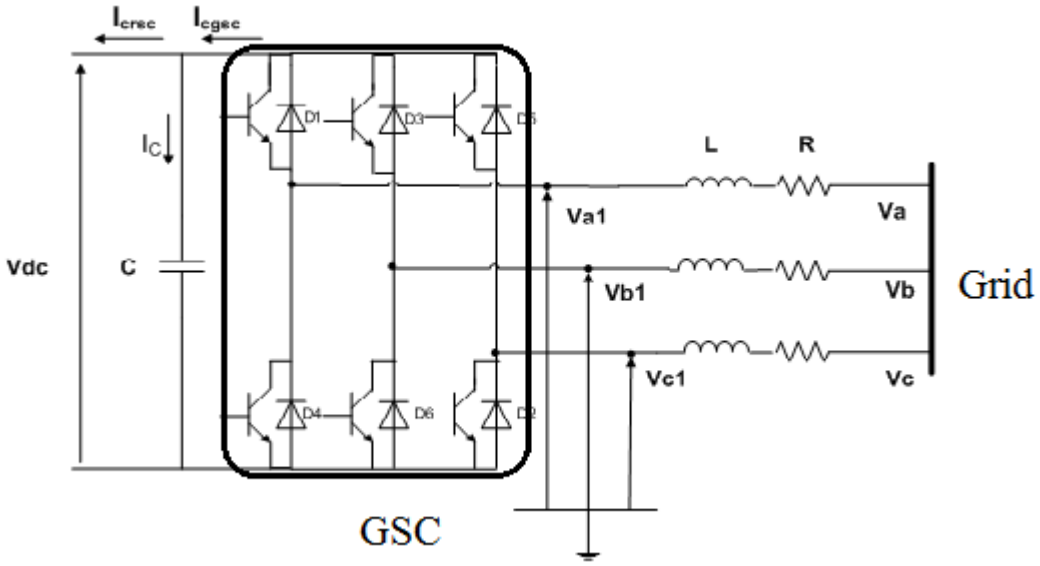

Fig. 3.13 A diagram of GSC-to-Grid connection

The relation between three-phase voltages of the Grid supply and Grid-side converter voltages are given by

$$\begin{bmatrix} V_a \\ V_b \\ V_c \end{bmatrix} = R\begin{bmatrix} i_a \\ i_b \\ i_c \end{bmatrix} + L\frac{d}{dt}\begin{bmatrix} i_a \\ i_b \\ i_c \end{bmatrix} + \begin{bmatrix} V_{a1} \\ V_{b1} \\ V_{c1} \end{bmatrix} \tag{3-37}$$

where i_a, i_b and i_c are three-phase grid-side converter currents, V_{a1}, V_{b1} and V_{c1} are three-phase grid-side converter voltages.

Three-phase voltages can be decomposed in the following dq-axis reference frame as

$$V_{cd} = Ri_{cd} + L\frac{di_{cd}}{dt} - \omega_e Li_{cq} + V_{cd1} \tag{3-38}$$

$$V_{cq} = Ri_{cq} + L\frac{di_{cq}}{dt} + \omega_e Li_{cd} + V_{cq1} \tag{3-39}$$

Where V_c is a voltage in phase c, V_{c1} is a voltage in phase c at GSC.

Since the d-axis of the reference frame is oriented along the grid voltage vector, the q-axis grid voltage is zero. The active power (P_c) and reactive power (Q_c) are given by

$$P_C = V_{cd}\, i_{cd} \tag{3-40}$$

$$Q_C = -V_{cd}\, i_{cq} \tag{3-41}$$

From (3-40) and (3-41), the active and reactive power is proportional to the d-axis and q-axis converter current (i_{cd}, i_{cq}), respectively.

As part of the DC-link, the energy stored in the DC-link capacitor is given by $CV_{dc}^2/2$.

The time derivative of the energy is equal to the sum of active GSC power (P_c) and RSC power (P_r). Neglecting harmonics due to transmission between grid and rotor, the DC-link equations are obtained as

$$\frac{1}{2} C \frac{dV_{dc}^2}{dt} = P_C - P_r \tag{3-42}$$

where $P_c = V_{cd}\, i_{cd}$, $P_r = V_{rd} i_{rd} + V_{qr} i_{qr}$ and $i_{crsc} = P_r/V_{dc}$ and $i_{cgsc} = P_c/V_{dc,}$ (see Fig. 3.13), hence

$$C \frac{dV_{dc}}{dt} = i_{cgsc} - i_{crsc} \tag{3-43}$$

From (3-42) and (3-43), it can be concluded that the DC-link voltage can be controlled using the d-axis GSC current while the reactive power is controlled using the q-axis GSC current as given in (3-41). Therefore, the d-axis and q-axis components of reference GSC currents for DC-link voltage and reactive powers control can be written as

$$i_{cdref} = PI(V_{dcref} - V_{dc}) \tag{3-44}$$

$$i_{cqref} = PI(Q_{cref} - Q_c\ ) \tag{3-45}$$

where PI is the proportional and integral gain and i_{cdref}, i_{cqref} are the d-axis and q-axis reference GSC currents for DC-link voltage and reactive power, respectively.

After rearranging (3-38) and (3-39), the GSC voltages can be expressed as

$$V_{cd1} = -Ri_{cd} - L\frac{di_{cd}}{dt} + \omega_e L i_{cq} + V_{cd} \tag{3-46}$$

$$V_{cq1} = -Ri_{cq} - L\frac{di_{cq}}{dt} - \omega_e L i_{cd} + 0 \tag{3-47}$$

Hence, the d-axis and q-axis reference voltages (V_{cdref}, V_{cqref}) for GSC current control can be expressed as

$$V_{cdref} = PI(i_{cd} - i_{cdref}) + feedforward\_term \tag{3-48}$$

$$V_{cqref} = PI(i_{cq} - i_{cqref}) + feedforward\_term \tag{3-49}$$

where PI is the proportional and integral gain.

The feed forward terms provide more accurate transient voltage compensation, and result in reducing transient current both in general operation and fault condition. Finally, these d-q axis reference voltages will be converted to 3-phase frame to generate modulation indices for the GSC PWM converter. Fig. 3.14 shows the block diagram of GSC control.

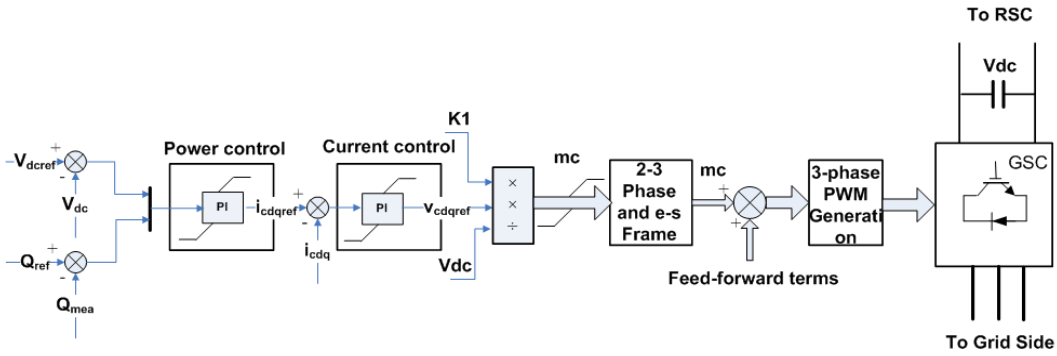

Fig. 3.14 Block diagram of GSC control

In order to offer preferable dynamic response to grid voltage dips, the feed-forward terms can be approximated as the stator voltage [39, 93]. To generate 3-phase PWM signals to drive the six-IGBT converter, the voltage demand needs to be scaled by using the index (K_1) and DC-link voltage (V_{dc}).

So the modulation index (m_c) for GSC is given by

$$m_c = K_1 * V_{cdqref} / V_{dc} \quad (3\text{-}50)$$

where $K_1 = ((2\sqrt{2}) * V_{rac} / \sqrt{3})$.

The ratio between DC and AC voltage of the grid side converter (see Fig. 3.13) is manipulated by the modulation factor in (3-50).

3.6 Rotor over-current protection

The stator windings of the DFIG are directly connected to the grid, while the rotor windings of the machine are connected to the grid through power electronic converters. During faults, high stator currents transfer from the stator to the rotor side of the DFIG because of the magnetising effect between stator and rotor. The resulting high currents can cause damage to the converter. In order to protect the converter from over-current, a so-called 'crowbar' is connected to short-circuit the rotor windings. When operating the crowbar, the PWM RSC controller is de-activated and will be reactivated after crowbar disengagement. The crowbar circuit consists of a three-phase diode bridge that rectifies the rotor currents and a single IGBT-diode parallel in series with a crowbar resistor(R_{cb}) as shown in Fig. 3.15.

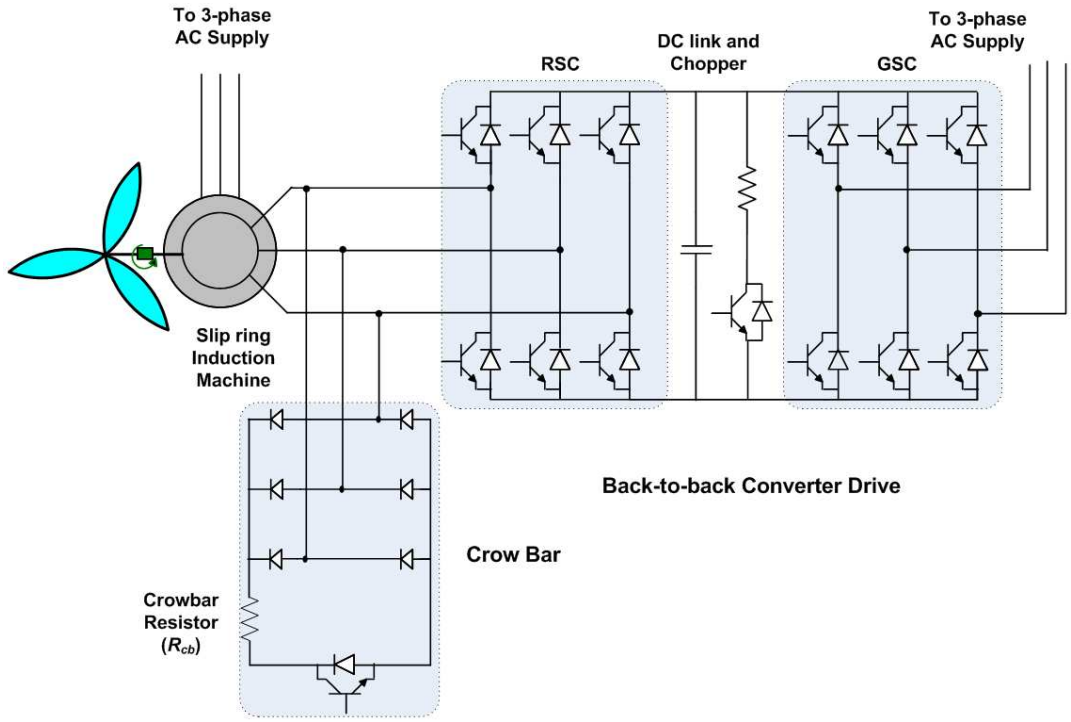

Fig. 3.15 A Crowbar and Converter Drive Circuit

The crowbar is required to protect the converter from high currents by shorting the rotor circuit to a crowbar resistor. In the meantime, an additional crowbar resistance to the rotor circuit helps the machine to reduce magnetisation more quickly, especially during fault conditions.

For DFIG fault-ride-through investigation, a switched rectifier bridge is represented by a three-phase y-connected resistor (R_{cb}') as shown in Fig. 3.16.

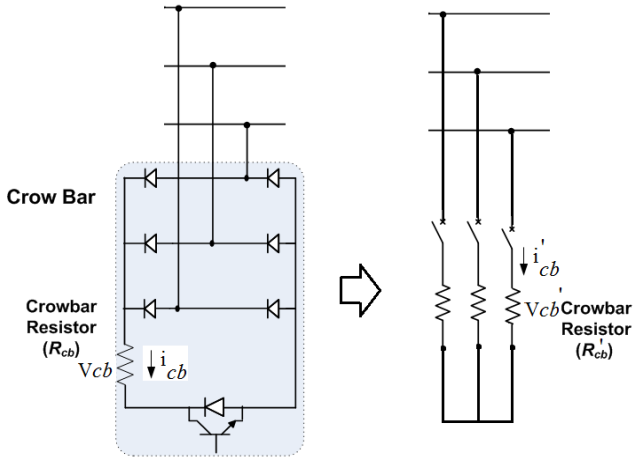

Fig. 3.16 A crowbar equivalent circuit

The crowbar equivalent circuit is connected between the rotor and RSC through a controllable breaker. The breaker is normally open but closed during the rotor over-current, typically over 2 pu. After the rotor circuit is short circuited by the crowbar resistor the rotor resistance will be increased as R_r + R_{cb}' where R_{cb}' = 0.55 R_{cb} as derived from the crowbar equivalent circuit by using the consumed power relationship of the crowbar resistor.

In an ideal rectifier circuit, an average DC voltage (Vcb) across the original crowbar is given by

$$Vcb = 1.35Vac \tag{3-51}$$

The power relationship between original and equivalent circuits can be expressed as.

$$Pcb = \frac{Vcb^2}{Rcb} = (1.35Vac)^2 . \frac{1}{Rcb} \tag{3-52}$$

While

$$Pcb' = \frac{3V'cb^2}{R'cb} = 3(Vac/\sqrt{3})^2 . \frac{1}{Rcb'} \tag{3-53}$$

Hence,

$$R'cb = \frac{1}{(1.35)^2} Rcb = 0.55Rcb \tag{3-54}$$

3.7 DC- brake chopper and DC-link

A DC-link brake chopper is used to prevent an over-voltage condition occurring on the DC-link, which is caused by transient rotor currents through diodes to the brake resistor when all of the IGBTs in RSC are turned off, thus protecting the converter. During grid faults DC-link voltage increases rapidly, and the brake chopper is automatically turned on/off whenever the DC-link voltage rises over/under its threshold value. For the DFIG FRT investigation, the DC brake chopper is represented by a resistor in series with an IGBT switch as seen in Fig. 3.17.

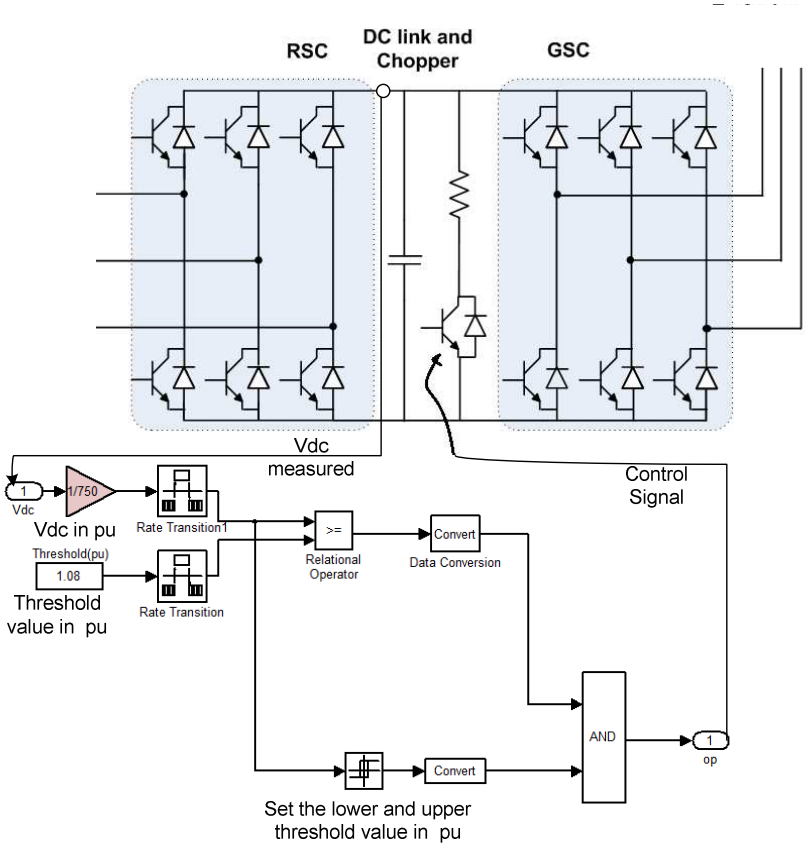

Fig. 3.17 A diagram of the brake-chopper control

While the DC-link voltage increases above the threshold value, the IGBT switch is triggered by the control signal resulting in the brake resistor operating. A diagram of the brake-chopper control signal is illustrated in Fig. 3.17.

The brake chopper is automatically set to operate above the upper threshold value of 810V (1.08pu) and to disconnect below the lower threshold level of 795V (1.06pu) with regard to the nominal DC-link voltage of 750V.

3.8 Line filter

The Line filter is connected between the GSC and the grid in order to prevent undesirable high frequency interference from PWM voltages generated by the inverter. The filter model consists of series R and L as shown in Fig. 3.18, and also the designed values are in Appendix A.

Fig. 3.18 Line filter

3.9 The grid supply and Fault

The grid supply is assumed to be an ideal stiff three-phase supply. In the DFIG model, the grid supply voltage is directly connected to the stator of the DFIG. For three-phase fault conditions, a magnitude and period of voltage dips can be set using the supply/fault profile block as shown in Fig. 3.19. The voltage vector is formed using the polar-to-cartesian block. After that the d-q component of voltage is transferred to a 3-phase voltage.

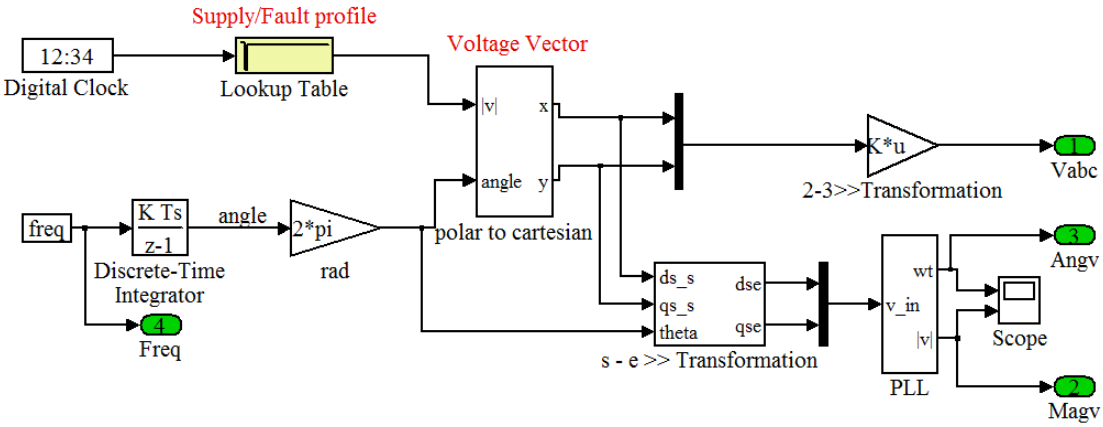

Fig. 3.19 The supply/fault model

3.10 Summary

In normal and fault conditions, the DFIG is operated at unity power factor: i.e. reactive power is zero. Active and reactive powers of the DFIG are independently controlled by PI controllers through RSC and GSC using a stator-voltage vector control method. Moreover, the generated active power of the DFIG is mainly controlled by the d-axis rotor current control while the d-axis GSC current is used to DC-link voltage control as illustrated in Fig. 3.20.

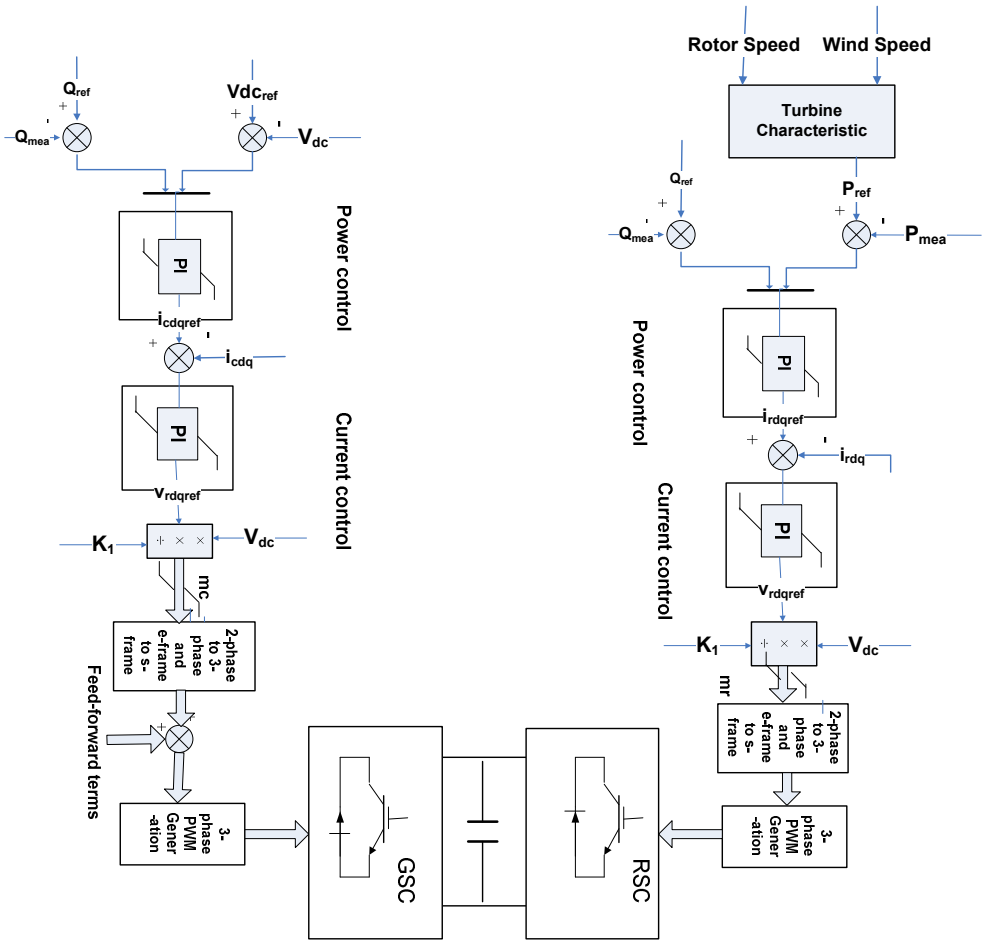

Fig. 3.20 Block diagram for RSC and GSC vector control scheme

In general operation, electrical power is supplied from the stator to the grid regardless of the speed slip. On the rotor of the DFIG, electrical power is supplied from the rotor to the grid at super-synchronous speed operation and absorbed by the rotor at sub-synchronous speed operation. For RSC, to control torque and active power, both optimum torque and power and speed curves are used to operate controllers. The generator speed is adjusted by controlling torque according to the torque-speed curve

while the active power is controlled by following with the electrical power-speed curve. To obtain the active power, the active power reference from the power curve is used to control the d-axis rotor current in the stator-voltage vector reference frame as mentioned in (3-29). The reactive power reference is set by the power factor demand, and also controlled by the q-axis rotor current in stator-voltage vector reference frame as mentioned in (3-30). For GSC, to control DC-link voltage and reactive power the DC-link voltage is controlled by the d-axis grid side converter current as mentioned in (3-44) while the reactive power is controlled by the q-axis grid side converter current as mentioned in (3-45).

In stator-voltage vector control, both stator and rotor quantities are transformed to d-q components in the reference frame which rotates at the same angular frequency of stator-voltage space vector. So the d-axis of the reference frame is aligned to the stator-voltage vector. The d-q axis rotor current reference and d-q grid converter current reference from the two controllers is independently used to provide the pulse width modulation factors for RSC and GSC (see Fig. 3.20). For the DFIG system model, all components are connected as illustrated in Fig. 3.1. Back-to-back converters with DC-link and chopper (see Fig. 3.15) and Line filter (see Fig. 3.18) are modelled using the Power System Block-set (PSB) found in Matlab/Simulink. For the mechanical and drive train (see Fig. 3.3), generator (see Fig. 3.8), supply/fault (see Fig. 3.19) and control system, they are built using standard Simulink Blocks. The crowbar is represented by an equivalent circuit (see Fig. 3.16). Moreover, machine, grid and converters are connected to each other using controlled voltage and current sources. The complete model for the simulations is shown in Fig. 3.21, and the detailed Simulink diagrams of DFIG System Model can be found in Appendix D.

Finally, some simulated results of 15% retained voltage lasting 500ms using the developed DFIG model are compared with experimental results as shown in Fig. 3.22 and will be discussed in section 4.2. More details of the model verification will be described in Chapters 4 and 5.

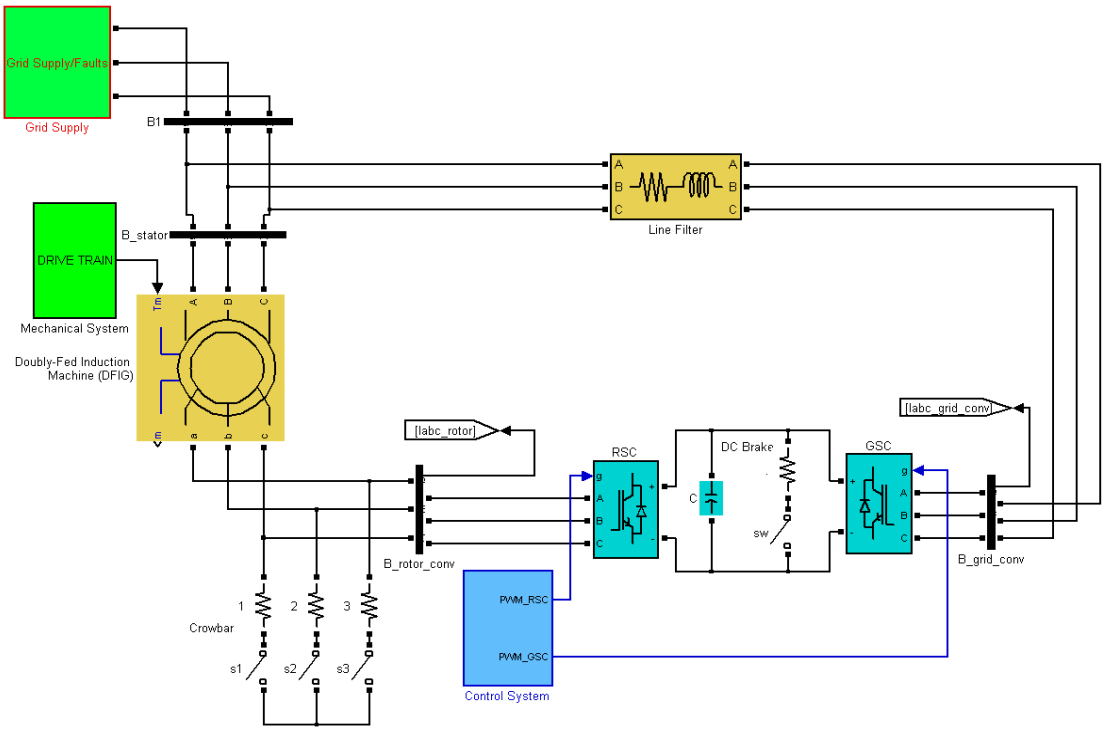

Fig. 3.21 A diagram of the completed model of the DFIG system

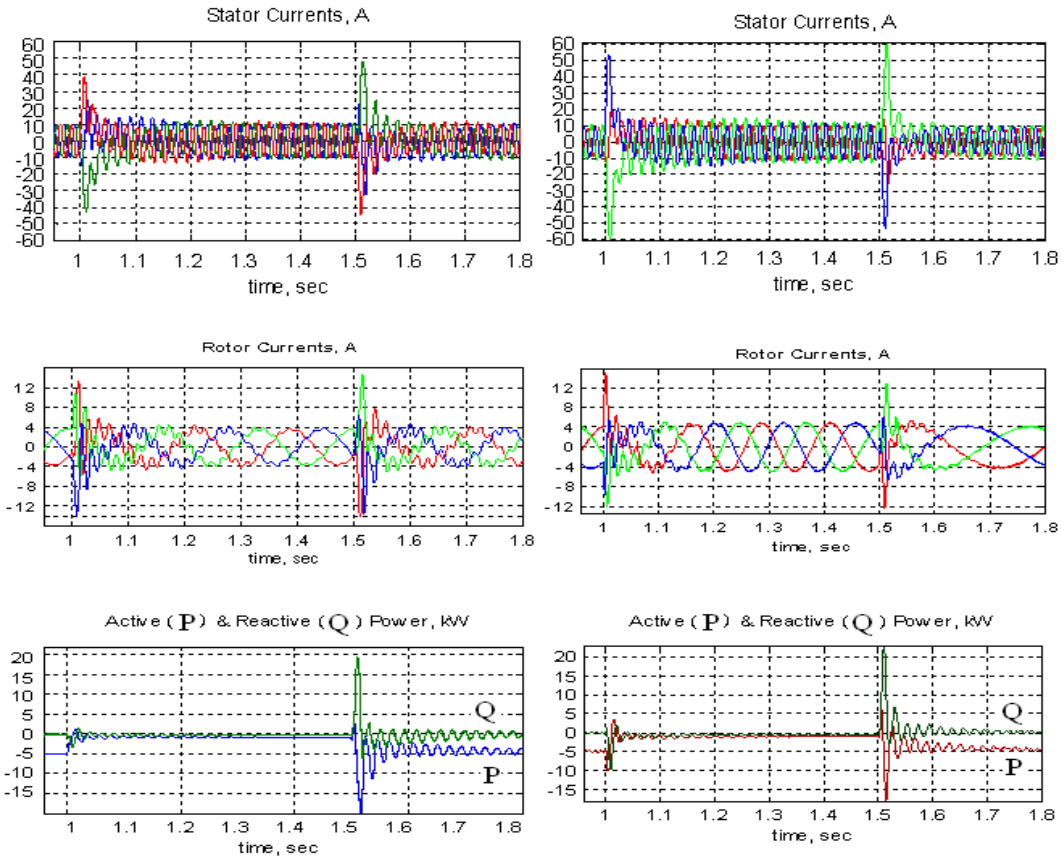

Fig. 3.22 Simulation (left side) and experiment (right side) wave forms for three phase faults at 15% of retained voltage lasting 500ms

Chapter 4 Verification of the model during healthy and faulted operating conditions

The behaviour of a wind turbine differs depending on the operating point. DFIGs commonly use two different control regimes, as mentioned in Chapter 2: first for optimal power production at low wind speeds, and the other for rated and maximum rotor speed conditions in high wind speed regions [47, 94]. In order to ensure the robustness of the model, the validation should at least cover tests for the two operating modes in the operational speed range. Four cases are considered in low and high speed conditions during normal operation, and three more cases in high speed conditions during fault conditions. Furthermore two cases of crowbar and DC-link chopper methods are verified. Finally a comparison between simulation and experimental results is made.

4.1 Initialisation of the DFIG model verification

The wind acting on a rotor wind turbine is very complex and includes both deterministic effects and stochastic variations due to turbulence, hence the need for an average wind speed [95] which is a constant value. For a verification of the model during normal operating and fault conditions, wind speeds are assumed to have constant value. As mentioned in Section 3.1, an average wind speed is typically about 10 m/s at which the DFIG generates 0.67 pu power output.

The DFIG model was validated using a laboratory test rig comprising four main elements: a grid fault emulator, a 10kW DC machine as a wind turbine simulator, a 7.5kW, 415V, 50Hz, four-pole DFIG machine and a control hardware assembly [96]. A dSpace dS1103 controller is used to communicate between the DFIG controller, wind turbine simulator, converters, DC motor and DFIG. The controller is activated in real time through a GUI designed using Control Desk software. The controller was developed using Matlab/Simulink and the code built for operation on the dSpace control board [96]. Details of the test rig can be obtained from [39].

A photograph of the laboratory DFIG test rig, a schematic diagram of the laboratory DFIG system and Grid fault emulator and switching sequence diagram are shown in Fig. 4.1, Fig. 4.2 and Fig. 4.3, respectively.

Fig. 4.1 DFIG test rig

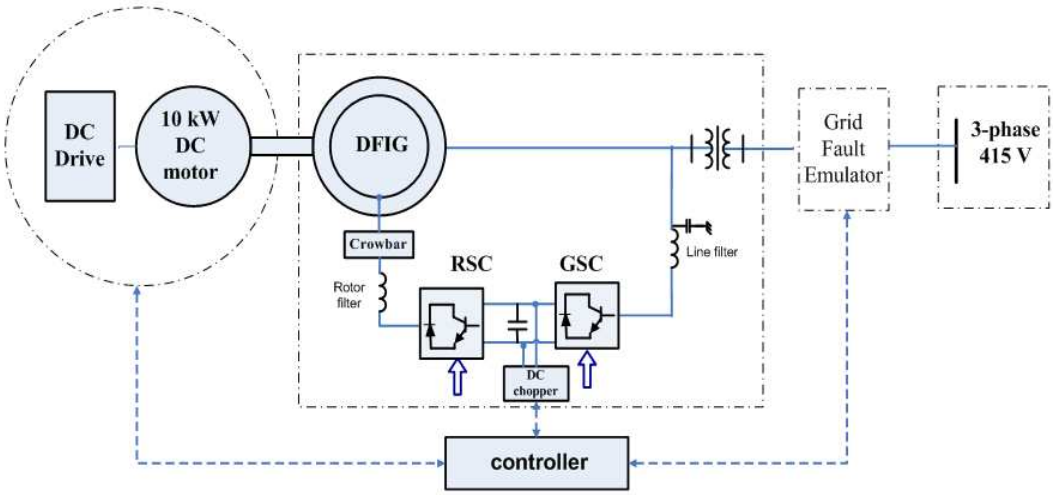

Fig. 4.2 Schematic diagram of the DFIG test rig

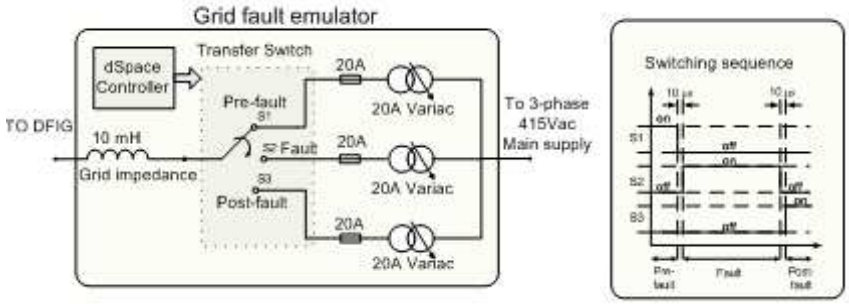

Fig. 4.3 Grid fault emulator and switching sequence diagram

The grid fault emulator was produced to apply balanced, rectangular grid fault voltage profiles of the specified grid code. Three independent voltage levels (pre-fault, fault and post-fault) were prepared in parallel on three of three-phase variacs. The three variac outputs were connected by a set of back-to-back IGBT transfer switches controlled from the dSpace control board. A fault test was performed by switching the voltage applied to the generator from one variac source to the next in sequence: from ‘pre-fault’ to ‘fault’ and then to ‘post-fault’ as required.

4.2 Verification of the model during normal operation

In verifying the DFIG model, it is assumed that the stator voltage (V_s) is always 1 pu. (or 340 Vpeak). A comparison between simulation and experimental stator voltages can be shown in Fig. 4.4.

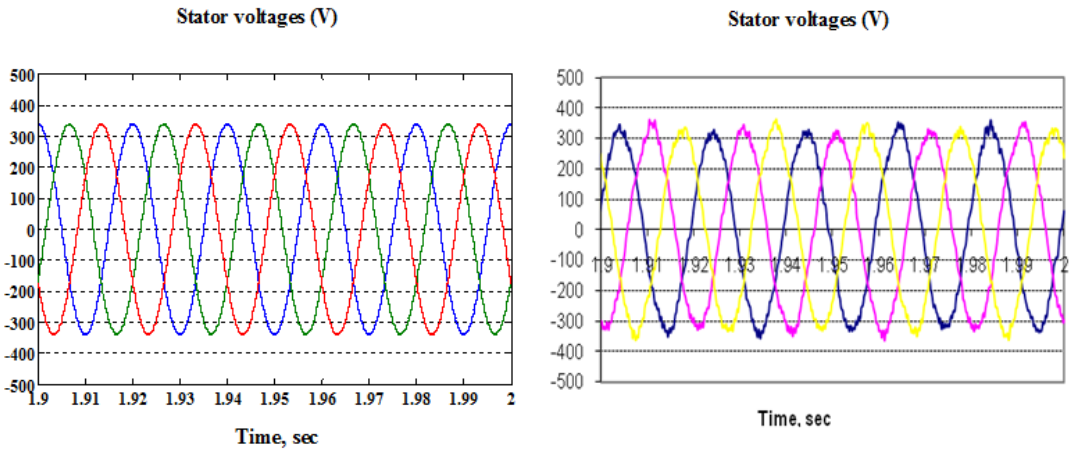

(a) Simulation (b) Experiment

Fig. 4.4 Stator voltage waveforms

Four cases are examined. The stator active power (P_s), DFIG speed (ω_r) and the stator voltage (V_s) are defined as shown in Table 4.1 while the stator reactive power (Q_s) is set to zero.

Table 4.1 Four cases of the normal operations

Case	Stator Active Power (pu)	Speed (pu)	Mode of operation
1	0.22	0.95	Sub-synchronous
2	0.12	1.03	Super-synchronous
3	0.22	1.02	Super-synchronous
4	0.37	1.02	Super-synchronous

First the DFIG supplies stator active power (Ps) of 0.22 pu at a sub-synchronous speed of 0.95 pu. Second, generating slightly less power of 0.12 pu with a super-synchronous speed of 1.03 pu is verified while in the third, more power is shown in mode of a super-synchronous speed of 1.02 pu. Finally 37% of power supplies to the grid at the same speed of 1.02 pu. For each case to be verified, the resulting simulated and measured stator currents, rotor currents, active and reactive powers are compared as follows.

Case I: Ps 0.22 pu at a speed of 0.95 pu

While operating at a speed of 0.95 p.u. (5% below synchronous) and generating 1.65kW (0.22 pu) at unity power factor, the resulting simulated and measured stator currents, rotor currents, and active and reactive powers are shown in Fig. 4.5. The experimental stator current waveforms show that more harmonics occur in comparison with the simulation while the latter shows a small difference in peak value of about 0.1A. Moreover, the simulated stator currents show that there are more ripples than the measured currents. For rotor currents, both simulation and experimental results show a similar rotor frequency of approximately 2.5 Hz which is slip times the stator frequency but a small difference in magnitude of 0.2A. Finally the simulated active and reactive powers contain more ripple than the experimental case because of controller tuning. However, the average value of active and reactive power magnitude of both waveforms is very similar.

Case II: Ps 0.12 pu at a speed of 1.03 pu

While operating at a speed of 1.03 pu (3% above synchronous) and generating 0.9kW (0.12 pu) at unity power factor, the resulting simulated and measured stator currents, rotor currents, and active and reactive powers are shown in Fig. 4.6. For stator currents, there is good agreement between simulation and experiment with a peak value of 1.77 A (0.12pu) and a frequency of 50 Hz. The stator current waveforms contain high frequency harmonics caused by the transmission of rotor harmonics into the stator. Further, the experimental waveforms show that more harmonics occur in comparison with the simulation because some damage to line filters or electronic equipment could occur after numerous tests. For rotor currents, both experimental and simulation waveforms have a similar frequency of 1.5 Hz but a small difference of about 0.4 appears in the peak value. For active and reactive powers, both simulation and experimental waveforms are in close agreement.

Case III : Ps 0.22 pu at a speed of 1.02 pu

While operating at a speed of 1.02 p.u. (2% above synchronous) and generating 1.65kW (0.22 pu) power at unity power factor, the resulting simulated and measured stator currents, rotor currents, and active and reactive powers are shown in Fig. 4.7. For stator currents, the experimental waveforms show that more pronounced harmonics occur in comparison with the simulation because some damage to line filters or electronic equipment could occur after numerous tests. However, there are fewer harmonics than

in the previous cases, because the DFIG is controlled to generate more power to the grids.

Other simulation waveforms in comparison with experiment are obviously similar, i.e. the rotor currents show a similar frequency of 1 Hz and a magnitude of 2 A. For active and reactive power, both experimental and simulation waveforms are similar.

Case IV: Ps 0.37 pu at a speed of 1.02 pu

While operating at a speed of 1.02 p.u. (2% above synchronous) and generating 2.78kW (0.37 pu) at unity power factor, the resulting simulated and measured stator currents, rotor currents, and active and reactive powers are shown in Fig. 4.8. The stator currents show a similar frequency of 50 Hz but a slight difference in magnitude of 5A. Rotor currents are very close agreement with a frequency of 1Hz and a peak value of 2.4A in both simulation and experiment. Finally, active power of 2.78kW (0.37pu) at unity power factor produced by the DFIG are in very good agreement between simulation and experimental waveforms.

4.2.1 Summary

The comparisons of simulation and experiment waveforms of four study cases in both sub- and super-synchronous modes show general good agreement. The experimental waveforms of stator currents show that more harmonics occur in comparison with the simulation because some damage to line filters or electronic equipment could occur after numerous tests. Stator current waveforms show less harmonics when the DFIG is generating more active power. These harmonics are caused by PWM switching on the rotor side. The simulation and measurement of rotor currents also are in good agreement, with frequency correctly related to machine slip. Active and reactive powers are similar in simulation and experimental results.

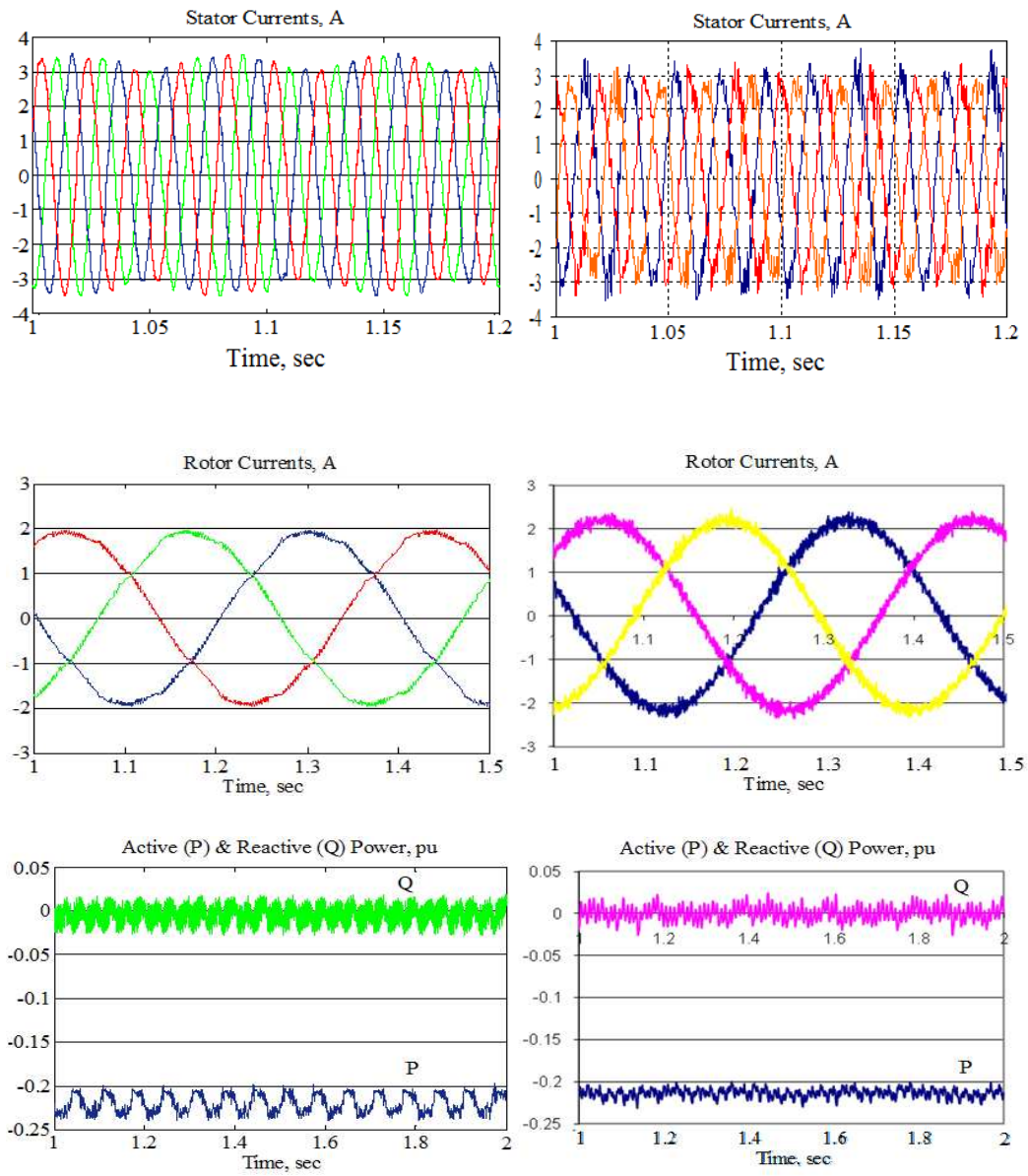

(a) Simulation (b) Experiment

Fig. 4.5 Waveforms for the normal healthy steady-state operation; Ps = 0.22 pu, speed = 0.95 pu

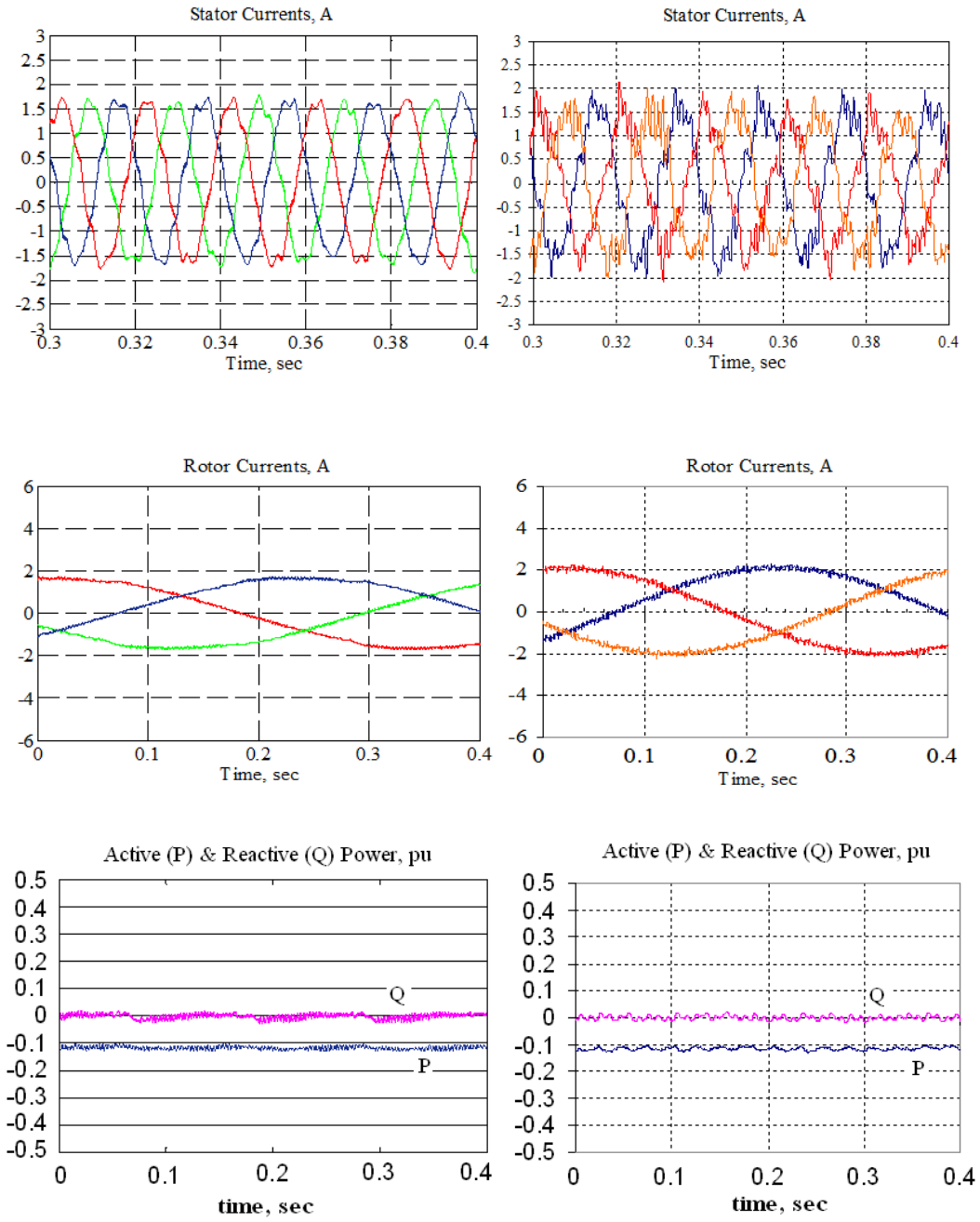

(a) Simulation (b) Experiment

Fig. 4.6 Waveforms for the normal healthy steady-state operation; Ps = 0.12 pu, speed = 1.03 pu

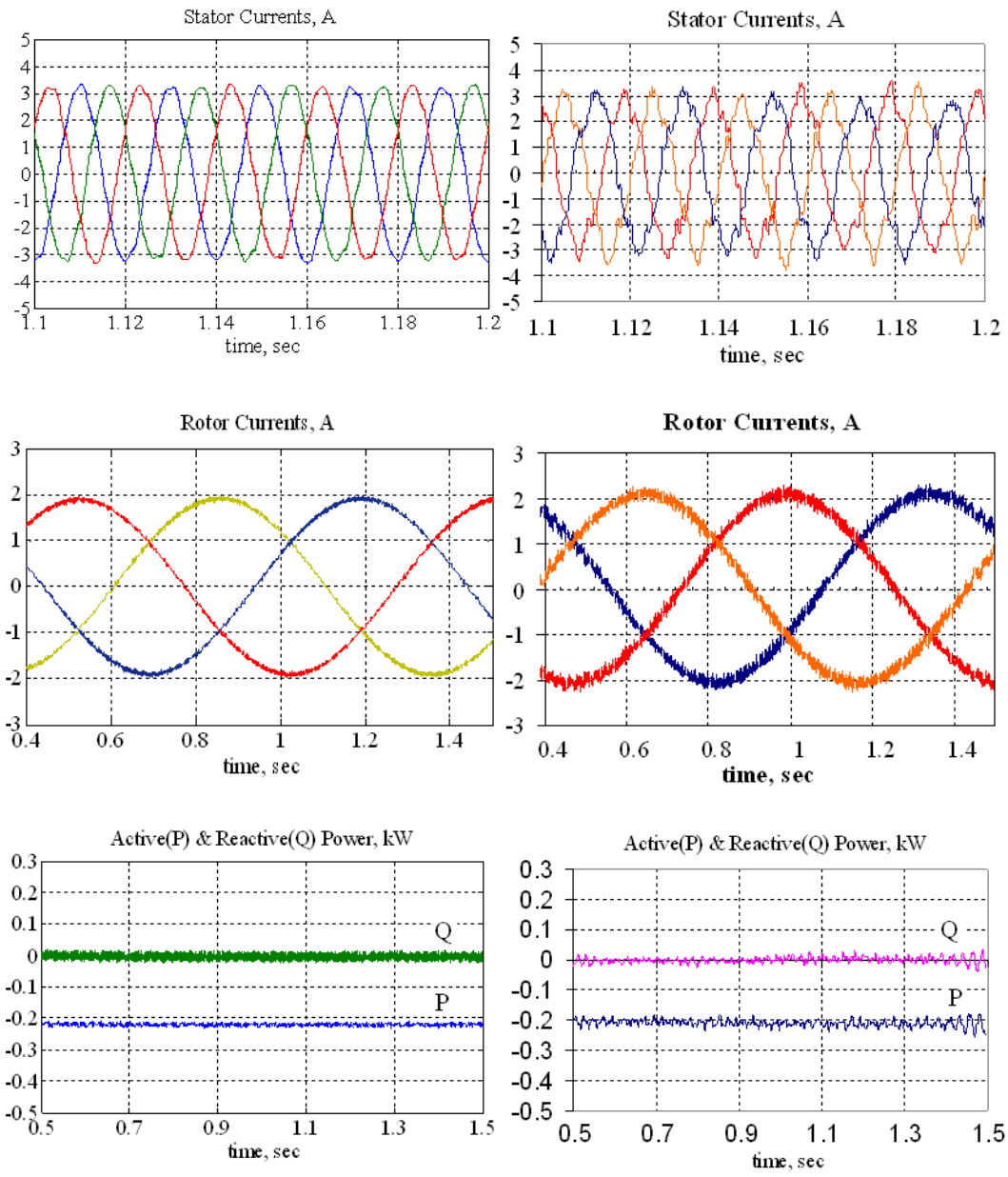

(a) Simulation (b) Experiment

Fig. 4.7 Wave forms for the normal healthy steady-state operation; Ps = 0.22 pu, speed = 1.02 pu

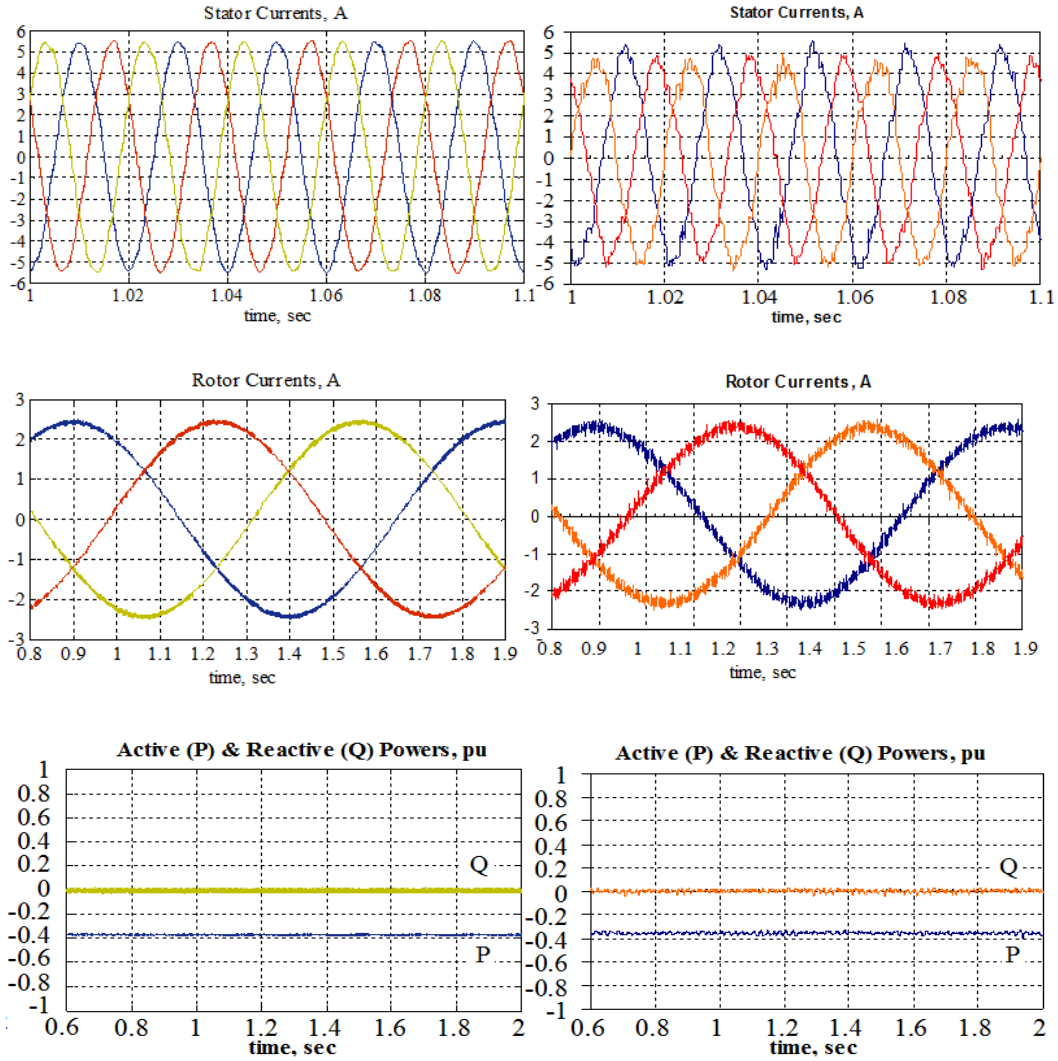

(a) Simulation (b) Experiment

Fig. 4.8 Wave forms for the normal healthy steady-state operation; Ps = 0.37 pu, speed = 1.02 pu

4.3 Verification of the DFIG model during fault conditions

In verifying the model under three-phase faults, the stator voltages are defined as a nominal value of 1 pu. The various stages of a grid fault event are defined in Fig. 4.9. The period occurring before fault initiation is called ‘pre-fault’ or ‘healthy volts’ period. This is followed by the ‘during fault’ period which occurs after the fault initiation event. Finally the period after fault clearance is defined as ‘post-fault’ or ‘recovery volts’ period.

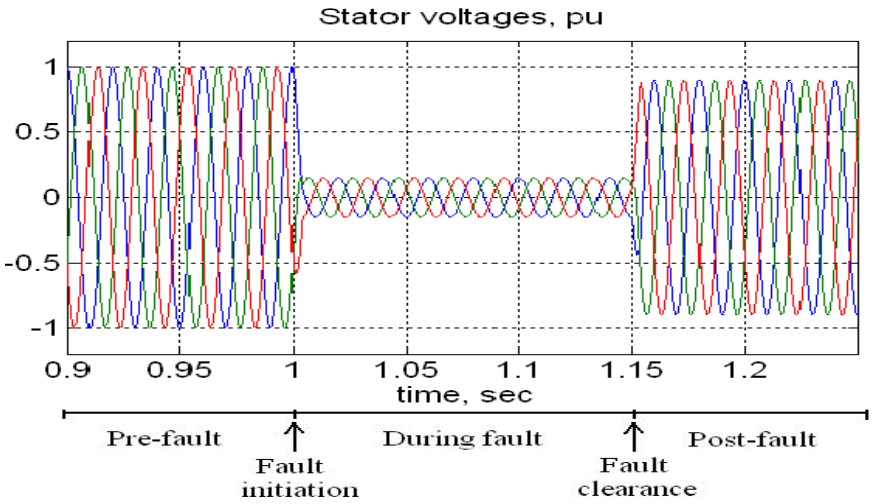

Fig. 4.9 Simulated balanced 3-phase voltage fault

Three fault scenarios of the DFIG model will be verified as shown in Table 4.2.

Table 4.2 Three cases of the fault scenarios

Case	Fault Voltage (pu)	Fault duration (sec)	Voltage Recovery (pu)
1	0	0.14	0.9
2	0.15	0.50	0.9
3	0.5	0.71	0.9

NB. All fault scenarios start at time of 1 sec.

Cases 1 and 3 for retained voltage at 0 and 50% respectively are chosen from GB grid code, while case 2 for 15 % retained voltage lasting 500ms is chosen from FRT requirements of the Irish grid code because they allow a greater duration than do the GB and German codes [4]. For recovery voltage, 90% of typical grid voltage remains after fault clearance.

In normal and fault conditions, the DFIG is operated at a speed of 1.12 pu and generates 5kW (0.67 pu) at unity power factor; i.e. reactive power is zero. Hence, both the PI controllers of the RSC and the GSC try to produce zero reactive power demand. The PI controllers of RSC try to produce the DFIG active power demand, while those of GSC maintain the desired DC-link voltage. During grid voltage dips the active power output

should be at least in proportion to the retained balanced voltage at the grid entry point, and the restoration of the voltage at least 90% of the nominal pre-fault level. Since the DFIG test rig generated considerable difficulty when carrying out the experiment, experimental results of the DFIG test rig are provided by [39] which was tested. Comparisons between simulation and experimental results of three cases are summarized in the following.

Case I: A 3-phase grid retained voltage of 0 pu

The applied fault is a 3-phase grid voltage dip from a normal voltage (1pu) to a fault voltage of 0pu. This fault is initiated at a time of 1s and is cleared at a time of 1.14s. The results are shown in Fig. 4.10.

Case II: A 3-phase grid retained voltage of 0.15 pu

Compared with the previous case this scenario envisages a voltage dip from normal (1pu) to a fault voltage of 0.15pu. The difference is that the clearance time is 0.5s. The results are shown in Fig. 4.11.

Case III: A 3-phase grid retained voltage of 0.50 pu

In contrast with the previous two cases, there is a voltage dip from normal (1 pu) to a fault voltage of 0.50 pu. The initiation time is 1s in this case and a clearance time of 1.71s. This is illustrated in Fig. 4.12.

The simulated and measured results of stator currents, rotor currents, active and reactive powers are shown in the following waveforms.

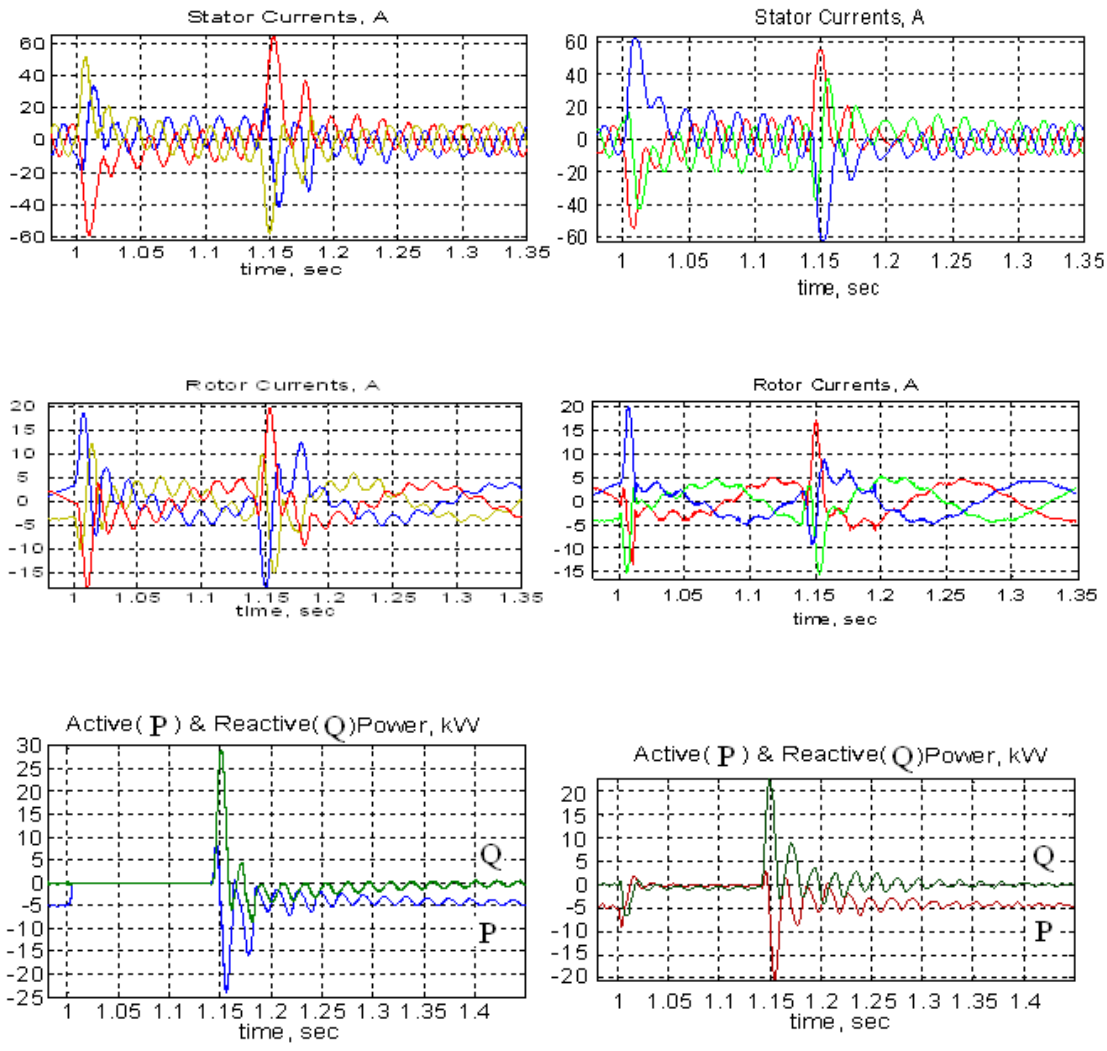

(a) Simulation (b) Experiment

Fig. 4.10 Waveforms for three phase faults; Fault voltage = 0 pu, Fault duration = 0.14 sec

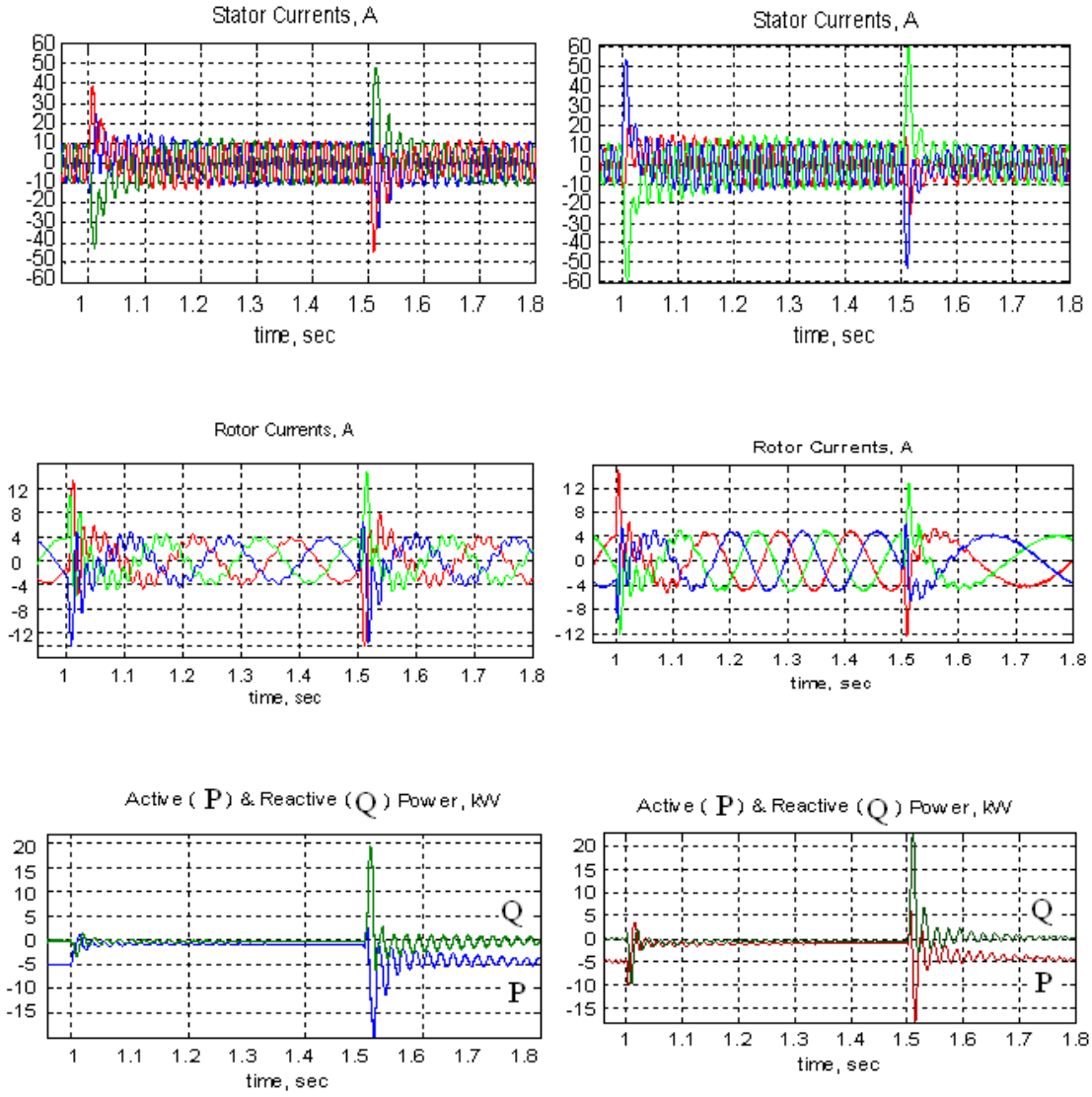

(a) Simulation (b) Experiment

Fig. 4.11 Waveforms for three phase faults; Fault voltage = 0.15 pu, Fault duration = 0.5 sec

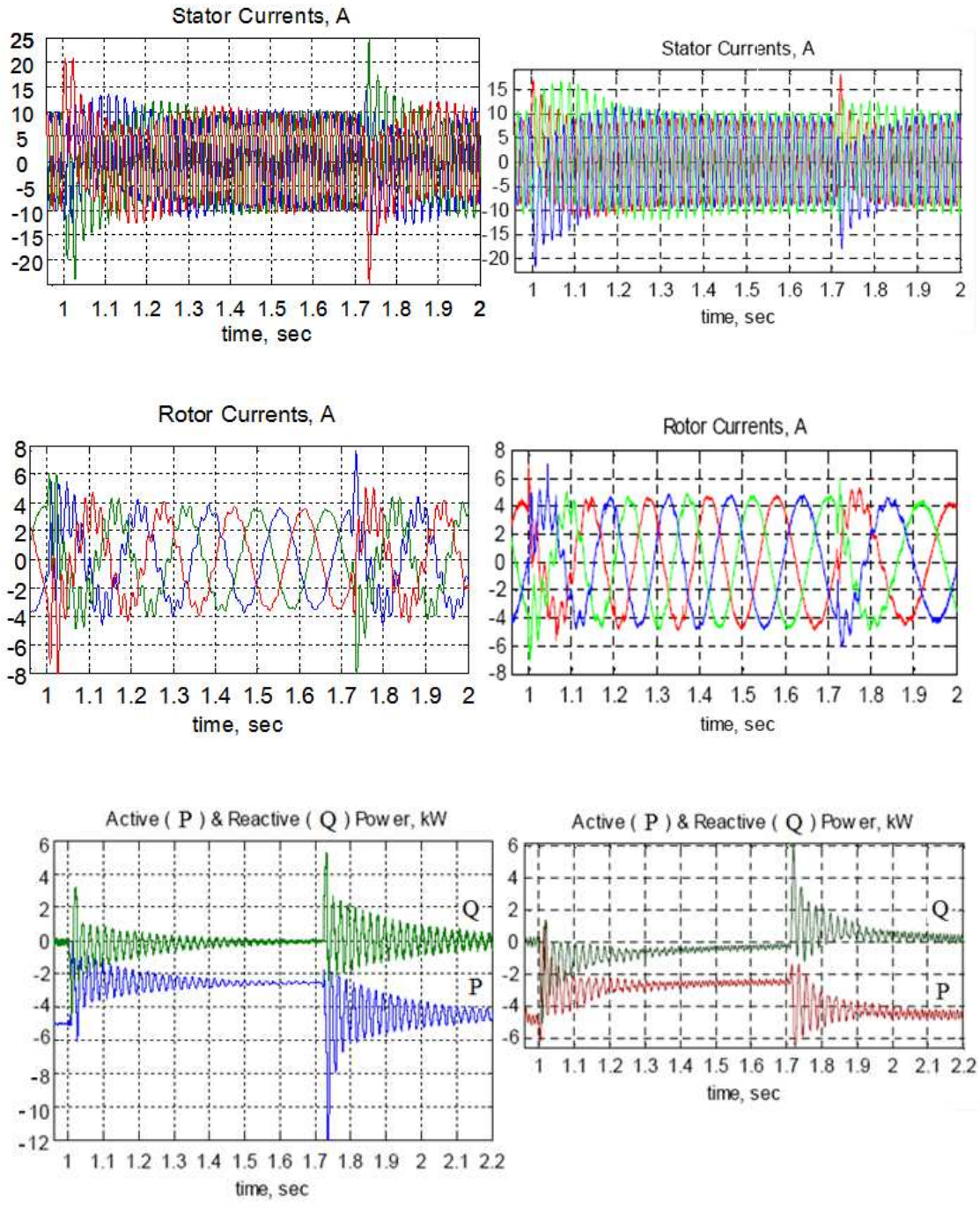

(a) Simulation (b) Experiment

Fig. 4.12 Waveforms for three phase faults; Fault voltage = 0.5 pu, Fault duration = 0.71 sec

4.3.1 Summary

Both simulation and experimental results of the three case studies are in reasonably good agreement. From stator and rotor peak currents in Fig. 4.11, Fig. 4.11 and Fig. 4.12, comparisons are drawn in the following table:

Table 4.3 Comparisons of absolute peak currents between simulation and experimental results during fault initiation and clearance

Case	**Absolute peak Stator current, |Is|**		**Comment**	**Absolute peak Rotor current, |Ir|**	
	Simulation	**Experiment**		**Simulation**	**Experiment**
1	60A (4.0pu)	60A (4.0pu)	Initiation	17.5A (3.7pu)	20A (4.2pu)
	60A (4.0pu)	60A (4.0pu)	Clearance	20A (4.2pu)	17.5A (3.7pu)
2	42A (2.85pu)	60A (4.0pu)	Initiation	14A (2.96pu)	14A (2.96pu)
	48A (3.25pu)	60A (4.0pu)	Clearance	14A (2.96pu)	14A (2.96pu)
3	22A (1.49pu)	22A (1.49pu)	Initiation	7A (1.48pu)	7A (1.48pu)
	25A (1.69pu)	18A (1.22pu)	Clearance	8A (1.69pu)	6A (1.27pu)

During fault initiation and clearance, stator and rotor currents transients reach a maximum value of 60A (4pu) and 20A (4pu), respectively. When the spike transient is on the rotor side, the power electronics devices (IGBTs and Diodes) inside the RSC risk being damaged and normally the RSC would trip on the over-current condition. Moreover, the current spikes are proportional to the voltage drop in each case: Case I with retained voltage at 0V, the peak is assumed to reach approximately 100% at 4pu while in cases II and III of 15% and 50% retained voltage the peaks appear lower at roughly 75% and 37%, respectively. At 50% retained voltage, both simulation and experimental results show gentler fault behaviour of both the stator and rotor currents where there is no need for fault ride through protection.

4.4 Verification of the FRT capability of the DFIG model using crowbar and DC-link brake methods

For fault ride-through requirements, a crowbar is generally used in the DFIG [25, 37, 97-102] while a DC-link brake chopper is either additionally [25, 28, 100, 103] or alternatively [39] used to support the FRT capacity. In this section the model with each FRT device is investigated and compared with the experimental results of crowbar and DC-link brake methods. Since the DFIG test rig proved considerably difficult when carrying on the experiment, experimental results of the DFIG test rig are provided by [39] which was tested.

4.4.1 Crowbar method

A crowbar is used to protect the converter. When the crowbar is operated, the rotor circuit connects to the crowbar resistor instead of the converter. In the test rig, the crowbar consists of a three-phase diode rectifier, an IGBT switch and a resistor. The equivalent circuit is represented by a three-phase resistor as shown in Chapter 3 (Fig. 3.16). The switch is triggered when the magnitude of the rotor current reaches a threshold value, which is generally twice the rated current.

In normal operation the crowbar is disconnected from the DFIG. During grid faults the FRT device connects to the rotor winding of the machine, thus diverting the current away from the converter to the crowbar resistor. The device helps to release the energy stored in the magnetic field of the machine from the rotor winding to the designed resistor. The crowbar activation is controlled by switching on an IGBT when the rotor over-currents reach a threshold value. Traditionally, the crowbar is engaged to completely demagnetise the rotor [28, 37, 92, 101, 104] and is typically activated for approximately 120ms. Because of this long period, the RSC control is deactivated and the DFIG is converted to a singly-fed induction machine which consumes reactive power, thus not supporting voltage during a grid fault. The result is obviously unsatisfactory for FRT grid requirements.

Investigation of the crowbar activation period:

In this investigation concerning full demagnetisation, the activation period of 120ms is designated as a timed crowbar operation and a 25Ω, 0.6kW crowbar resistor chosen to reduce the rotor time constant to ¼ of the original machine's value. The crowbar is removed when the magnitude of the dq-axis rotor current exceeds the threshold value

and the rotor-side PWM controller is immediately restarted with zero current to the rotor circuit connection.

Crowbar test condition: As mentioned in 4.4.1, the crowbar is activated and the RSC PWM switching is stopped (all IGBTs 'OFF'), when the magnitude of the rotor current exceeds 2pu. The rotor current and power PI controllers are reset to zero output while the GSC controllers continue operating. After 120ms, the crowbar is deactivated. If the rotor current remains over 2pu, the crowbar is re-engaged for another 120ms. When the crowbar is disconnected, the RSC PWM and rotor current PI control are immediately restarted. After 40ms delay, which is an acceptable period to lose power control [92], the power PI control starts operating; noting that before the power PI control is resumed the change rate of the rotor current reference value is limited at1.5 pu/s to secure current control stability.

The active power was set to -0.67pu (5kW) generation at unity power factor with the DFIG operating at the rated speed of 1.12 pu (pre-fault). Comparison between the simulation and experimental results is shown in Fig. 4.13.

Discussion: During the fault, the DFIG generates reduced active and reactive power and loses control for 120ms after fault clearance. As a result, high active power production and high reactive power consumption above 50% appear in this period (see Fig. 4.13) while stator over-currents are produced. The simulation results appear promising when compared with the experimental results. Rotor currents measured between crowbar and rotor-side converter are instantly reduced to zero during the initiation and clearance periods when the crowbar is activated to connect the crowbar resistance across the rotor circuit as shown in both simulation and experiment. During those periods the peak rotor current is below 2pu (9.5A). The effect of the crowbar operation prevents the RSC from high over-currents. After 120ms the power control is resumed and delivers active power of 0.9pu at unity power factor. Failing to satisfy FRT requirements after fault initiation and clearance, the generator must resume active and reactive power control immediately in order to minimise mechanical and electrical problems such as mechanical stress on the machine shaft and voltage collapse of the grid.

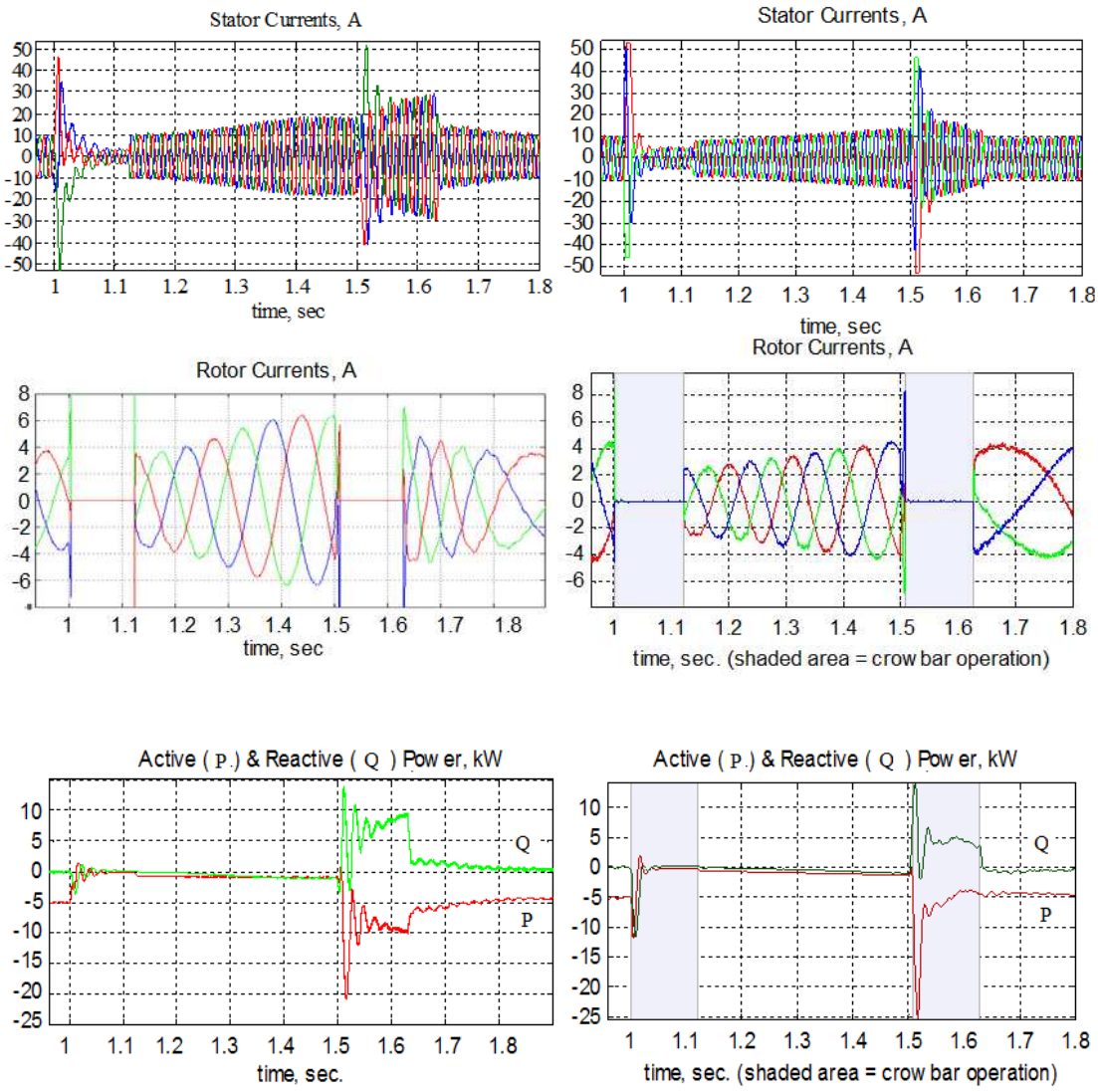

a) Simulation b) Experiment

Fig. 4.13 Results in case of crowbar activation period of 120ms

4.4.2 DC brake chopper method

The DC-brake chopper is used for the DC-link voltage protection. When the DC-link voltage rises above a threshold value, the chopper circuit is engaged by IGBT switching control. A diagram of the DC-brake chopper modes can be seen in Fig. 4.14.

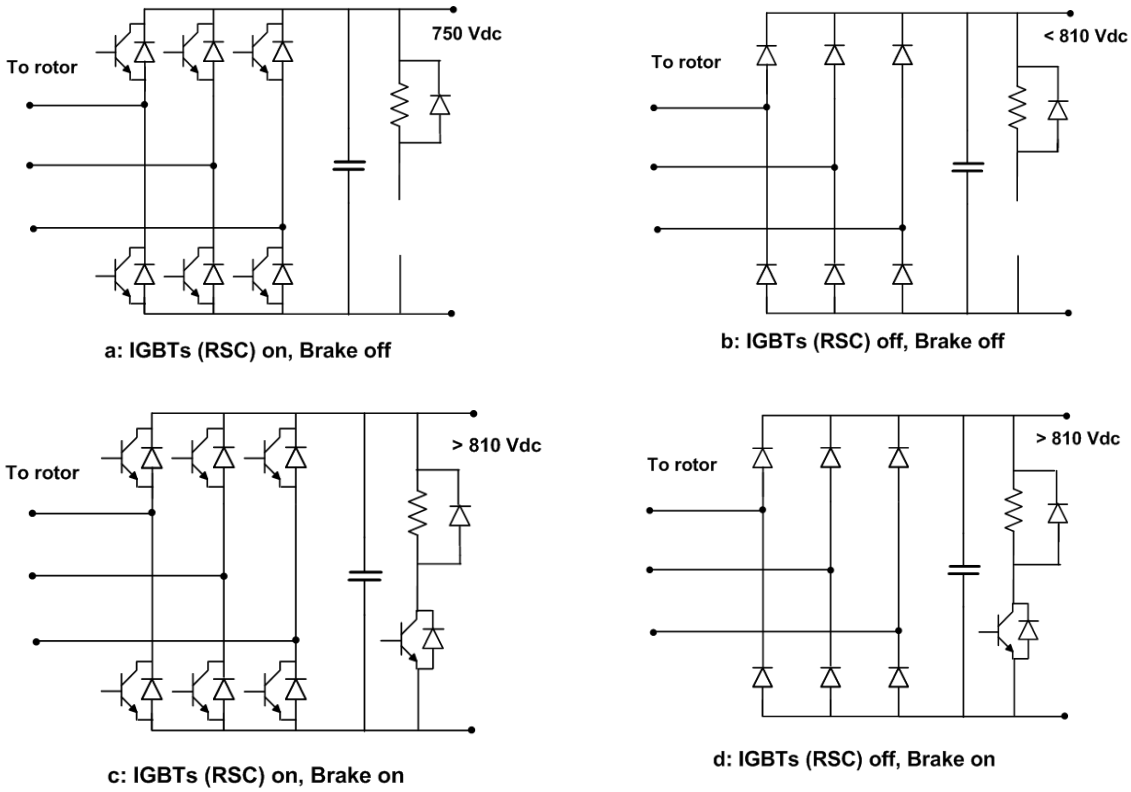

Fig. 4.14 DC-brake chopper operation modes

In normal operation, the DC-brake chopper is off as shown in Fig. 4.14a. There are two modes, illustrated in Fig. 4.14c and Fig. 4.14Fig. 4.14d, during a DC-brake operation. During grid faults, rotor currents flow into the DC-link resulting in a rapid voltage rise. If the DC-link voltage rises above a threshold value of 1.08 pu (810Vdc), the brake chopper will be engaged, as illustrated in Fig. 4.14c. To protect the converter from over-currents, all IGBTs of the RSC are switched-off; however, the currents still continue to flow through the anti-parallel diodes as shown in Fig. 4.14b. When the DC-link voltage reaches a pre-set threshold value, the brake chopper is engaged as shown in Fig. 4.14d. After application of the DC-brake chopper, the voltage is decreased and remains below the lower threshold, whereupon the brake chopper will be disengaged; for example in the test rig, the lower level is set at 795Vdc. All IGBTs in the RSC can resume switching when the rotor current returns to a safe, pre-defined level.

Investigation of the DC-brake chopper control delay:

For the DC-link brake test (no crowbar), the RSC's anti-parallel diodes are overrated to accommodate the maximum rotor over-currents. The DC brake chopper is independently operated by its own controller using a DC-link voltage measurement. As

mentioned above, the DC-brake chopper is turned on at 810V and off at 795V. As with the crowbar method, when the measured rotor current magnitude reaches the threshold value of approximately 2pu the rotor-side PWM is turned-off, i.e. all IGBTs are switched off. The period when the rotor PWM is turned off and vector control is temporarily stopped is defined as the rectification period. During this period rotor currents are flowing through the anti-parallel diodes in the rotor side converter.

DC-link brake test condition: A 15% fault is applied to the DFIG at t=1 sec. When the magnitude of the rotor current exceeds 2pu, the RSC PWM switching is stopped (all IGBTs 'OFF'). The rotor current and power PI controllers are reset to zero output while GSC controllers are allowed to continue operating. When the rotor current decreases to below 2pu, the PWM reactivation delay is set at 20ms. After 20ms which is acceptable [92], the rotor-side PWM is restarted with only current control using the interim current reference from the equation [39] below.

$$i^{e*}_{r} \text{ (interim ref)} = [-1.00P_{ref} + 0.64|V_s|j]$$

where P_{ref} is stator active power (pu) and $|V_s|$ is a magnitude of stator voltage(pu)

The power control resumption is delayed for a further 20ms to allow the current controller to settle. Comparison between simulation and experimental results is discussed in the following.

Discussion: Before fault initiation the DFIG is operated at 12% above synchronous speed (1.12pu). Fig. 4.15 shows a comparison between simulation and experimental DC-link, stator current and rotor current waveforms, generated active and reactive power and rotor speed.

The DC-link voltage is kept under 870Vdc for simulation and 850Vdc for experiment on either fault initiation or clearance. In both cases the brake resistor was operated above 810V. After 33ms the transient over-currents reduce and the DC-link brake cuts the voltage down to 810V. Similarly, at fault clearance a peak of 850V was cut down to 810V. While the brake chopper was operated, the grid–side converter had been operated and controlled the DC-link voltage back to 750V within 300ms after fault clearance. The results show more oscillation in the simulation than in the experiment because of the difference in the rotor speed. The stator current dc component gradually decreases,

and takes a longer time than the rotor currents because the effective stator time constant is longer than the rotor time constant.

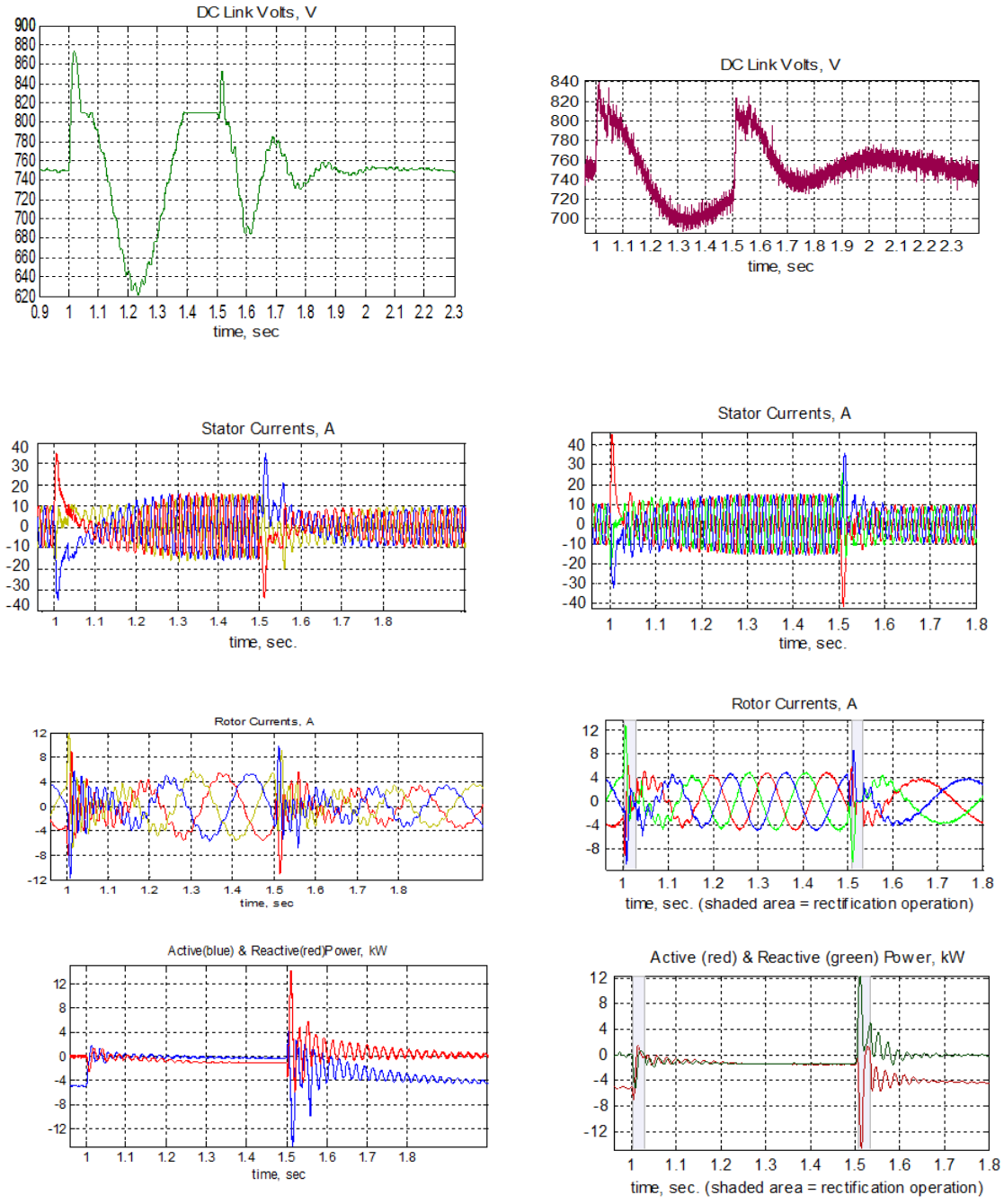

a) Simulation b) Experiment

Fig. 4.15 DC-brake control delay

The rotor currents show an oscillation with a frequency of 50 Hz on a rotor frequency after fault initiation and clearance both in simulation and experiment. The rotor frequency depends on the increased rotor speed during and after the fault as shown in Fig. 4.16. The rotor speed oscillates in the range of 1.06 to 1.17pu in both simulation

and experiment. The oscillating rotor speed frequency is 1.67 Hz for the simulation and 1 Hz for the experiment. However, speed oscillations still occur in the typical range from 0.2 to 2 Hz [40, 105].

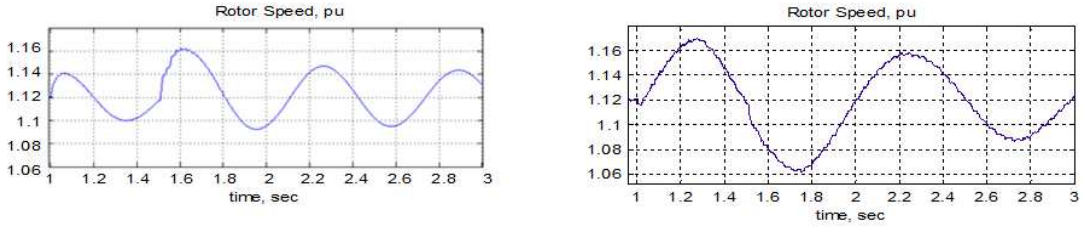

a) Simulation b) Experiment

Fig. 4.16 Rotor speed oscillation

For active and reactive power, during the fault the DFIG supplied 5% and 20% active power for simulation and experiment respectively and 18% reactive power both in simulation and experiment. After fault clearance the reactive power oscillates significantly from the average value of 4KVar consumption down to zero within 300ms. This period lasts longer in simulation.

4.4.3 Summary

The FRT performance of the DFIG has been investigated under experimental conditions, i.e. the crowbar activation period and the DC-brake control delay. For investigation into the crowbar activation period, rotor currents between crowbar and rotor-side converter are immediately reduced to zero during the initiation and clearance periods when the crowbar is operated. After the fault clearance of 120 ms in a period of crowbar activation the DFIG loses power control and consumes high reactive power which clearly does not satisfy FRT grid requirements.

For investigation into the DC-brake control delay, stator currents are gradually decreased and take a longer time than the rotor currents because the effective stator time constant is longer. The rotor currents have an oscillation after fault initiation and clearance but a slight difference in the rotor frequency and rotor speed both in simulation and experiment.

However, the oscillating rotor speed is still in the range of 1-2 Hz which generally happens in practice. After fault clearance, the DFIG supplies high active power and consumes high reactive power in the recovery of 30ms, but powers oscillate from the average value of 50% down to zero which lasts longer in simulation. However, the results are acceptable for FRT grid requirements.

Chapter 5 **Investigation of DFIG Fault ride-through capability**

A combined scheme using both crowbar and DC-brake chopper is reviewed, providing a crucial element for DFIGs FRT. There are three cases in section 4.3: after model validation, the case of 0.15pu fault voltage is used for the purpose of investigating the FRT capability of the DFIG. This is because a duration of 140ms fault for the FRT requirement of GB grid code provides a contrast to a period of 500ms fault for those of Ireland and USA grid codes, of which the FRT requirement profile was presented in section 1.4. After that the developed model including both FRT devices (crowbar and DC-brake chopper) will be employed to investigate the DFIGs FRT performance with different values of crowbar resistance in the worst case of zero fault voltage with a fault duration of 500ms.

5.1 Review of a combined scheme (both crowbar and DC-brake chopper) for DFIG FRT capability

[103, 106] compared the use of a combined scheme (both crowbar and brake chopper) with the crowbar system only, and found that using the combined scheme provided better results of DC-link voltage during fault at the DFIG terminals: i.e. the DC-link was kept within acceptable values. [107] and also [108] presented how using both crowbar and chopper devices effectively reduced the resulting DC voltage, because during the fault period the crowbar protects high current from the rotor side of machine to the converter. However, operating the crowbar leads to loss of the generator controllability of the rotor side converter. Thus the DC-brake chopper provides a better performance, reducing the DC-link voltage while the DFIG operation is connected.[25, 81, 109, 110] recommended that a crowbar be used to by-pass the rotor circuits to the dissipating resistor, thus decreasing high currents which could damage the rotor side converter during the fault. While in this period a DC chopper is used to limit the DC-link voltage, thus keeping the DC-link voltage below the upper threshold.

Moreover, as verified using the crowbar method in section 4.4, during a fault the longer the crowbar is removed, the more reactive power is absorbed. ***This can be improved by using auto-switching control of the crowbar according to the determined rotor***

current magnitude, and the DC-link voltage ripple is controlled by auto-switching the DC-brake chopper with respect to the threshold level. Simulation results show the effectiveness of combined crowbar and DC-brake chopper.

5.2 Investigation of the FRT capability using a combined scheme

To investigate the fault ride through performance using a combined scheme, the pre-fault conditions are as follows: the DFIG operating at a speed of 1.12 pu (1680rpm) and generating 0.67 pu (5kW) at unity power factor. A 7.5kW-DFIG, 415V, 1290V (rotor line-to-line voltage rms) base is chosen. A 10.4A stator and 3.35A rotor currents are base values resulting from the voltage and power bases. The rotor converter rating is generally chosen to be equal to the rating of rotor current which is 3.35A, rms. The crowbar connection between the RSC and rotor of DFIG is set to operate at an absolute peak rotor current of 9.5A (2pu), with the DC-brake chopper across DC-link connecting between RSC and GSC set to switch on at DC voltage of 810V (1.08pu) and off 795V (1.06pu). The simulation results of the investigation are shown in Fig. 5.1 and Fig. 5.2.

The results show the stator currents, rotor currents and active and reactive powers in the case of 0.15pu fault voltage, comparing before and after applying FRT protection (crowbar and chopper). In the FRT protection case the RSC currents are different, because the crowbar can protect the converter after peak currents reach 2pu while in the case of there being no crowbar and DC brake chopper protection the converter could be damaged. If the DC-brake chopper protection was not present then the DC link voltage would increase until the capacitor was damaged. Therefore, as part of the FRT capability of a DFIG, the crowbar is used to protect the converter while the DC-brake chopper helps the system to release energy across the DC link and also prevent capacitor damage.

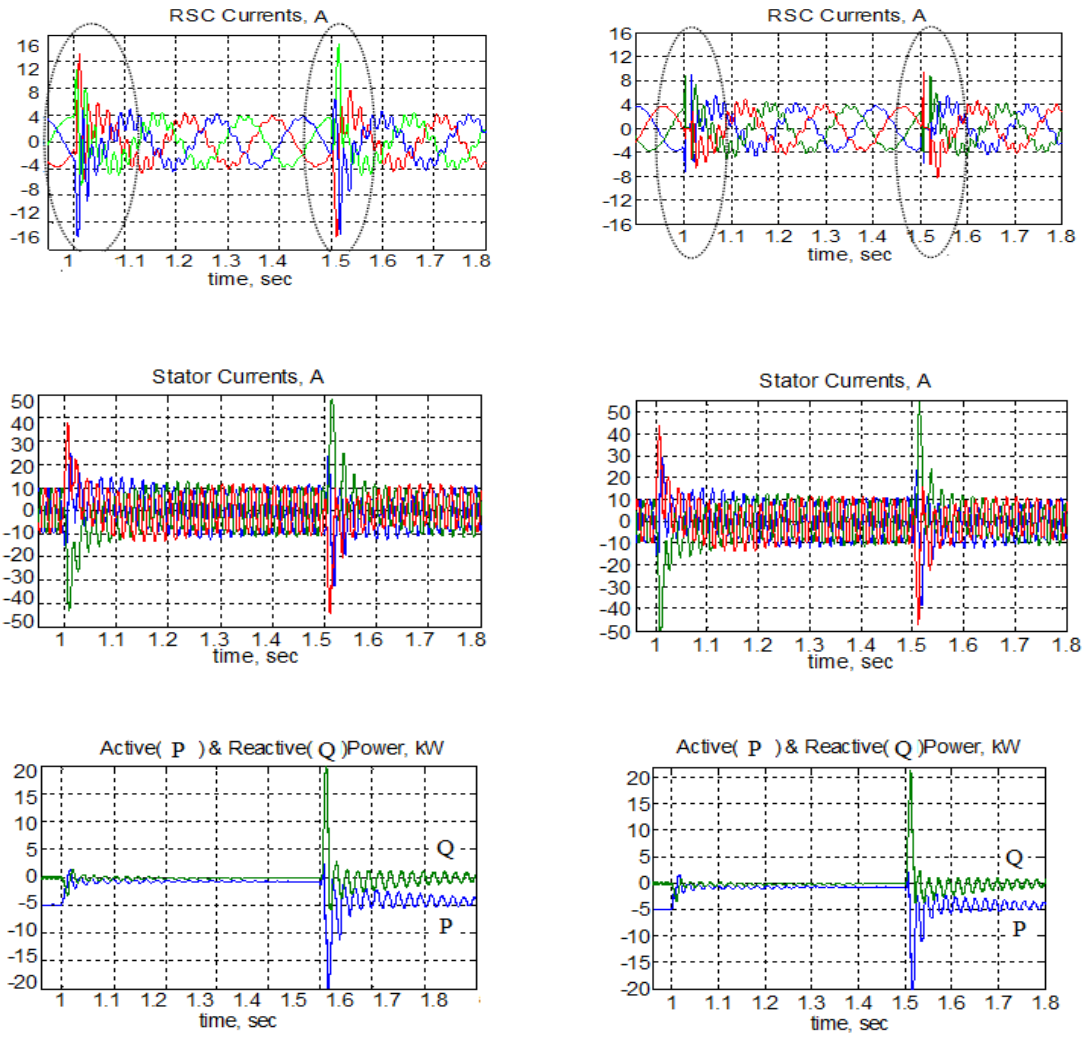

a) Before FRT protection b) After FRT protection

Fig. 5.1 Simulated waveforms of stator currents, rotor currents and active and reactive powers

Details of FRT protection are shown in Fig. 5.2, for a fault voltage of 0.15pu at the initiated time of 1 s and a clearance time of 1.5 s. The crowbar begins operating when the peak RSC current is increased to 9.5A (2pu). In the operation period of 20 ms (see Fig. 5.3) after fault initiation and clearance, the crowbar is activated to connect the crowbar resistance across the rotor circuit to protect the converter. In the meantime the machine performs as a singly-fed induction machine in operating mode, in which the DFIG is not controlled by the RSC. For the DC brake chopper, its brake resistor is operated when the DC-link voltage is increased above the threshold value of 810V (1.08pu) according to the laboratory design.

In the case of no FRT devices, the voltages rise to the value of 1000 V after fault initiation and 1200 V after fault clearance; this is undesirable for the DC-link capacitor, which could be damaged.

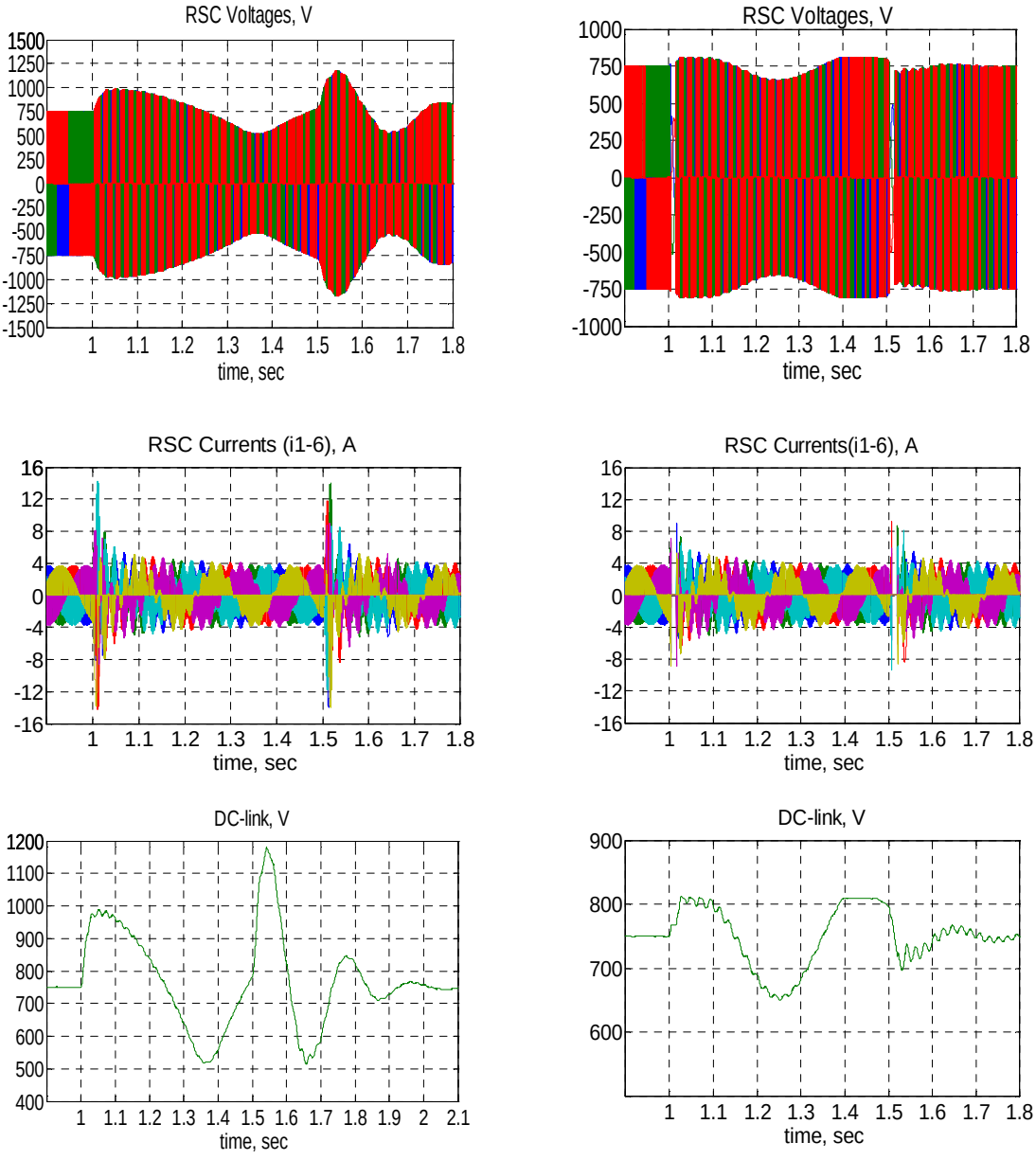

a) Before FRT protection

b) After FRT protection

Fig. 5.2 Simulated waveforms of rotor side voltages, currents and DC-link voltage

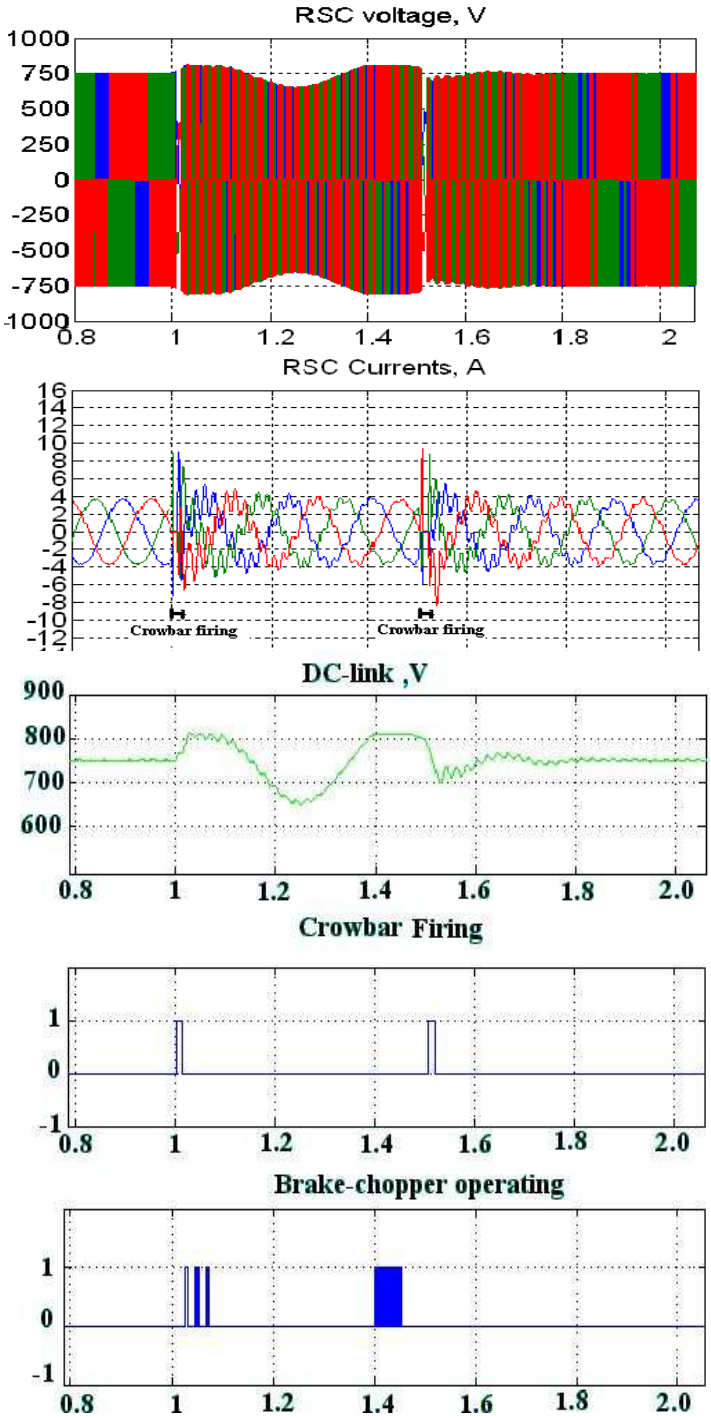

Fig. 5.3 Simulated RSC voltages and currents and DC-link voltage with crowbar and DC chopper operation during the FRT

The model simulation can demonstrate more detail of voltages and currents of RSC and the DC-link voltage, shown in Fig. 5.4. Currents in the RSC (i_{R1}-i_{R6}) were defined in Fig. 3.7 (Chapter 3). i_{R1}, i_{R3} and i_{R5} are currents in the top part while i_{R4}, i_{R6} and i_{R2} are currents in the bottom part of IGBTs with anti-parallel diodes. The solid colour shows

IGBT currents with high switching frequency in the RSC during their operation, controlled by PWM switching. The currents in the RSC during control interruption and crowbar activation occur during the period from 1.004s to 1.016s and from 1.506s to 1.52s approximately.

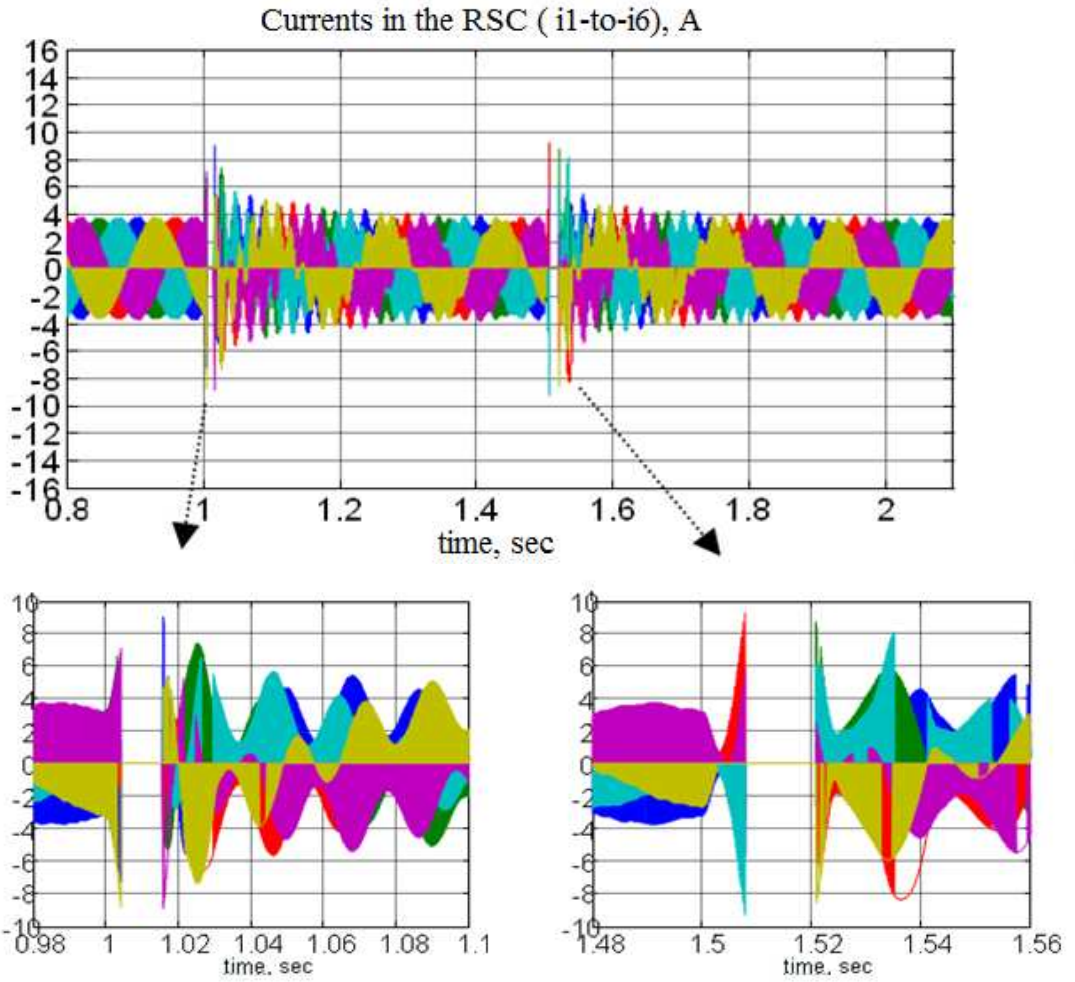

Fig. 5.4 Simulated currents on top and bottom legs of the RSC during grid fault with crowbar and brake chopper

In the period mentioned above, the switching of the IGBTs is stopped by the protection logic, but current and energy still flow into the DC-Link through the freewheeling diodes causing a very fast voltage increase. The simulation results show no current flows through the diodes in this period.

Fig. 5.5 shows the RSC line-to-line voltage when the IGBTs are switched off during crowbar operation. The shape of RSC voltage is changed from PWM switching to sinusoidal waveform because of voltages across the crowbar resistor, and no currents flow through both IGBTs and anti-parallel diodes in this period.

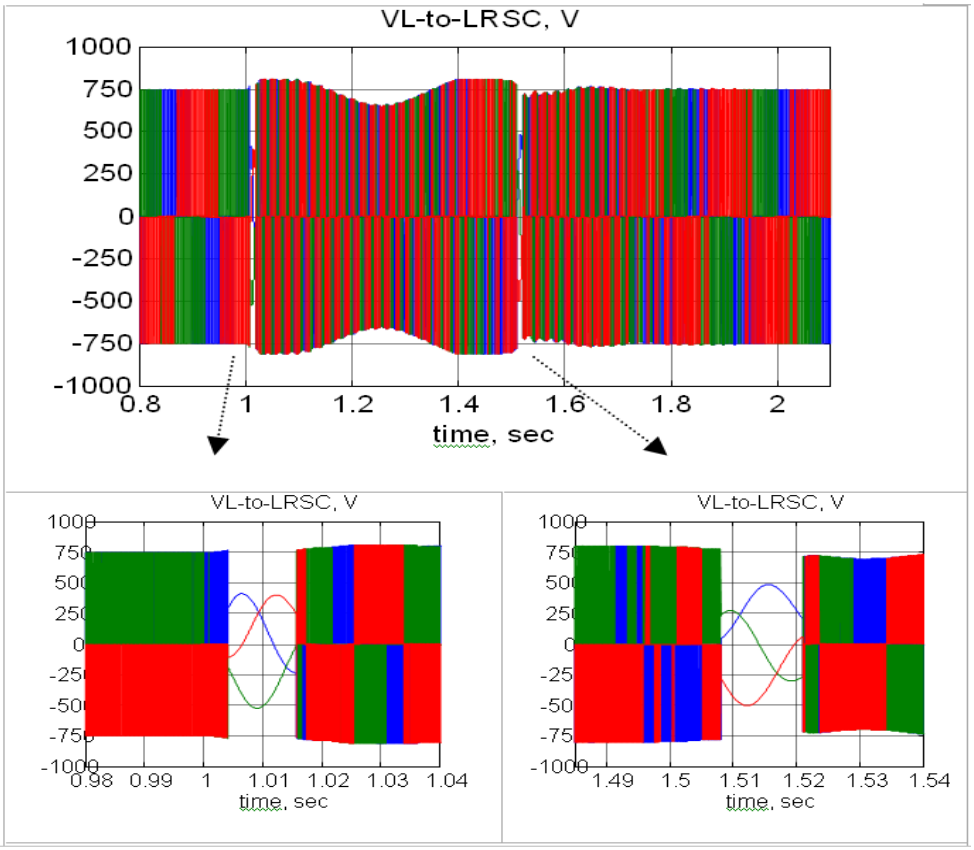

Fig. 5.5 Simulated Line-to-Line voltages of the RSC during grid fault

5.2.1 Summary

In investigating DFIG fault ride-through capacity, the results show that stator currents, rotor currents and active and reactive powers are the same as in case II (retained voltage of 0.15 pu) which does not have crowbar and chopper protection. However, in the FRT protection case, the results are different because of the protection of both the rotor-side converter and the DC-link capacitor. Moreover, this simulation shows the behaviour of voltages and currents when IGBTs are switched off and only diodes conduct the currents. Based on the previous results during fault conditions, it will certainly rescue the converter and DC-link capacitor although the simulation is not verified by experiment.

Further study of FRT capability of the DFIG is concerned with the effectiveness of the use of a crowbar or a DC-link brake chopper under specified conditions.

5.3 Investigation of the FRT capability using a combined scheme with different values of crowbar resistors

Different values of crowbar resistor are used in the wind turbine system, resulting in different behaviour. In this section, the behaviour of the DFIG system under grid faults influenced by the value of crowbar resistors is investigated.

Whenever rotor currents are increased above a threshold value of 2 pu, a three-phase crowbar resistor is applied by activating power electronic switches connected in series with a resistor. In the meantime the rotor circuit of the DFIG is switched from the voltage supplied from the RSC and bypass rotor currents to the crowbar resistor (R_{CB}). As a result, the DFIG behaves as a squirrel cage induction generator with an increased rotor resistance (R_r+R_{CB}) as shown in Fig. 5.6.

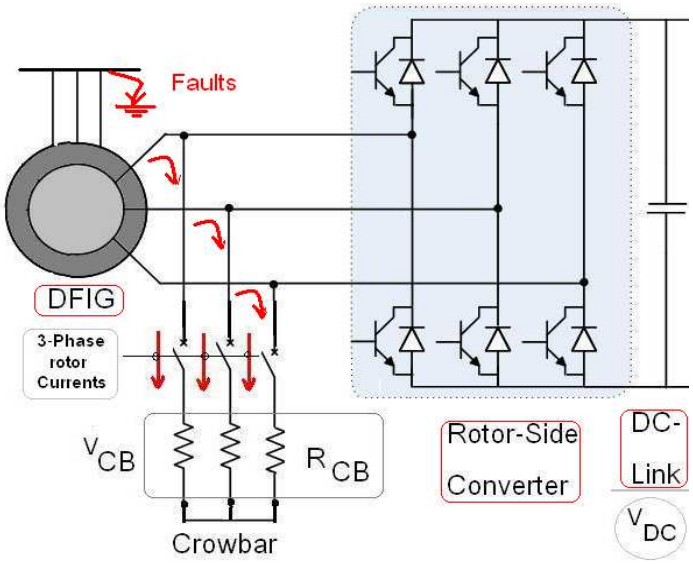

Fig. 5.6 Schematic diagram of a DFIG with a crowbar connected to the rotor circuit

During a normal condition, the amplitude of the rotor voltage is approximately given by

$$e_r = \frac{L_m}{L_s}\lambda_s \omega_s \approx sV_s \tag{5-1}$$

where s is the slip (the difference between synchronous and rotor speed). This voltage is proportional to the slip time of stator voltage which is quite small.

During a voltage dip, in contrast, high induced voltages occur in the rotor and can result in losing control of the converter. The induced rotor voltage resulting from changes of the rotor flux can be calculated from (3-6) and (3-7) as

$$\bar{\lambda}_r = \frac{L_m}{L_s}\bar{\lambda}_s + \sigma L_r \bar{i}_r \tag{5-2}$$

Where σ is the leakage factor; $\sigma = 1 - \frac{L_m^2}{L_s L_r}$

Substituting the rotor flux in the rotor voltage in (3-5), the voltage is obtained:

$$\bar{V}_r^r = \frac{L_m}{L_s}\frac{1}{\omega_b}\frac{d\bar{\lambda}_s^r}{dt} + (R_r + \frac{\sigma L_r}{\omega_b}\frac{d}{dt})\bar{i}_r^r \tag{5-3}$$

There are two terms in (5-3): The first is the electromotive force (EMF) induced by the stator flux and represented as e_r. This refers to the rotor voltage when the rotor is in an open-circuit situation ($i_r = 0$). The second term exists when rotor currents occur, resulting in voltage drop in the rotor resistance (R_r) and also the rotor transient inductance (σL_r). Per-phase equivalent circuit of the rotor circuit can be seen in Fig.5.7

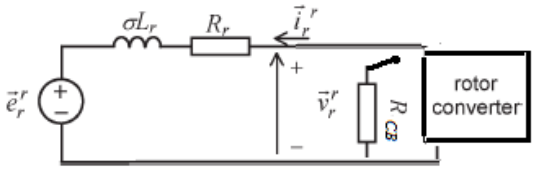

Fig. 5.7 Per-phase equivalent circuit of the rotor circuit

As seen in the circuit, the use of a crowbar is very important in protecting the rotor-side converter from over-currents, and also supporting the FRT capability of a DFIG wind turbine. The minimum value of crowbar resistance is chosen to limit the rotor over-current, typically within 2 pu, while the maximum value should be concerned to avoid over-voltage on the converter. For analysis of the optimum value of the crowbar resistance, a simplified three-phase of RSC with a Y-connected crowbar is modelled using the SimPowerSystems toolbox as shown in Fig. 5.8.

All IGBTs in RSC are inactivated, resulting in having only free-wheeling diodes in circuit. The grid-side converter has very good control of the dc-link voltage, as researched in [28], so the DC-link voltage can be assumed to be constant at a nominal voltage. In contrast, in this DFIG model with the combined scheme the DC-link voltage can be decreased below a nominal voltage, depending on the fault duration.

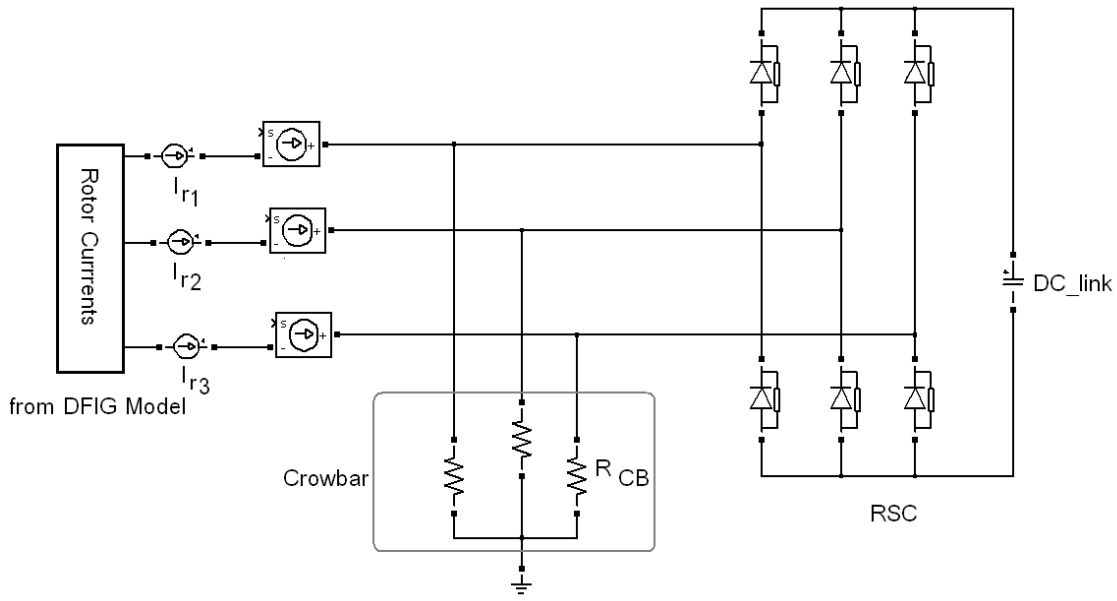

Fig. 5.8 A simplified three-phase diagram of RSC of DFIG including a Y-connected crowbar during no IGBTs-switching

In order to protect the converter and the DC-link capacitor, the over-voltage at the crowbar should be limited in the following condition.

$$V_{CB} = I_{CB}.R_{CB} \le \frac{V_{dc}}{\sqrt{3}} \tag{5-4}$$

As seen in (5-4), the diodes (in Fig. 5.8) will start conducting when the voltage across the crowbar resistor is given by

$$V_{CB\max} = I_{r\max}.R_{CB} \approx \frac{V_{dc}}{\sqrt{3}} \tag{5-5}$$

V_{CBmax} is also the upper limit value of the RSC voltage (V_{rmax}) which is caused by the maximal rotor current, so the optimum value of the crowbar resistance can be given by

$$R_{CBop} = \frac{V_{dc}}{I_{r\max}\sqrt{3}} \tag{5-6}$$

In the normal condition the DFIG is operated at a speed of 1.12 pu to generate stator active power of 0.67 pu at unity power factor, i.e. reactive power is zero. During a fault, the three-phase supply voltage dips from normal voltage (1 pu) to fault voltage (0 pu) at time = 1 sec and the fault is cleared at time = 1.5 sec. When the rotor current occurs over 2 pu, the crowbar is activated and the machine behaves like a squirrel cage induction machine where the stator winding remains connected to the grid. At the same time the IGBTs RSC is switched off, and the rotor currents flow through the crowbar

resistor instead. Whenever the rotor current decreases to less than 2 pu, the crowbar is inactivated and the IGBTs switching is reconnected. Two cases, of with and without crowbar protection are studied. Further, different crowbar resistance values (from 5 to 20 times rotor resistance) are investigated, as shown in Table 5.1.

Table 5.1 studied cases of various crowbar resistance

Case no.	Crowbar resistance (pu)	Note
1	Without a crowbar	Having only a DC-link brake protection
2	With a crowbar (from 5 to 20 times of rotor resistance)	Having both a crowbar and DC-link brake protection

5.3.1 DFIG behaviour under fault conditions, having only DC-link brake chopper protection (without a crowbar)

The DFIG is controlled to generate stator active power (P_s) of 1.0 pu at unity power factor as a normal condition with independently controlled d-axis and q-axis rotor current components. While a three-phase fault is initiated at time = 1 sec and cleared at time = 1.5 sec, the DFIG loses power control from 1 sec to 1.5 sec. After a fault clearance time of 500 msec the generator resumes pre-fault operation, generating stator active power of 5 kW(0.67 pu) while the machine has no reactive power consumption as shown in Fig. 5.9.

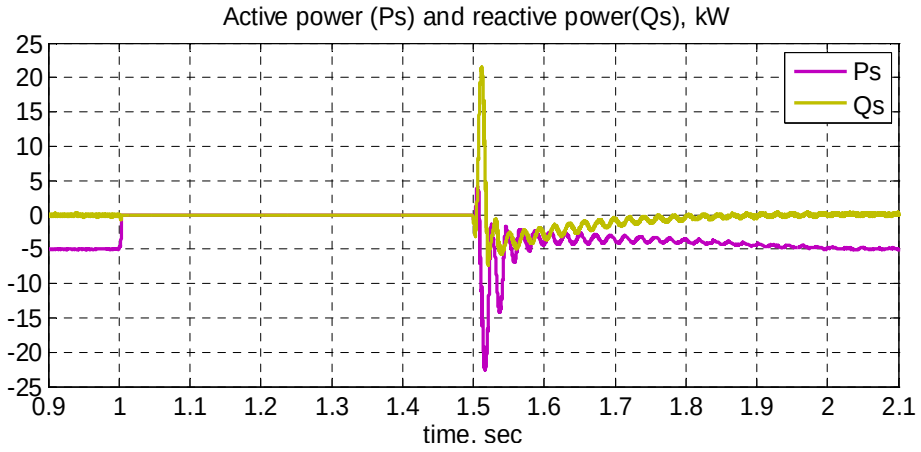

Fig. 5.9 The stator active (P_s) and reactive power (Q_s) response

The rotor current apparently reaches above 2pu at fault initiation but around 17.5 A (3.7 pu) after fault initiation and clearance, as shown in Fig. 5.10. These high rotor

currents can damage the rotor-side converter (RSC), in the case of there being only a DC-brake chopper without a crowbar.

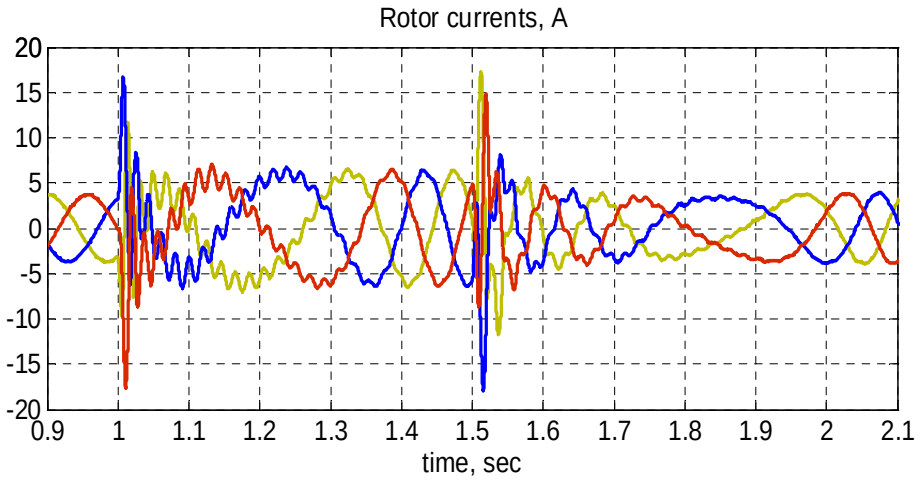

Fig. 5.10 Simulation results for the rotor currents

During the fault occurrence (between time=1 and 1.5 sec) electromechanical torque (T_e) falls from 0.67 pu to 0 pu because of demagnetization of the DFIG while turbine torque (T_w) will be decreased by using a speed controller. As a result, the turbine speed (ω_m) rises slightly with very low frequency, but is rather constant as shown in Fig. 5.11. After fault clearance at time =1.5 sec, turbine torque is immediately increased from zero and by then a speed controller is restarted to control the generator speed, thus reducing high speed to a normal speed of 1.12 pu.

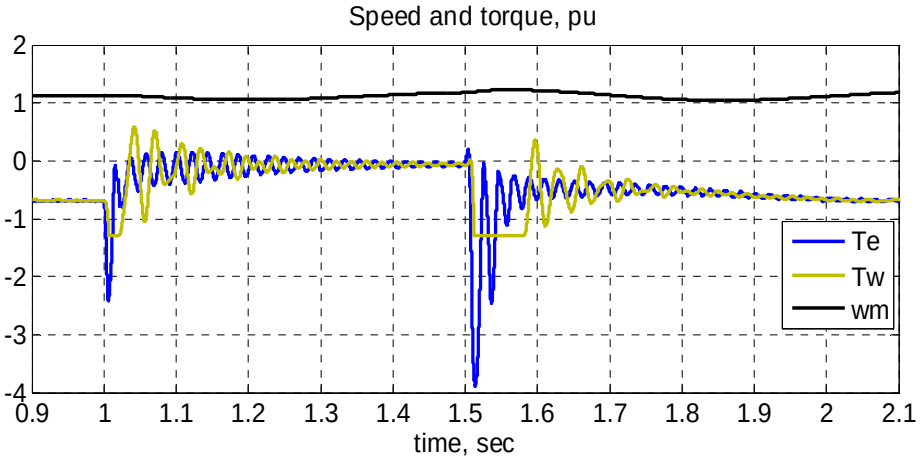

Fig. 5.11 Speed, Electromechanical torque and Turbine torque response

As for DC-link voltage, this starts increasing rapidly from 750 V (a nominal value) to 880 V (a peak value) at fault initiation. The DC-link voltage has been reduced by engaging a brake chopper with upper/lower threshold levels. After fault clearance, the controller will resume normal activity to return to a nominal voltage as shown in Fig. 5.12.

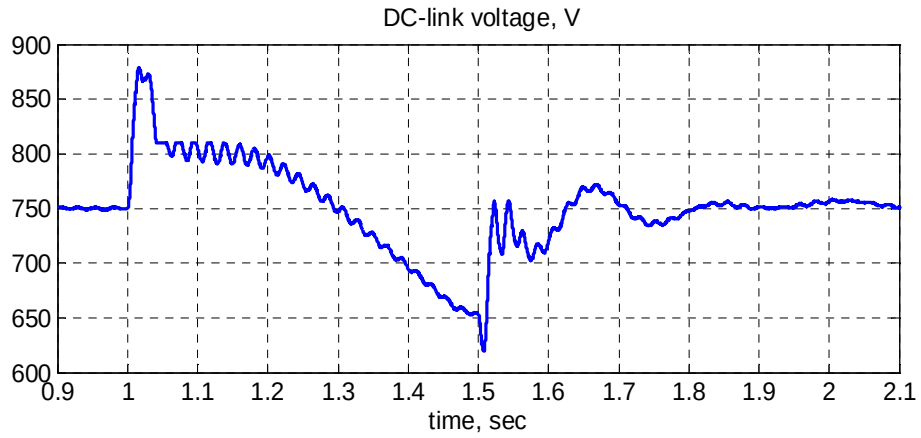

Fig. 5.12 DC-link voltage response without a crowbar protection

5.3.2 DFIG behaviour under fault conditions, having both a crowbar and a DC-link brake chopper protection (a combined scheme)

The DFIG is operated as mentioned in the previous section (having only a DC-link brake chopper) but also adding a crowbar for protection. To find the minimum value of crowbar resistance, four different crowbar resistance values are investigated, i.e. R_{CB} = 5Rr, 10Rr, 15Rr and 20Rr. Simulation results of rotor currents are shown in Fig. 5.13. During three-phase faults initiated at time = 1 sec and cleared at time = 1.5 sec, rotor currents are increased from fault initiation to fault clearance and then, after fault clearance time of 500 msec, decrease to normal operating value. The peaks of rotor currents occur in a very short time at both fault initiation time and fault clearance time.

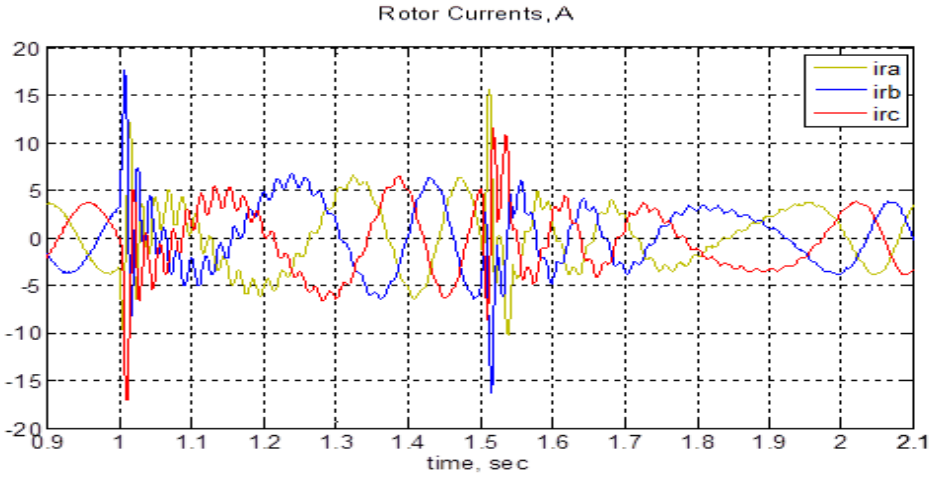

a) R_{CB}=5Rr

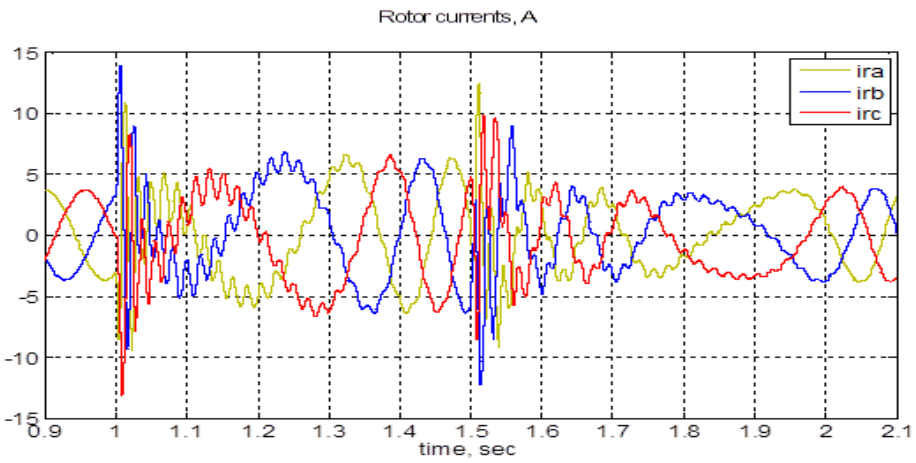

b) R_{CB}=10Rr

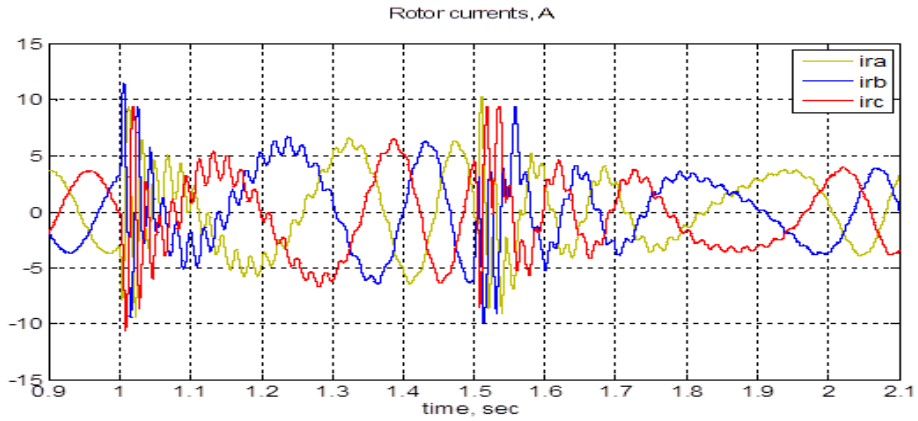

c) 15Rr

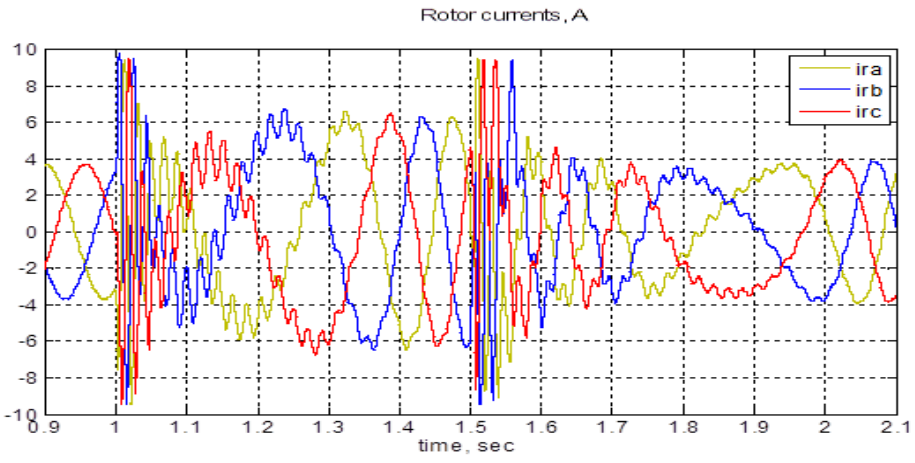

d) R_{CB}=20Rr

Fig. 5.13 Simulated rotor currents at different crowbar resistance values

After using crowbar resistances of 5Rr, 10Rr, 15Rr and 20Rr, the results show that the peaks of rotor currents have been reduced from 3.7 pu (without crowbar protection) to 2.9, 2.7, 2.5 and 2.0 pu, respectively. Moreover, the trend of increasing the value of the

crowbar resistance from 5 to 20 times the rotor resistance (5-20×Rr), thus resulting in the reduced peak of rotor currents, may be drawn and is shown in Fig. 5.14. Therefore, the rotor currents are precipitated in a safety level of 2 pu with use of the minimum crowbar resistance value of 20 times the rotor resistance value (20Rr). As a result, the rotor-side converter will be protected from high rotor currents.

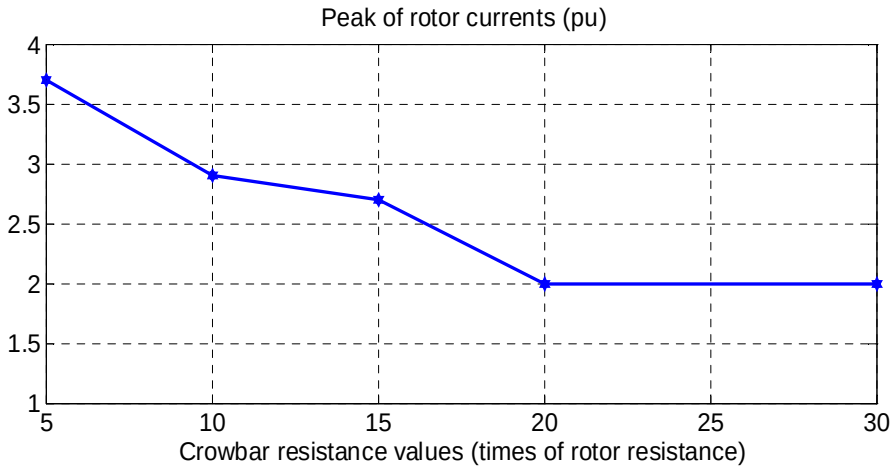

Fig. 5.14 Relations between crowbar resistance (times of rotor resistance) and peak of rotor currents (pu)

Moreover, a comparison of the DC-link voltage using different crowbar values shows that the DFIG with a combined scheme (a DC-brake chopper and a crowbar) keeps the voltage within acceptable levels better than using the DC-brake chopper only, as seen in Fig. 5.15. Also, active and reactive powers appear in the behaviour, as in case I (retained voltage of 0 pu) in Chapter 4 which does not have crowbar and chopper protection as shown in Fig. 5.16.

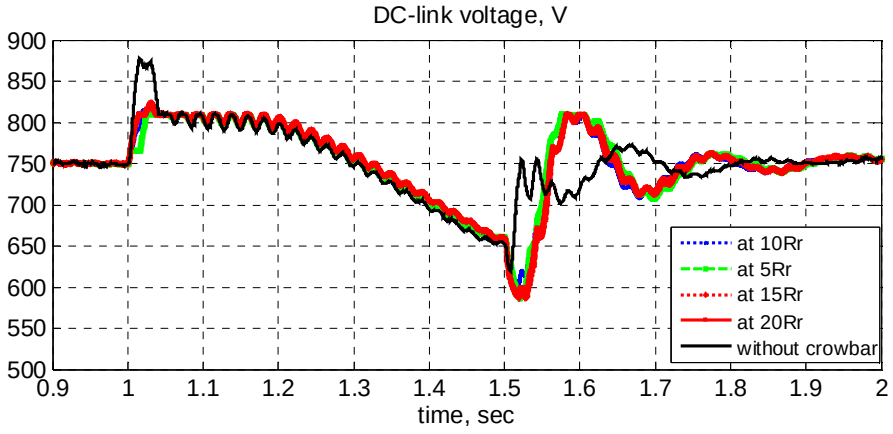

Fig. 5.15 DC-link voltage in different crowbar values

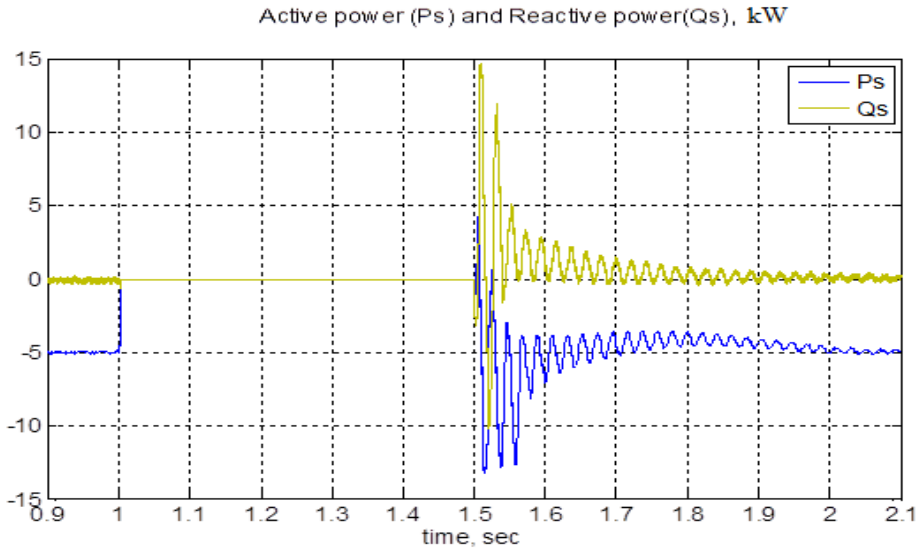

Fig. 5.16 Active and reactive power response with a combined scheme

5.3.3 Summary

In the study of DFIG fault ride-through capacity with a combined scheme (a crowbar and a DC-brake chopper), the results show that rotor currents have been decreased from 3.7 to 2 pu. After using crowbar resistance values from 5 to 20 times rotor resistance value, the minimum crowbar resistance can be designed with a value of 20Rr. Active and reactive powers are almost the same as in case I (retained voltage of 0 pu) which does not have crowbar and chopper protection. However, in the FRT protection case, especially a combined scheme, both the rotor-side converter and the DC-link capacitor will be well protected. Moreover, this simulation shows the behaviour of voltages and currents when IGBTs are switched off and only diodes conduct the currents.

5.4 2-MW wind turbine based on DFIG

To review and investigate FRT management, a 7.5-kW machine was used to study FRT capability using the combined scheme. According to [111], currently wind turbines with 1.5-3 MW rated power are commonly installed in on-shore projects. The commercial wind turbines available in the market with power ranges between 1.5 and 3 MW are summarised in [112]. To be realistic and re-confirm the effectiveness of the proposed model, a 2-MW DFIG was chosen for investigation while seeking accuracy in the developed model.

In the normal condition the 2-MW DFIG is operated at a speed of 1.12 pu to generate stator active power of 0.67 pu at unity power factor. During fault, the three-phase supply voltage dips from normal voltage (1 pu) to fault voltage (0 pu) at time = 1 sec and the fault is cleared at time = 1.5 sec. When rotor current occurs over 2 pu, the crowbar is engaged and the DFIG behaves like a singly-fed induction machine where the stator winding remains connected to the grid. In the meantime the IGBTs switching control of RSC is lost, and the rotor currents flow through the crowbar resistor instead. Whenever the rotor current is lower than 2 pu, the crowbar is disengaged and the IGBTs switching is reconnected. Two cases, having crowbar protection and without crowbar protection, are studied. Further, different crowbar resistance values (from 5 to 20 times rotor resistance) are investigated for a large 2-MW DFIG.

5.4.1 2-MW DFIG behaviour under fault conditions, using a combined scheme (with DC-link brake chopper and crowbar)

To investigate the fault ride-through performance using a combined scheme, the pre-fault conditions are as follows: DFIG operating at a speed of 1.12 pu (1680rpm) and generating 0.67 pu (1.34 MW) at unity power factor. A 2 MW-DFIG, 690 V, 2156 V (rotor line-to-line voltage rms) base are chosen. A 1.673 kA stator and 0.536 kA rotor currents are base values resulting from the voltage and power bases. Parameters of 2 MW-DFIG are included in Appendix A. The rotor converter rating is generally chosen to be equal to the rating of rotor current which is 536A, rms. The crowbar connecting between RSC and rotor of DFIG is set to operate at an absolute peak rotor current of 1.52 kA (2 pu) and the DC-brake chopper across DC-link connecting between RSC and GSC is set to switch on and off at a DC voltage of 1080 V (1.08 pu) and 1060 V (1.06 pu), respectively. The simulation results of the investigation are shown in Fig.5.17.

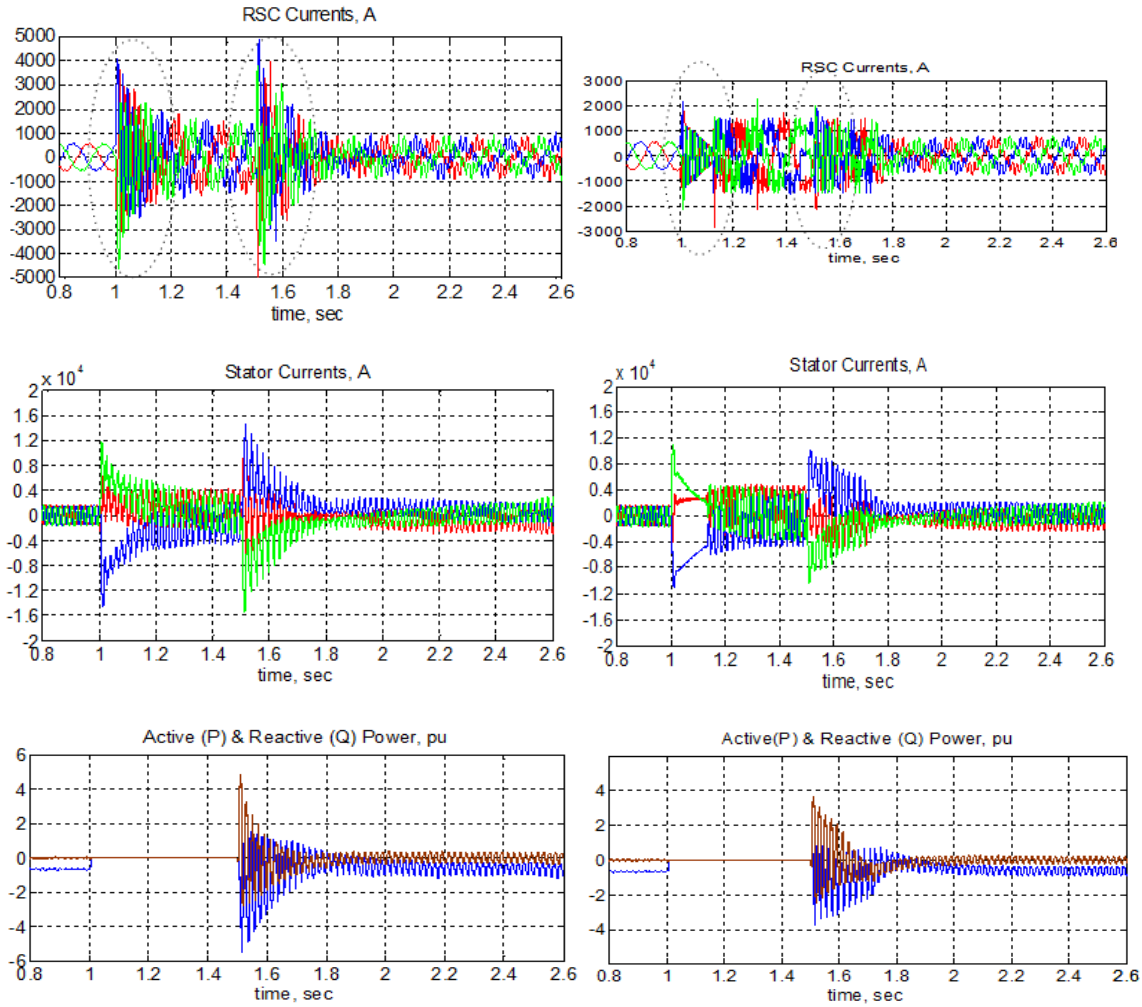

a) Before FRT protection b) After FRT protection

Fig.5.17 Simulated waveforms of stator currents, rotor currents and active and reactive powers

The results show the stator currents, rotor currents and active and reactive powers for a 2-MW DFIG in the case of 0 pu fault voltage, comparing before and after having FRT protection (crowbar and chopper). In the FRT protection case the RSC currents are different, because the crowbar can protect the converter after peak currents reach 1.52 kA (2 pu) while in the case of no crowbar and DC brake chopper protection the converter could be damaged. Without the DC-brake chopper protection then the DC link voltage would increase until the capacitor was damaged. Therefore, to re-confirm the effectiveness of the proposed model as part of the FRT capability of a DFIG, the crowbar is absolutely used to protect the converter while the DC-brake chopper helps the DFIG release energy across the DC link and also prevent capacitor damage. Details of FRT protection are shown in Fig.5.18, for a fault voltage of 0 pu at the initiated time of 1 s and a clearance time of 1.5 s.

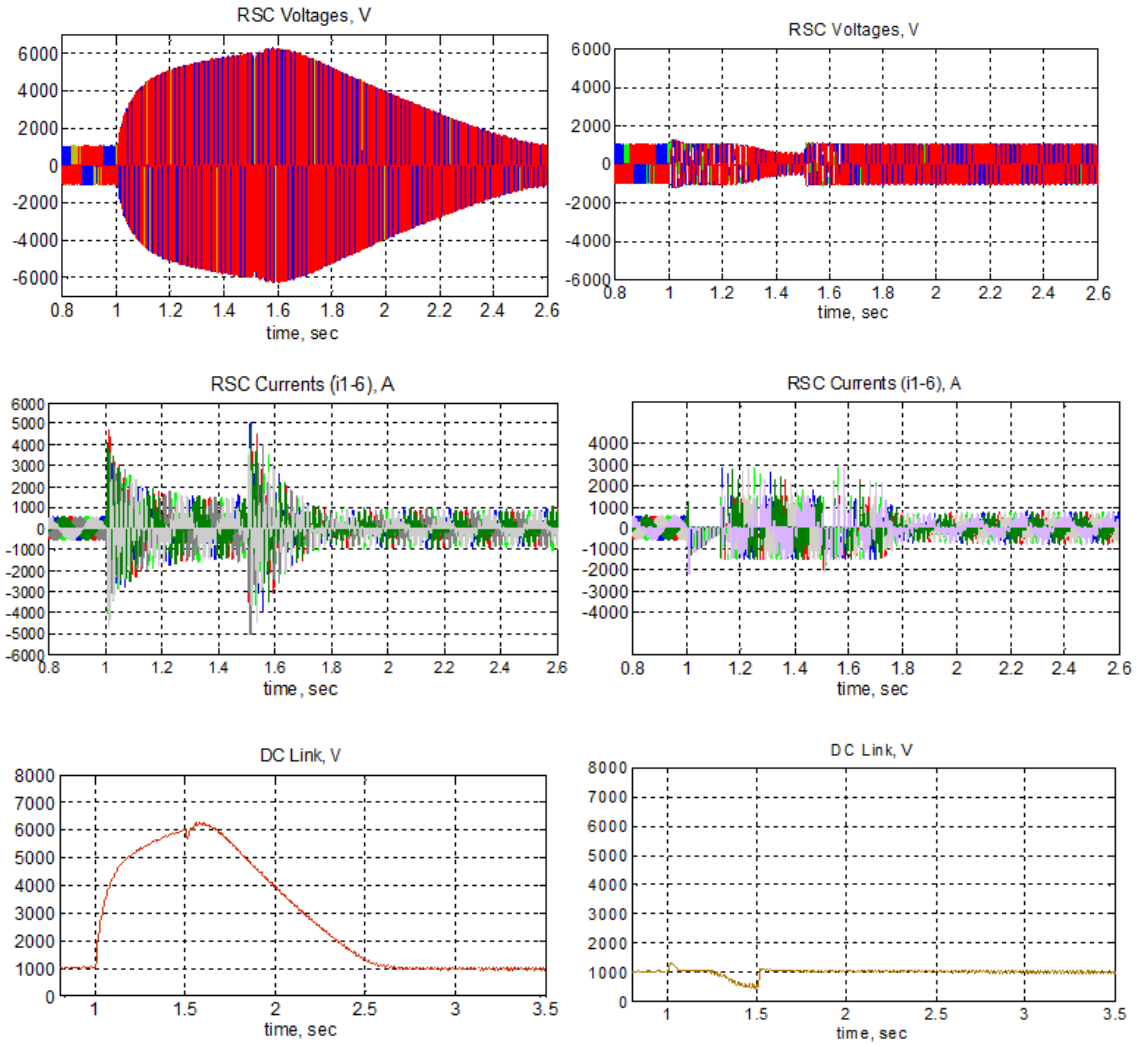

a) Before FRT protection b) After FRT protection

Fig.5.18 Simulated waveforms of rotor side voltages, currents and DC-link voltages

The crowbar starts operating when the peak RSC current is increased to 1.52 kA (2pu). After fault initiation and clearance, the crowbar is activated to connect the crowbar resistance across the rotor circuit to protect the converter. In the meantime the machine performs as a singly-fed induction machine operating mode, in which the DFIG is not controlled by the RSC. For the DC brake chopper, its brake resistor is operated when the DC-link voltage is increased above the threshold value of 1080V (1.08pu) (see Fig.5.18b) as in the same previous design.

In the case of no FRT devices, the voltages rise to the value of 6000 V after both fault initiation and fault clearance (see Fig.5.18a) which causes damage to the DC-link capacitor.

5.4.2 2-MW DFIG behaviour under fault conditions, having only DC-link brake chopper protection (without a crowbar)

The 2-MW DFIG is controlled to generate stator active power (Ps) of 0.67 pu at unity power factor as a normal condition with independently controlled d-axis and q-axis rotor current components. While a three-phase fault is initiated at time = 1 sec and cleared at time = 1.5 sec, the DFIG loses power control from 1 sec to 1.5 sec. After the fault clearance time of 600 msec, the generator resumes pre-fault operation to generate active power of 0.67 pu (1.34 MW) while no reactive power has been consumed; as shown in Fig. 5.19.

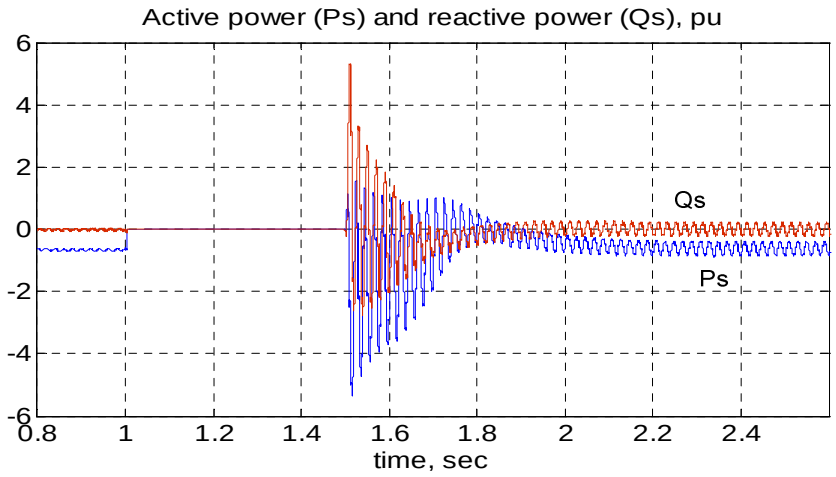

Fig. 5.19 Simulated stator active (P_s) and reactive power (Q_s) response for 2-MW DFIG

The rotor current apparently reaches above 2 pu at fault initiation, but around 4.5 kA (about 3 pu) after fault initiation and clearance as shown in Fig. 5.20. These high rotor currents can damage the rotor-side converter (RSC), in the case of having only a DC-brake chopper without a crowbar.

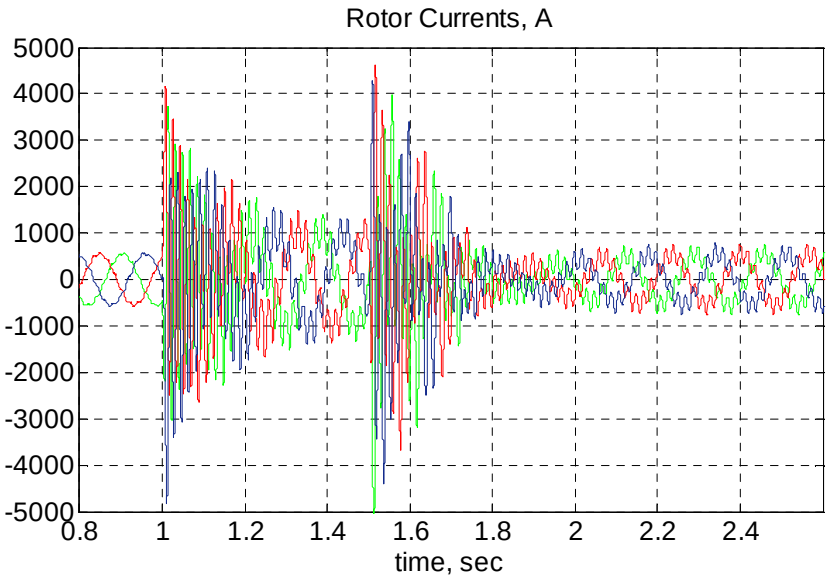

Fig. 5.20 Simulated rotor currents for 2-MW DFIG

For DC-link voltage, this starts rapidly increasing from 1000 V (a nominal value) to 1750 V (a peak value) at fault initiation and also fault clearance. The DC-link voltage has been reduced by engaging a brake chopper with upper/lower threshold levels. After fault clearance with a duration of 200 msec, the controller will resume normal activity to return to a nominal voltage as shown in Fig.5.21.

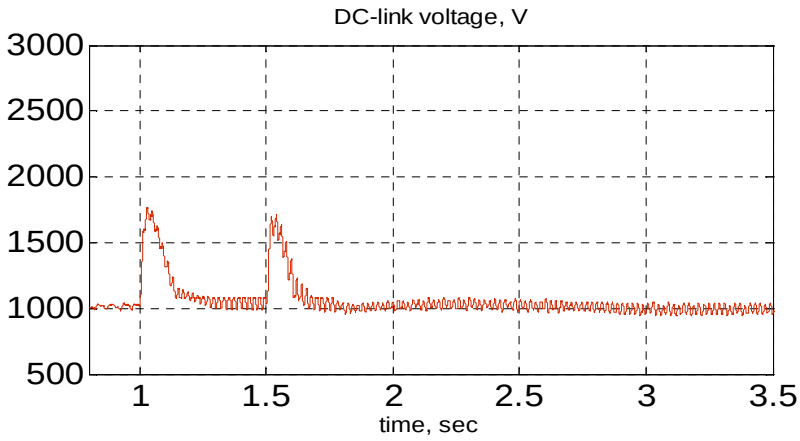

Fig.5.21 Simulated waveforms of rotor side voltages, currents and DC-link voltages

5.4.3 2-MWDFIG behaviour under fault conditions, having both a crowbar and a DC-link brake chopper protection (a combined scheme)

The 2-MW DFIG is operated while having a DC-link brake chopper and crowbar protection. To find the minimum value of crowbar resistance, four different crowbar resistance values are investigated, i.e. R_{CB} = 10Rr, 15Rr and 20Rr. Simulation results of rotor currents are shown in Fig. 5.22. During three-phase faults initiated at time = 1 sec and cleared at time = 1.5 sec, rotor currents increased over 2pu from fault initiation with a duration of 100 msec and still increased over 2pu after a fault clearance time of 300msec with the crowbar resistance value of 10 times rotor resistance (10Rr) (see Fig. 5.22a). When using a crowbar resistance greater than 15 times rotor resistance (15Rr) (see Fig. 5.22b and Fig. 5.22c), rotor currents increased over 2pu from fault initiation with a duration of 100msec and decreased to normal operating value after a fault clearance time of 300msec with an oscillation at frequency of 50 Hz. The rotor current frequency is related to machine slip which depends on the increased rotor speed during and after the faults. The peaks of rotor currents occur in a very short time at both fault initiation time and fault clearance time.

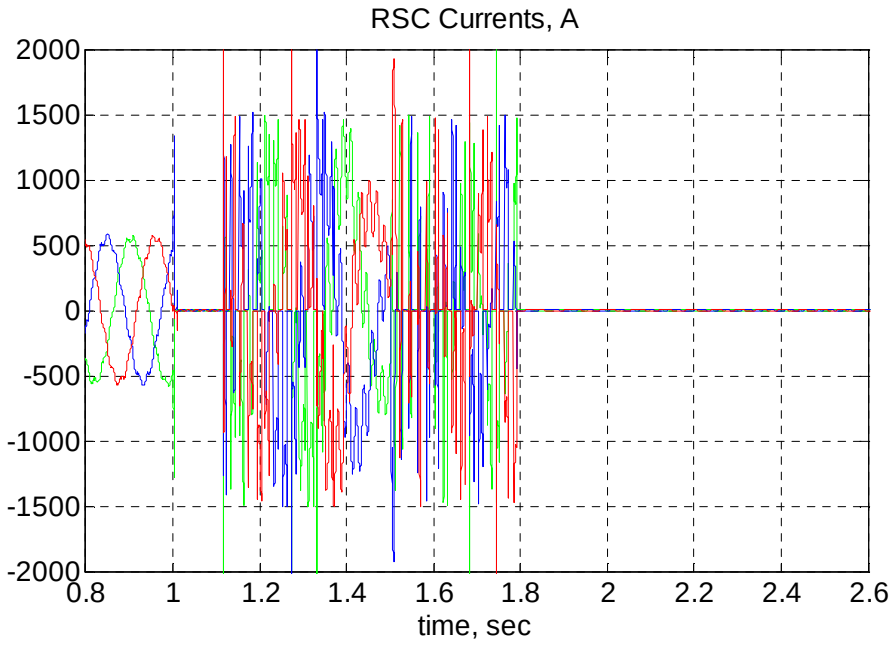

a) Rcb = 10Rr

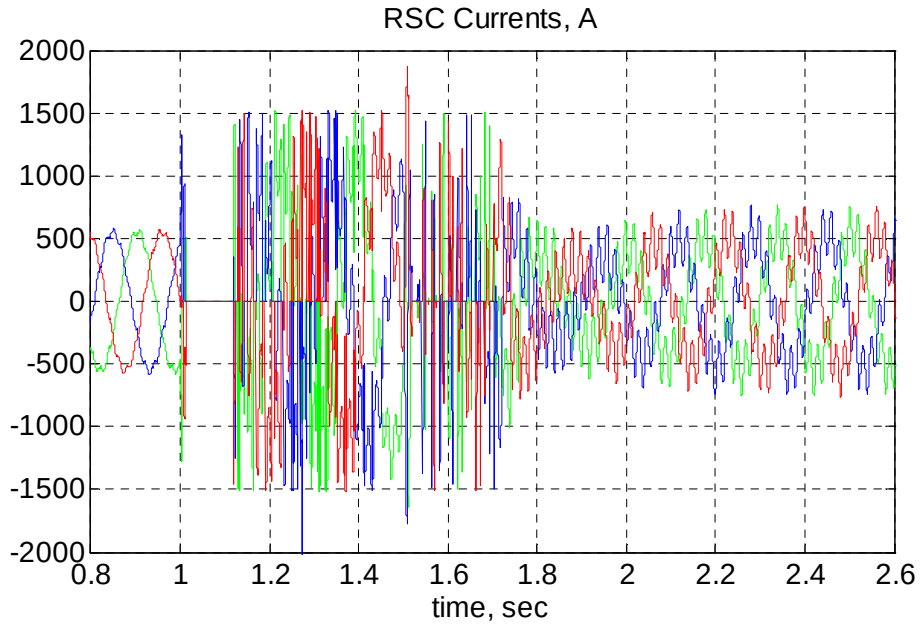

b) Rcb = 15Rr

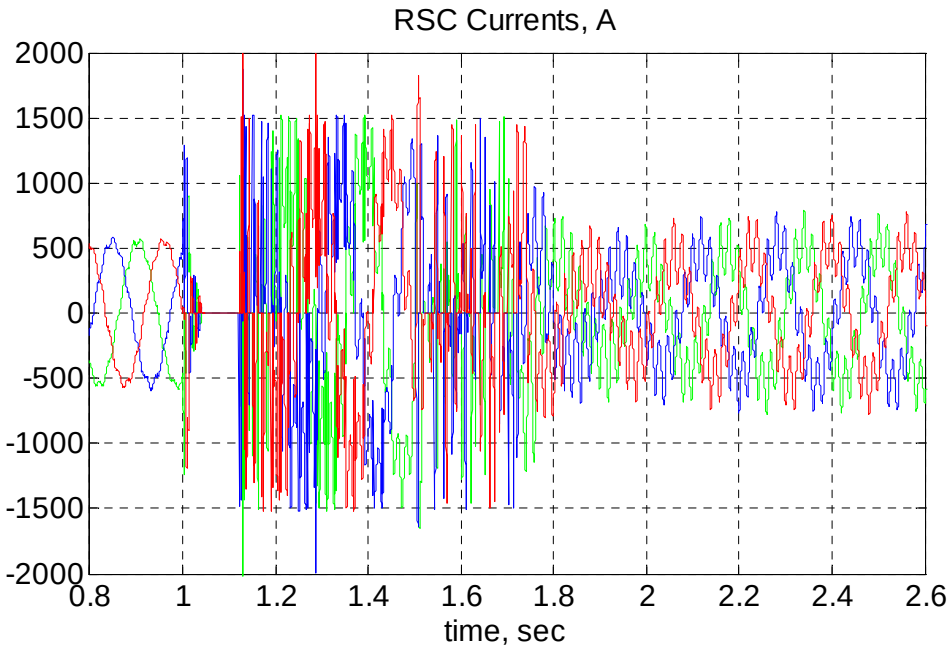

c) Rcb = 20Rr

Fig. 5.22 Simulated rotor currents at different crowbar resistance values for 2-MW DFIG

Furthermore, in the case of having no crowbar protection, high power flowing into the rotor makes the DC-link voltage rise quickly from 1000 V (a nominal value) to 1750 V (a peak value) at fault initiation and also fault clearance. When using a different

crowbar value, a comparison of the DC-link voltage shows that the DFIG with a combined scheme (a DC-brake chopper and a crowbar) still keeps the voltage within limits better than when having only the DC-brake chopper. This is as seen in Fig. 5.23.

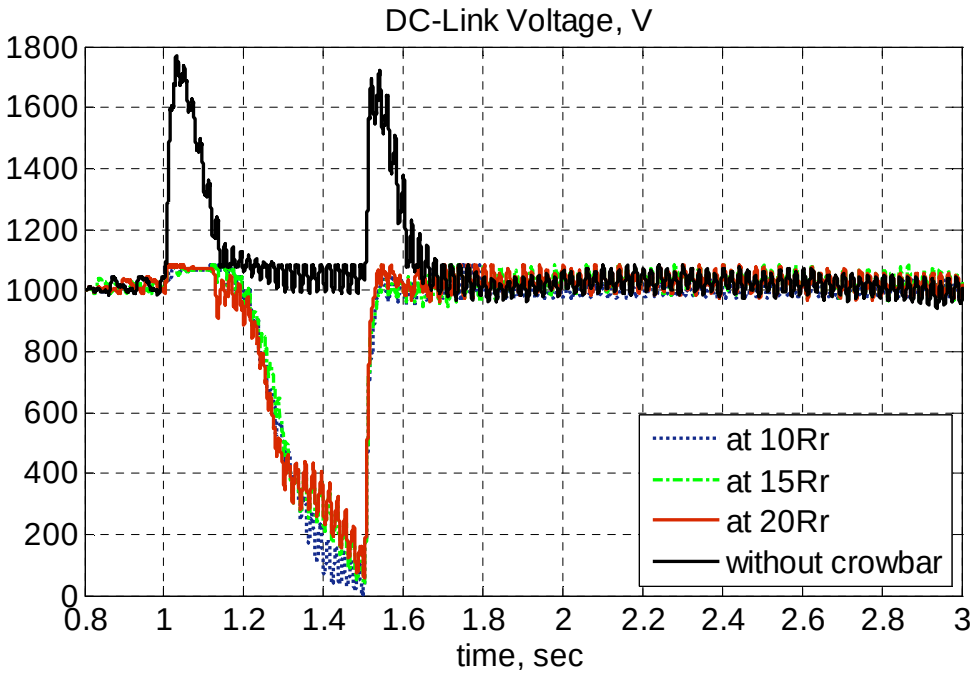

Fig. 5.23 Simulated DC-Link voltage in different crowbar values for 2-MW DFIG

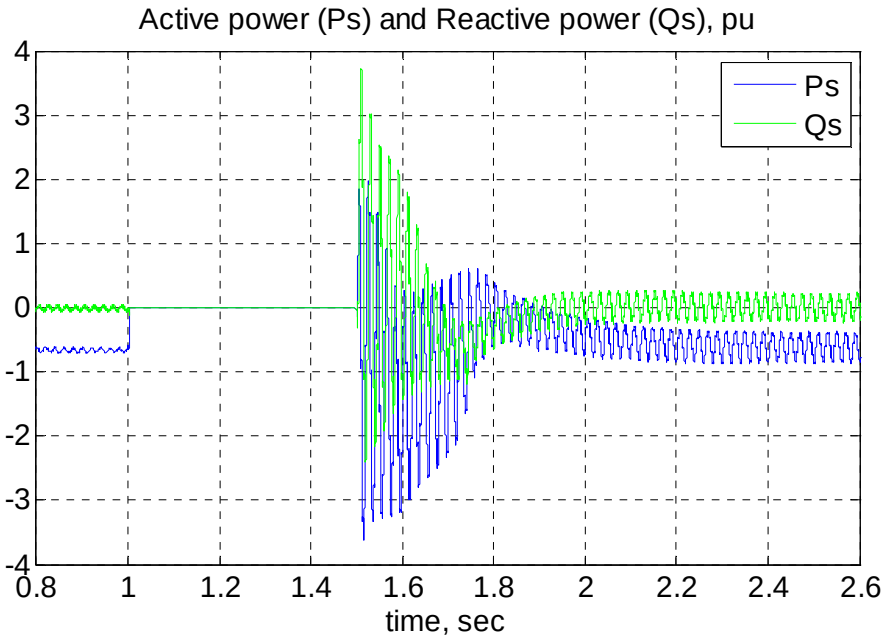

Fig. 5.24 Simulated active power (Ps) and reactive power (Qs) for 2-MW DFIG

The stator active (Ps) and reactive power(Qs) from the 2-MW DFIG is controlled to generate active power (Ps) of 0.67 pu at unity power factor as a normal condition with

independently controlled d-axis and q-axis rotor current components. While a three-phase fault is initiated at time= 1 sec and cleared at time = 1.5 sec, the DFIG loses power control from 1 sec to 1.5 sec. After fault clearance time of 600 msec, the generator resumes pre-fault operation to generate average active power of 0.67 pu (1.34 MW) while no reactive power has been consumed as shown in Fig. 5.24.

5.4.4 Summary

In the study of fault ride-through capacity for a 2-MW DFIG with a combined scheme (a crowbar and a DC-brake chopper), the results show that rotor currents have been cut off from 5.3 to 2 pu. After using crowbar resistance values from 10 to 20 times rotor resistance value, establishing the crowbar resistance value at 20Rr can again be confirmed as the minimum value.

Active and reactive powers are almost the same as in the case which does not have crowbar and chopper protection. However in the FRT protection case, especially a combined scheme, both the rotor-side converter and the DC-link capacitor will be well protected. Moreover, this simulation for a 2-MW DFIG can show the behaviour of voltages and currents when IGBTs are switched off and there are only diodes to conduct the currents during crowbar activation.

Chapter 6 Thesis summary, conclusions and recommendations

This chapter briefly summarises the most important results obtained in the course of this work. Conclusions and suggestions for future work are given later.

6.1 Thesis Summary

A brief summary has been made of the research performed in the literature, identifying some omissions of DFIG wind turbine models in Section 2.6. The fifth-order DFIG model, including detailed modelling of the converter, is important to give more accurate results.

A new DFIG model allowing for the switching effects of IGBT and anti-parallel diode devices has been proposed for fault ride-through investigation. The Simulink model of DFIG system is developed using a stator-voltage vector control method in Chapter 3, including Appendix D. The verification of the model during normal operation shows general good agreement between simulation and experiment; while the model is verified during fault conditions, both simulation and experimental results are in good reasonable agreement as summarised in Section 4.3.1. Moreover, the verification of the FRT capability of the DFIG model using crowbar and DC-link brake methods, i.e. the crowbar activation period and the DC-brake control delay, has been investigated and is summarised in Section 4.4.3. For investigation into the crowbar activation period of 120 ms after fault clearance, both simulation and experimental results show that the DFIG loses power control and consumes high active power resulting in failure to satisfy FRT grid requirements. For investigation into the DC-brake control delay, both simulation and experimental results are acceptable for FRT grid requirements but the rotor-side converter will be put at risk if there is no protection. This problem can be helped using a combined scheme (crowbar and DC-brake chopper). Further, the developed model can provide simulation results of the behaviour of voltages and currents when IGBTs are switched off and only diodes conduct the currents; these have not been presented in contemporary literature. The model is therefore proven to be useful for analysing converter behaviour during fault conditions.

After verification of the DFIG model during normal and fault conditions, the model is used to investigate DFIGs FRT using a combined scheme (crowbar and DC-brake chopper). This is the subject of on-going research and an interesting trend, as reviewed in Section 5.1. Clearly results from the combined scheme show that both the rotor-side converter and the DC-link capacitor will be protected, compared with having only a DC-link brake for protection. However, having both a crowbar and DC-link brake protection is more effective if the minimum value of the crowbar resistance will be designed at a value of 20 times the rotor resistance.

6.2 Conclusions

The DFIG is widely used for large grid-connected, variable-speed wind turbines. As the amount of installed wind power increases, it is increasingly important that turbine generators remain connected and support the grid transmission network during transient system disturbances: so-called FRT, as specified by various national grid codes. To study the FRT capability of the DFIG, an accurate model of the DFIG system is needed. DFIG modelling is a contemporary research area being pursued by many researchers. They have studied control schemes in more detail, rather than power electronic devices. The assumed ideal converter model has been used in many publications. The main problem is the inability to deal with switching off IGBT devices and leaving the rotor circuit connected to a diode bridge rectifier. Taking into account the behaviour of rotor converter diodes and IGBTs, there remains a need to fill a gap which has not been addressed in contemporary literature, and also help to support the essential qualities of the combined scheme in enabling the DFIG to deal with FRT. This is also in order to help overcome the drawbacks raising concerns in many publications.

The Matlab/Simulink model for a vector controlled DFIG is developed to investigate drive FRT characteristics, allowing for the switching effects of IGBT and anti-parallel diode devices. The developed model can be used to predict machine and converter current and voltage waveforms during three-phase supply faults, and to investigate the FRT capability of the DFIG wind turbine. Further, including the switching behaviour of the rotor converter diodes and IGBTs, the model can be used to predict a fault scenario when switching off the IGBT devices and leaving the rotor circuit connected to a diode bridge rectifier. Comparisons between simulation and experiment are discussed in order to validate the model. Finally, the combined scheme for the FRT capability with different crowbar resistors is investigated.

The conclusions from the results of this thesis can be drawn up as follows:

- Validation of the model during normal conditions in both sub- and super-synchronous modes shows close agreement for stator current, rotor current and active and reactive power.
- Comparisons between simulation and experimental results during fault conditions are in reasonable agreement. Within 20ms of fault initiation and clearance, stator and rotor currents undergo a transient and reach the maximum value of 60A (4pu) and 20A (4pu), respectively.
- The model can show how fault currents in diodes can rise to 4 pu in the worst 3-phase fault scenario with zero retained voltage corresponding to the experimental results.
- The model can also be used to investigate the transient behaviour of the DFIG drive system during supply fault conditions when the converter IGBTs are switched off and the rotor converter appears to be a simple diode bridge rectifier.
- The model can be used to investigate the FRT performance of the DFIG in accordance with the transmission system grid code with and without protection devices, i.e. a crowbar or DC-brake chopper which is helpful in designing the system protection.
- The simulations compared favourably with experimental results for two FRT protection schemes: crowbar activation period and DC-brake chopper delay. The results are acceptable for use in designing the protection and in predicting the FRT performance according to grid requirements, i.e. using only the crowbar in a long period of 120 ms which can cause power interruption and consumption of high reactive power in either fault initiation or clearance which is unsatisfactory for FRT grid requirements. While using a DC-brake chopper within the timed delay of current and power control permits the transient rotor over-currents flowing through the rotor converter diodes to the DC-link to support FRT grid requirements.
- Finally, the model can be used for the study of the combined scheme with both a crowbar and DC-brake chopper arrangement which has different crowbar resistance values in order to design the minimum crowbar resistance.

6.3 Recommendations and Further work

The DFIG model should extend to other network components, i.e. a transmission line, a transformer, etc., in order to study more details in voltage response to the grid during faults.

Investigation into the FRT performance of the DFIG under unbalanced fault conditions should be validated in order to compare with balanced three-phase faults.

Aerodynamics and drive train should be studied in more detail in order to improve the mechanical model in controlling power, pitch and speed of a wind turbine.

Other control approaches are needed to study in comparison with a classical PI control in order to improve the FRT capability of the DFIG under fault conditions

Duration of crowbar activation when using a combined scheme should be investigated to find an optimum time.

The usage of an impedance crowbar should be studied and compared with the usage of a resistance crowbar.

Appendix A

A.1 Per unit system

The per unit system is commonly used in power system simulation. It is convenient to represent all quantities in terms of a per unit (pu) value. The pu value can be given by

$$pu = \frac{true\_value}{base\_value} \quad \textbf{(A.1)}$$

After the base values (power, voltage and frequency) have been defined, other base values can be calculated as follows.

The base values are chosen:

$S=VA_b$ = three-phase rated power = $(3/2)V_bI_b=7500\ W$ (A.2)

V_b= peak value of rated phase voltage = 415*√ (2/3) = 339 V (A.3)

f_b= rated frequency = 50 Hz (A.4)

Base values of other quantities:

I_{sb} = peak value of rated phase stator current = √2*10.434 = 14.756 A (A.5)

I_{rb} = peak value of rated phase rotor current = √2*10.434*0.32 = 4.72 A

$\omega_b = 2\pi f_b$ = 314.16 elec. rad/s (A.6)

$\theta_b = 1.0$, elec.rad (traditional choice) (A.7)

$\omega_{mb} = \omega_b(2/pole)$ = 157.08 mech. rad/s ; *Poles =4* (A.8)

$$Z_b = V_b / I_b = 22.963 \text{ ohm} \tag{A.9}$$

$$L_b = V_b / (I_b \omega_b) = 0.07309 \text{ H} \tag{A.10}$$

$$\lambda_b = V_b / \omega_b = 1.075 \text{ Wb.turns} \tag{A.11}$$

$$RPM_{nom} = 3000 \tag{A.12}$$

Mechanical parts:

$$T_b = 3/2(pole/2)\lambda_b I_b, \text{ Nm} = VA_b / \omega_{mb} \tag{A.13}$$

$$\omega_b, _{HS} = \omega_b / (pole/2) \tag{A.14}$$

$$\theta_b, _{HS} = \theta_b / (pole/2) \tag{A.15}$$

$$RPM_{nom,HS} = RPM_{nom} / (pole/2) \tag{A.16}$$

$$H = \frac{J\omega_{mb}^2}{2.VA_b} \tag{A.17}$$

$$J_b = 2\frac{VA_b}{\omega_{mb}^2} = 2\frac{T_b}{\omega_{mb}} \tag{A.18}$$

$$K_{shaft,b} = \frac{VA_b}{\omega_{mb}^2} = \frac{T_b}{\omega_{mb}} \tag{A.19}$$

$$D_b = \frac{VA_b}{\omega_{mb}^2} = \frac{T_b}{\omega_{mb}} \tag{A.20}$$

$$B_b = \frac{VA_b}{\omega_{mb}^2} = \frac{T_b}{\omega_{mb}} \tag{A.21}$$

DFIG quantities can be found in Table A1.

Table A1. Parameters of a 7.5kW DFIG test rig.

Quantity	**Parameter**	**Value**	**pu**
Mechanical Parts:		(refer to high speed side)	
Turbine inertia (refer to high speed side)	J_t	-	5.25
Turbine friction	B_t	-	0.0
DFIG high-speed shaft inertia	J_g	-	1.44
DFIG high-speed shaft friction	B_g	-	0.12
Coupling stiffness	K_{shaft}	Typically between 0.3 and 0.6 pu [35]	0.44
Coupling damping	D	-	1.0
Electrical Parts:			
Generator	**Parameter**	**Value**	**pu**
Stator	R_s	0.68 ± 0.005 Ω	0.04
	L_{ls}	9.04 ± 0.08mH	0.1482
Rotor	R_r	0.46 ± 0.005 Ω	0.02
(refer to stator side)	L_{lr}	9.04 ± 0.08mH	0.1232
Magnetisation	L_m	226 ± 11 mH	3.08
Turns ratio	a	0.32	
Number of pole	P	4	
Nominal voltage	V_s	415 V	1
DC Link	**Parameter**	**Value**	**pu**
Voltage	V_{dc}	750 V	1
Capacitor	C	705 μF	-
Brake resistor	R_{brake}	180 Ω	-
Line filter	**Parameter**	**Value**	**pu**
Inductance	L_{filter}	10.6mH	-

Table A2. Parameters of a 2MW DFIG wind turbine

Quantity	**Parameter**	**Value**	**pu**
Mechanical Parts:		(refer to high speed side)	
Turbine inertia (refer to high speed side)	J_t	-	5.25
Turbine friction	B_t	-	0.0
DFIG high-speed shaft inertia	J_g	-	1.44
DFIG high-speed shaft friction	B_g	-	0.12
Coupling stiffness	K_{shaft}	Typically between 0.3 and 0.6 pu [35]	0.44
Coupling damping	D	-	1.0
Electrical Parts:			
Generator	**Parameter**	**Value**	**pu**
Stator	R_s	-	0.00488
	L_{ls}	-	0.09241
Rotor	R_r	-	0.00549
(refer to stator side)	L_{lr}	-	0.09955
Magnetisation	L_m	-	3.95279
Turns ratio	a	0.32	
Number of pole	P	4	
Nominal voltage	V_s	690 V	1
DC Link	**Parameter**	**Value**	**pu**
Voltage	V_{dc}	1000 V	1
Capacitor	C	30 mF	-
Brake resistor	R_{brake}	1 Ω	-
Line filter	**Parameter**	**Value**	**pu**
Inductance	L_{filter}	2 mH	-
Resistance	R_{filter}	1 mOhm	-

The induction machine

The generator operating at the rated speed of 1.12 pu (1680rpm) and generating power of 0.67 pu (5kW for a 7.5- KW DFIG, 1.34 MW for a 2MW DFIG).

Stator and rotor time constant

The stator time constant (T_s) is defined by $T_s = L_s/R_s$ where $L_s = L_{ls} + L_m$. Similarly, the rotor time constant (T_r) is given by $T_r = L_r/R_r$ where $L_r = L_{lr} + L_m$.

Brake resistor value

The brake resistor was sized to dump twice the rated converter power during grid faults or 50% of the rated DFIG power which equated to 3.75kW. The resistance can be calculated by the equation $P_{brake} = V^2_{dc}/ R_{brake}$. For experiment, a voltage threshold is set at 810Vand the calculated resistance is 175Ω. Because the grid fault durations are quite short, the low power resistor is acceptable. Hence an 180Ω, 0.6kW resistor was chosen for a DFIG test rig.

Crowbar value

From section 3.7, the equivalent value of the crowbar resistor can be given by $R'_{cb}=0.55R_{cb}$. Because the crowbar is connected between RSC and rotor winding of DFIG, the crowbar resistance should be limited to prevent current flow through diodes in the RSC to DC-link. Hence, a limitation can be described by $i_{cb}R_{cb}<V_{dc}$. For experiment, a 18Ω, 0.6kW resistor was employed in the test rig; as a result, the calculated equivalent resistor of a 9.9Ω was used in the simulation for a 7.5kW DFIG while one of 0.026 Ω was used in a 2-MW DFIG simulation.

DC link

The DC-link voltage can be designed by using the standard ratings of power electronics in which 600V/1200V/1700V are typical device upper voltage limits. In the test rig, a 1200V-rated IGBT is used, so the 750V DC-link is defined as the DC-link voltage base for a 7.5- KW DFIG but the 1000V DC-link for a 2-MW DFIG.

Appendix B

B.1 Space vector theory

In AC circuit theory, the complex phasors are commonly used to represent the quantities which vary sinusoidally in time while in the behaviour of a machine, a number of physical quantities can be considered as periodic functions which are sinusoidally distributed in space around the periphery of the machine in the air gap. Thus, similarly the time phasor is used in AC circuit, the space vector is used to analyse the performance of the machine [113].

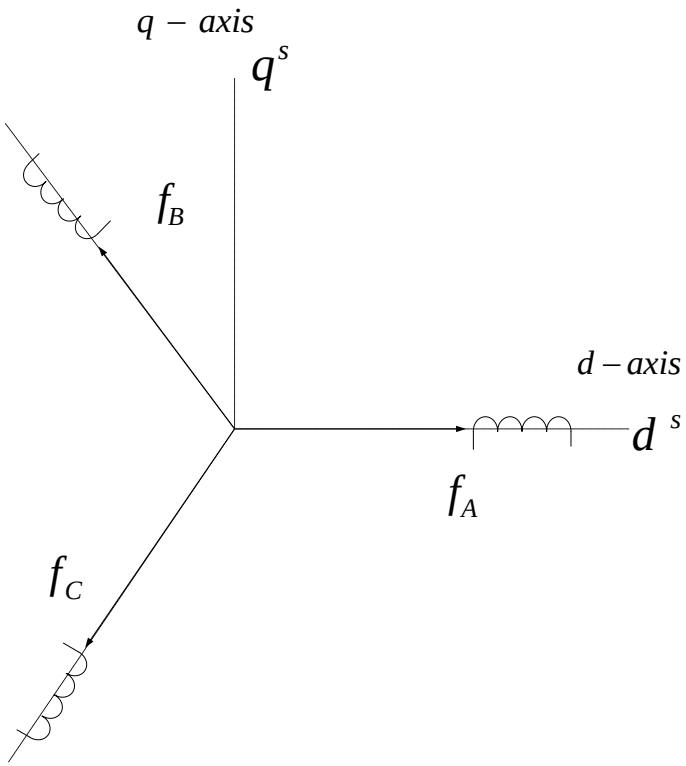

Fig. B.1 A symmetrical three-phase stator winding and reference frame

A symmetrical three-phase stator winding system is considered, where all three phases are displaced by 120^{θ} as shown in Fig. B.1 and the instantaneous values of stator quantities in the three phases A, B and C can be obtained as the sum of the space vectors of the same quantity. The stator quantities *(f_s)* can be current, voltage, flux density, flux linkage, etc and expressed as

$$c\bar{f}_S = \left(\bar{f}_A + \bar{f}_B + \bar{f}_C \right) \tag{B.1}$$

$$\bar{f}_S = \frac{1}{c}.\left(1.f_A + a.f_B + a^2.f_C \right) \tag{B.2}$$

Where $\bar{f}_s$ is the space vector of stator quantities expressed in the stator reference frame, $\bar{f}_A, \bar{f}_B, \bar{f}_C$ are the component space vector and $1, a$ and a^2 are unit vectors in the direction of the magnetic axes of phases A, B and C, respectively, $1 = \exp(0^\theta), a = \exp(j120^\theta)$ and $a^2 = \exp(j240^\theta)$. Hence, the space vector of the stator current in the stator reference frame can be expressed.

$$\bar{i}_S = \frac{1}{c}.\left(1.i_A + a.i_B + a^2.i_C \right) \tag{B.3}$$

With *c = 3 / 2* as a constant value.

Similarly other quantities such as the stator voltage, flux linkage and flux density can be obtained using the same approach as above. Fig. B.2 shows the space vector of the stator current and its d-q component in a stator reference frame.

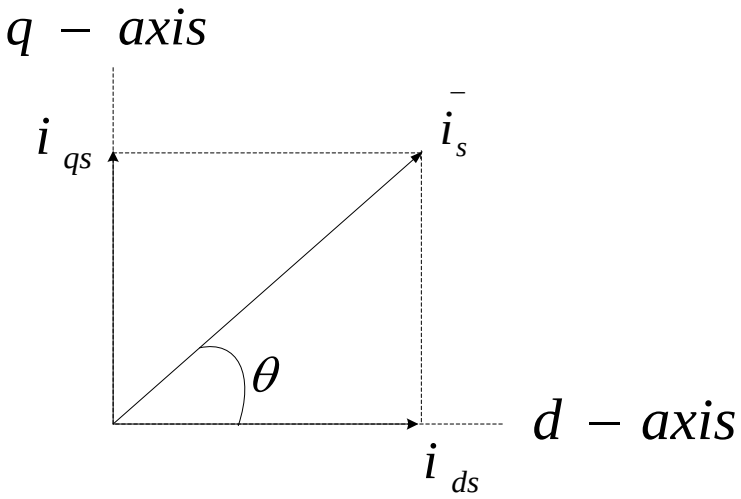

Fig. B.2 The space vector of the stator current in a stator reference frame

B.2 Three phase to stator reference frame transformations

The stator current space vector in the stator reference frame is defined as

$$\underline{i}_S^s = \frac{1}{c}.\left(1.i_A^s + a.i_B^s + a^2.i_C^s\right) \tag{B.4}$$

$$\underline{i}_S^s = i_{ds}^s + ji_{qs}^s \tag{B.5}$$

Where

$$a = \exp(j120^\theta) = \cos(120^\theta) + j\sin(120^\theta) = -\frac{1}{2} + j\frac{\sqrt{3}}{2}$$

$$a^2 = \exp(j240) = \cos(240^\theta) + j\sin(240^\theta) = -\frac{1}{2} - j\frac{\sqrt{3}}{2}$$

B.3 Three phase to rotor reference frame transformations

The stator current space vector in the rotor reference frame is defined as

$$\underline{i}_S^r = \underline{i}_S^s.\exp\left(-j\theta_r\right) \tag{B.6}$$

$$\underline{i}_S^r = i_{ds}^r + ji_{qs}^r \tag{B.7}$$

So it corresponds to the reference system on Fig. B.3.

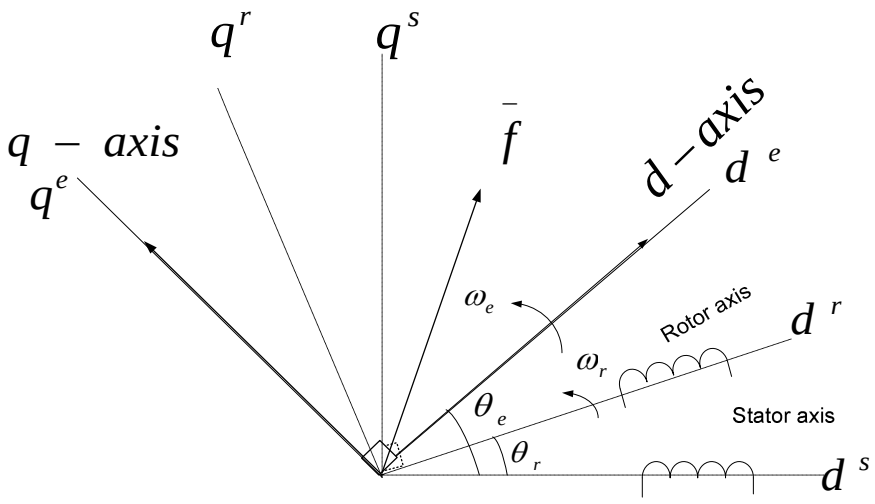

Fig. B.3 Reference frames for the induction machine

B.4 Three phase to synchronous or excitation reference frame transformations

As shown in Fig. B.3, the stator current can be referred to the synchronous or excitation reference frame.

$$\underline{i}_s^e = \underline{i}_s^s . \exp\left(-j\theta_e\right) \tag{B.8}$$

$$\underline{i}_s^e = i_{ds}^e + j i_{qs}^e \tag{B.9}$$

Similarly, other components such as voltage and flux linkage can be transformed to some other reference frame, like the procedure used in the space vector of current. Moreover, the same method can be used for transferring the rotor space vector from the rotor to another reference frame, or vice versa using an angle as depicted in Fig. B.3.

To make it more convenient in terms of writing, all quantities in stator voltage vector reference frame will be written without superscript ‘e’ on the top.

Appendix C

C.1 The DFIG test rig

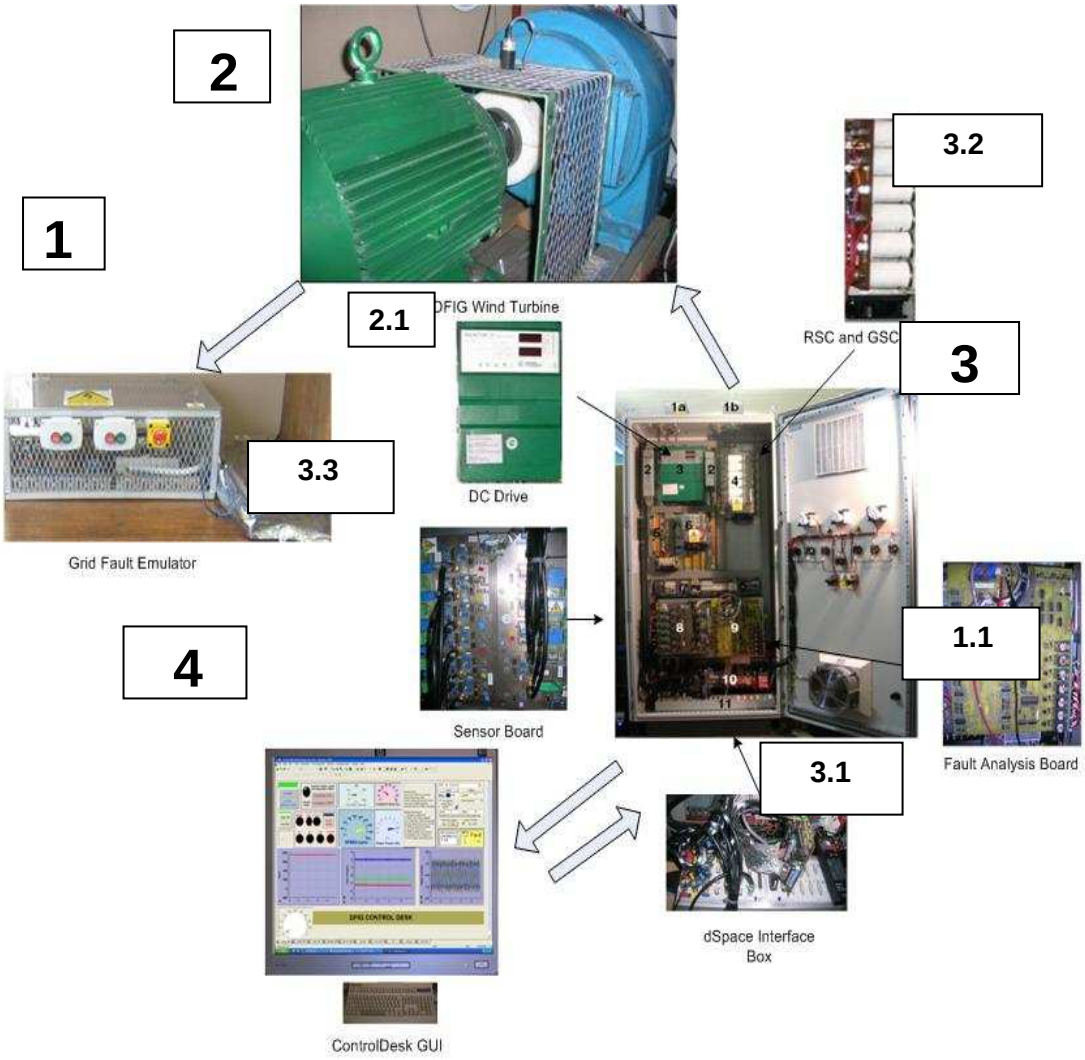

Fig.C.1 A picture of the DFIG test rig

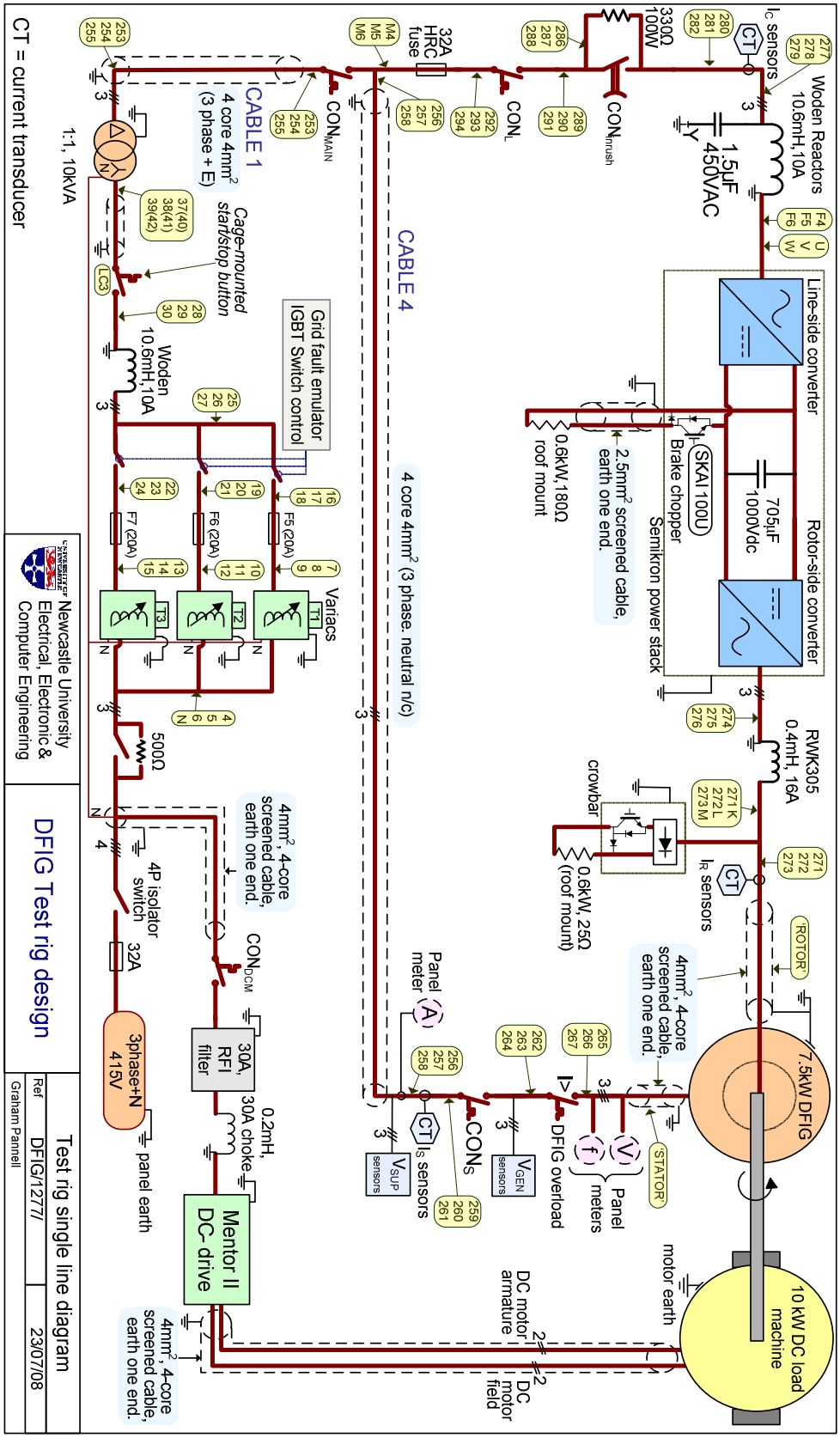

Fig.C.2 Test rig single line diagram [39]

The Test rig and pictures comprise four main elements (in Fig. C.1): a grid fault emulator (1) was defined through a fault analysis board (1.1), a wind turbine simulator (2) was controlled DC drive (2.1), a DFIG system and a control hardware assembly (3). A dSpace dS1103 controller (3.1) was used to communicate between the DFIG controller and wind turbine simulator and hardware such as converters (3.2), DC motor and DFIG (2). All signals were isolated and reduced by the sensor board (3.3) before sending to the dSpace controller. The controller was activated in real time through a GUI designed using Control desk software (4). The controller was developed using Matlab/Simulink and the code was built for operation on the dSpace control board.

The Test rig was designed and built by the research team with collaboration between Newcastle University and a British company.

Appendix D

D1. The detail Simulink diagrams of DFIG System Model

In modelling the DFIG system model, there are 9 main parts: 1) Grid-Supply Fault Model 2) DFIG Model 3) Rotor-Side Converter (RSC) 4) RSC Control System 5) Grid-Side Converter(GSC) 6) GSC Control System 7) Crowbar Model 8) DC-Brake Chopper Model and 9) Mechanical System Model, as shown in Fig.D1.

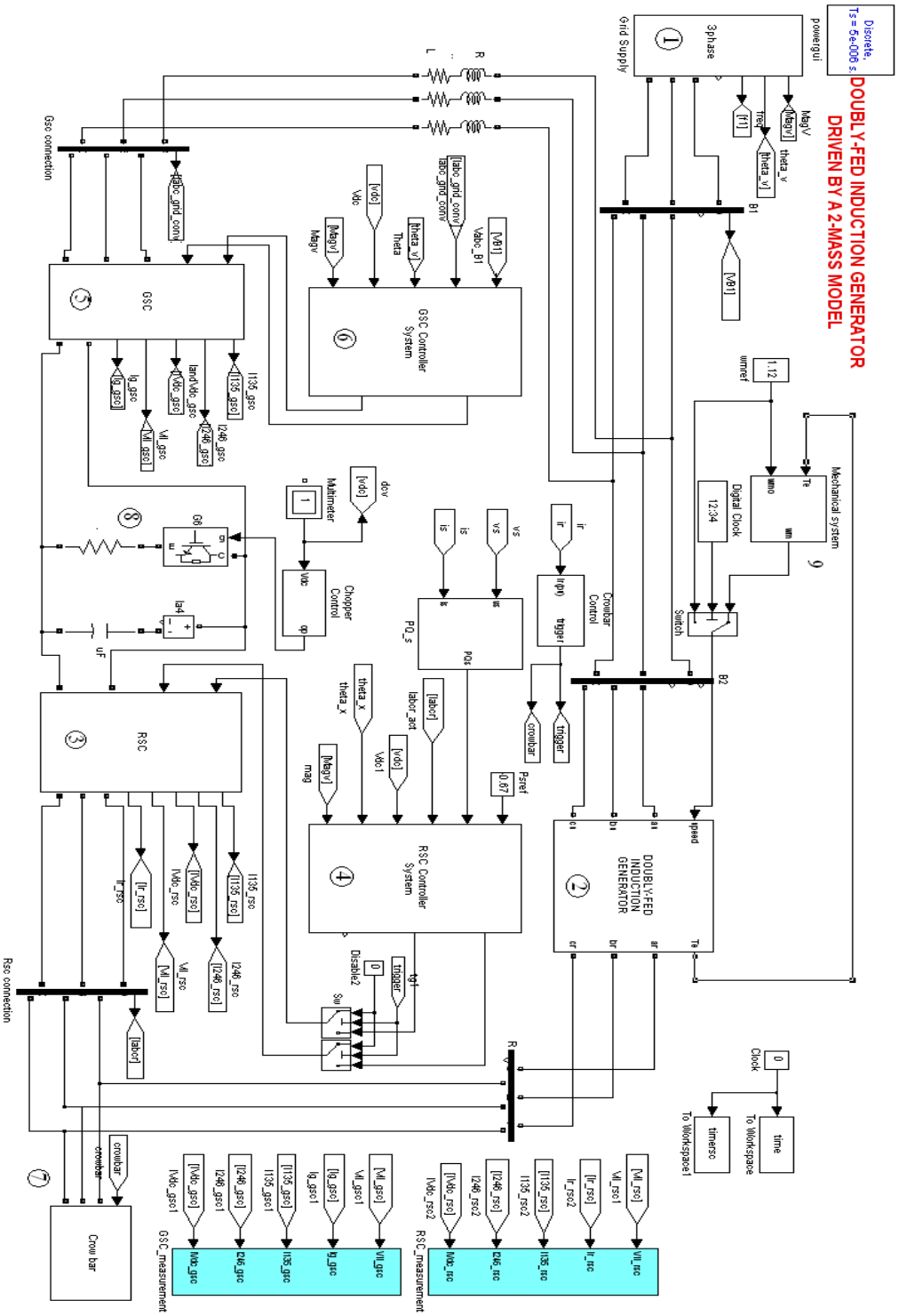

Fig. D1 Block diagram of the DFIG System Model

Sub-blocks of the model are illustrated in Fig. D2

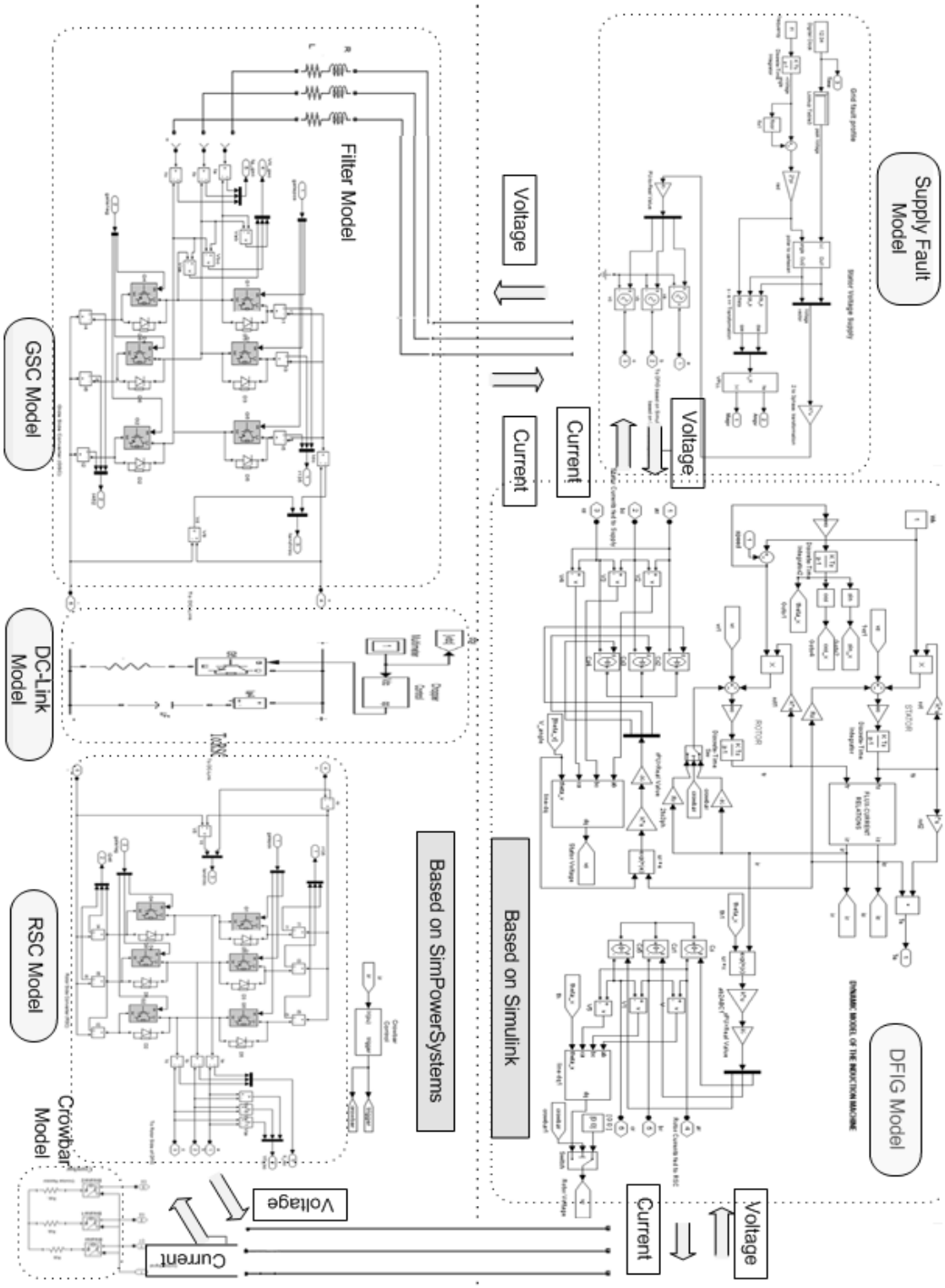

Fig.D2 Sub-blocks of the DFIG System Model

As a block diagram above, modelling of the upper two sub-block parts (Supply Fault and DFIG Model) are based on the Simulink platform while those of the lower three sub-blocks parts (GSC, DC-Link and RSC with a Crowbar) are based on he SimPowerSystems platform.

Voltage and current signals in both platforms are interactive, with voltage and current signal controlled. Details of each part are described in the following.

1. Grid Supply Fault Model

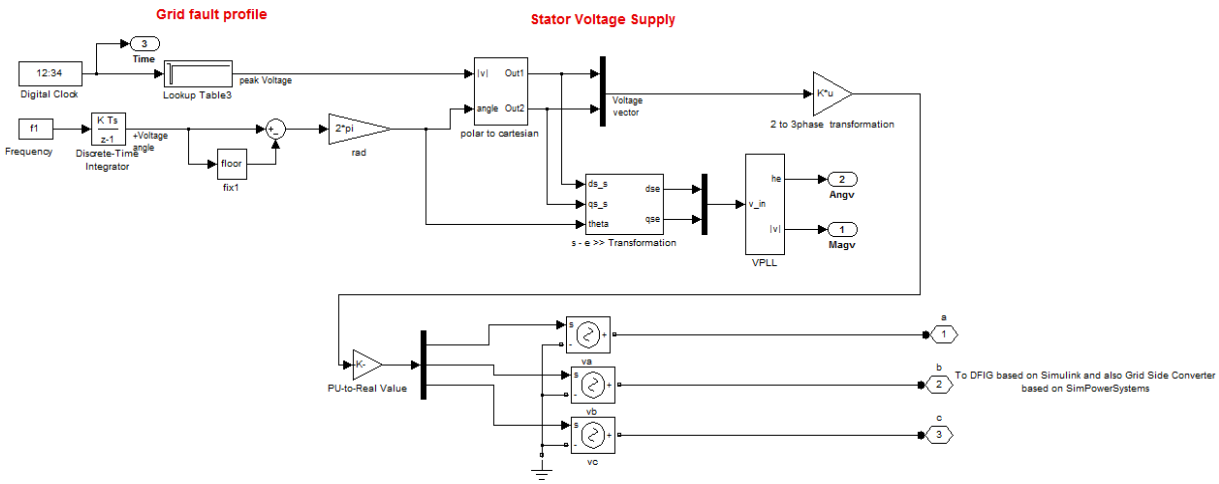

Fig.D3 Block diagram of Grid Supply Fault Model

Fig. D3 shows the grid supply model in which the magnitude of voltage is assigned in a look-up table at different times, while a voltage angle is defined by an integral of the voltage frequency. After that a supply voltage vector will be defined on the Simulink environment. In order to connect to a grid side converter modelled on SimPowerSystems platform to the supply voltage, the voltage is transformed from two to three phase. The three-phase voltage will be fed through a voltage-controlled voltage source to the stator side of DFIG and later to the grid side converter.

2. DFIG Model

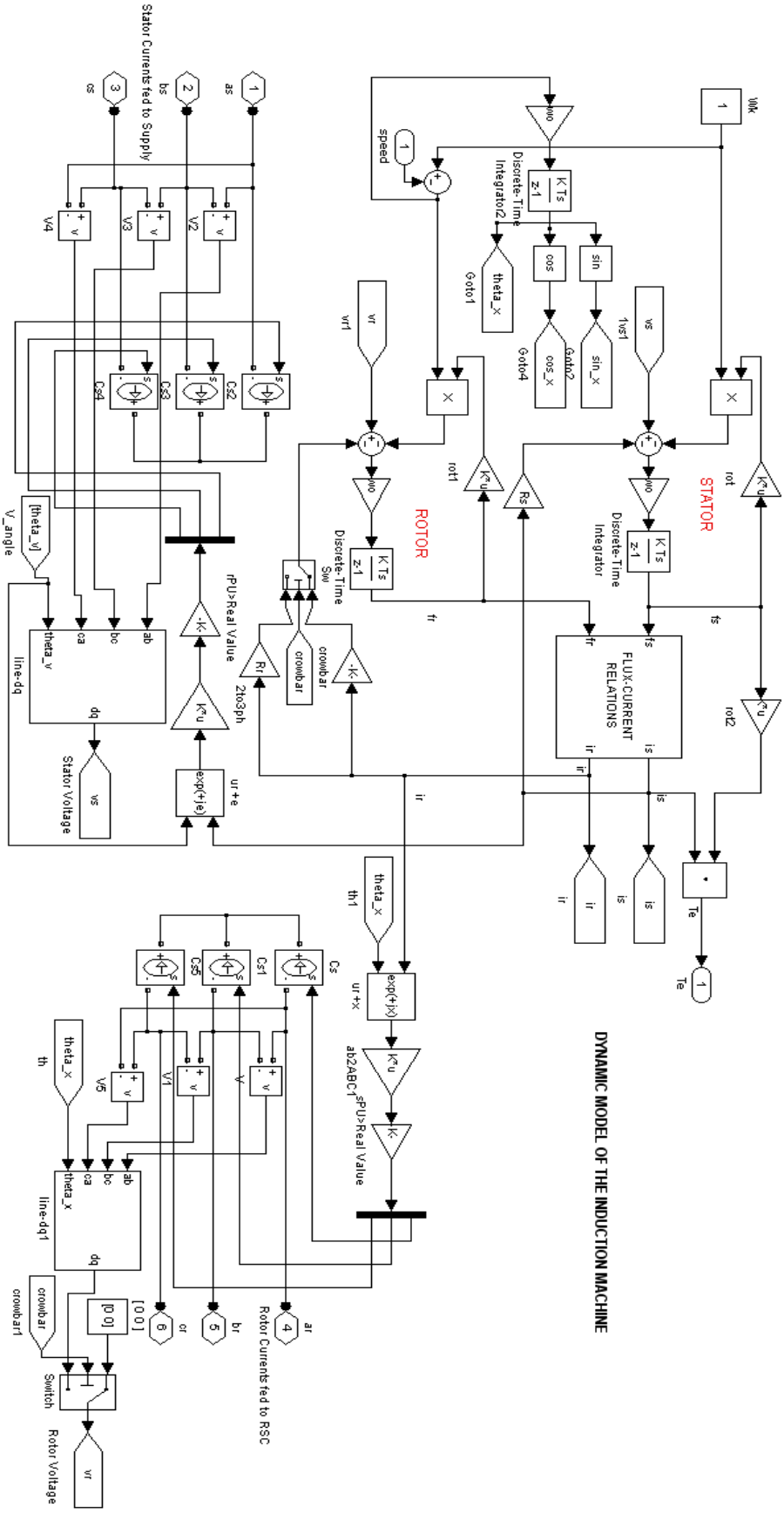

Fig.D4 Block diagram of a dynamic DFIG Model

Fig. D4 shows a dynamic DFIG model as explained in Section 3.4. Both stator voltage supply (v_s) and rotor voltage supply (v_r) in the DFIG model are supplied by grid supply and rotor side converter (RSC) respectively fed through a voltage-controlled voltage source, as shown in Fig.D4. Since the DFIG has been modelled using stator voltage vector control, both stator and rotor voltages on their natural frame are transferred to a stator-voltage vector frame using a sub-block (named as ''line-dq'') and shown in Fig.D5 and Fig.D6. As noted above, in the DFIG model the rotor-side converter is disabled during crowbar operation, while zero voltages are supplied to the rotor side.

In stator voltages, after supplying three-phase line-to-line voltage all three-phase voltages are transformed to the stator voltage reference frame of which the d-axis is aligned to the stator vector as a block diagram shown in Fig.D5.

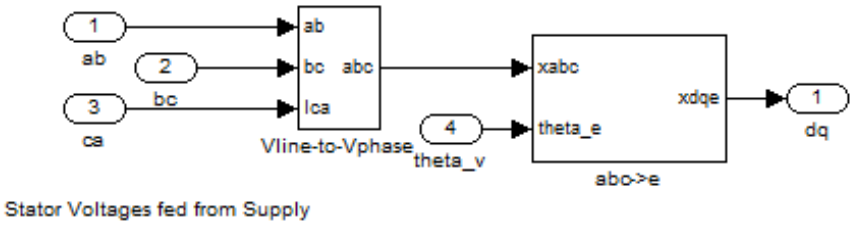

Fig. D5 Line-to-line stator voltage to dq component

While in the rotor-side of the DFIG, three-phase voltages fed from RSC are also transformed to the stator voltage reference frame of which the d-axis is aligned to the stator voltage vector as a block diagram shown in Fig.D6.

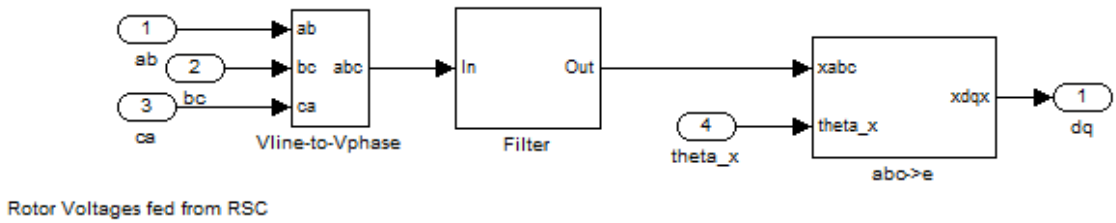

Fig. D6 Line-to-line rotor voltage to dq component

Further, during crowbar activation the rotor resistance of the DFIG (Rr) will be added to crowbar resistance (Rcb$'$) in the model, resulting in rotor resistance rise in the value of Rr+Rcb$'$. Also the rotor voltages are set to be zero (short-circuited), i.e. no rotor

voltages are supplied from RSC. As a result, only rotor currents are fed through the current-controlled current source to the crowbar and RSC based on SimPowerSystems platform as seen above in Fig D2.

3. Rotor Side Converter Model (RSC)

A three-phase PWM RSC model is composed of six IGBTs and anti-parallel diodes as shown in Fig. D7. Each IGBT and anti-parallel diode is simulated by a resistor, inductor and DC-voltage source connected in series with a switch as defined in the SimPowerSystems library. This model is suitable for simulating the fast electrical dynamics of the DFIG system.

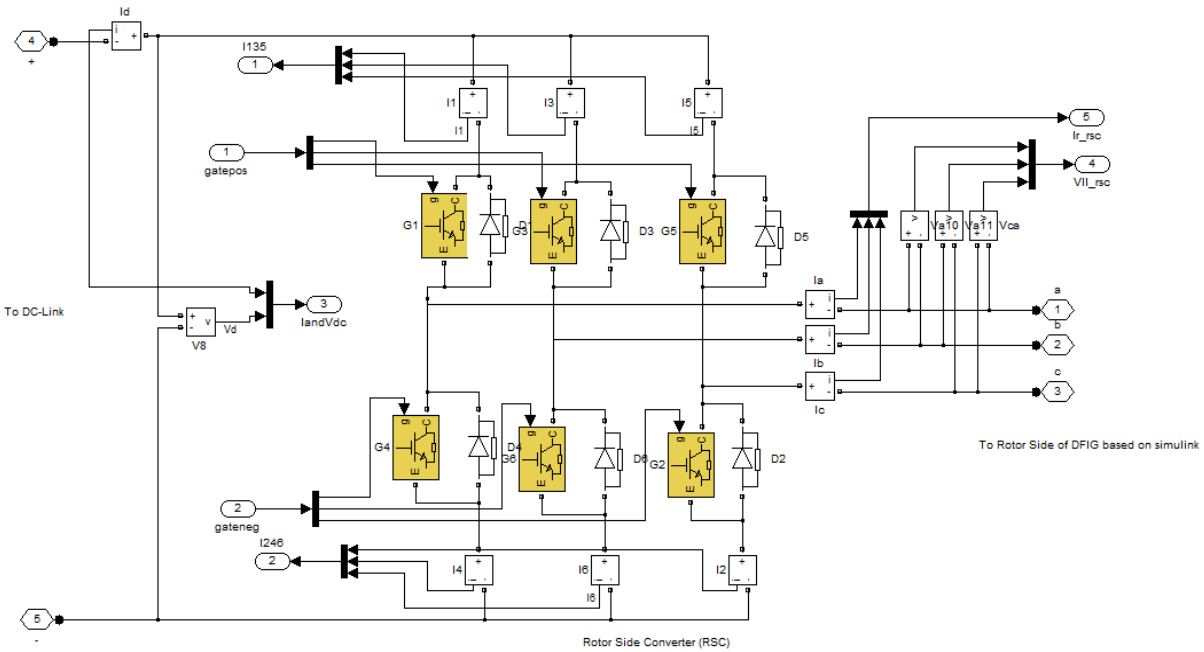

Fig. D7 A three-phase rotor side converter (RSC) model

In modelling the IGBT, their parameters are defined in the following Table.

IGBT parameter	**Value**
Snubber Resistance	1e5 Ω
Snubber Capacitance	∞
Ron	1e-3 Ω
Lon	0 H
Tf(s), Tt(s)	1e-6, 2e-6

And diode parameters are as follows:

Diode parameter	**Value**
Snubber Resistance	1e5 Ω
Snubber Capacitance	∞
Ron	1e-3 Ω
Lon	1e-6 H

4. RSC control system

As described in Chapter 3, the active and reactive stator powers of DFIG can be independently regulated by controlling the d-axis and q-axis rotor currents through the rotor side converter. Hence, to design the proper switching signals of six IGBTS, the reference power assigned by turbine characteristic, the calculated stator active and reactive powers, the rotor currents, DC-link voltage, rotor angle and stator voltage are needed for the input signals of the RSC control system as shown in Fig.D8.

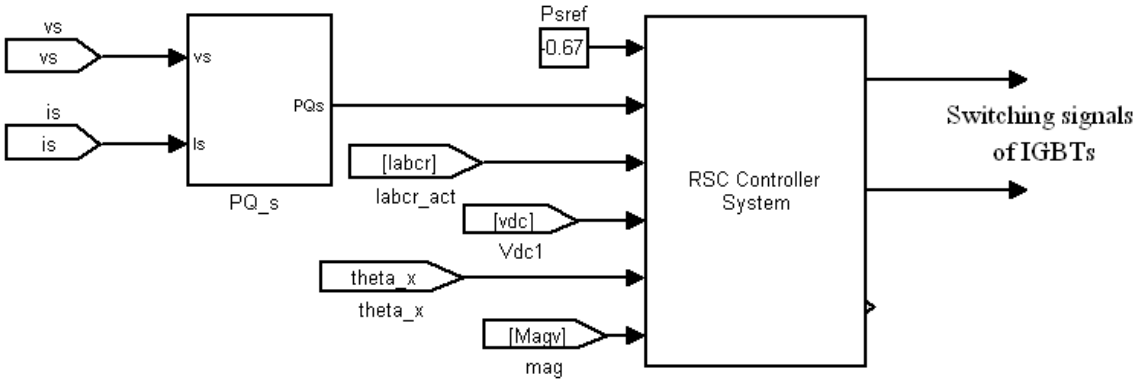

Fig. D8 A RSC control system

The reference stator active power (Psref) of 0.67pu can be calculated at the typical wind turbine speed of 1.12pu, while other values (Vs, is, ir, vdc, theta_x and MagV) will be measured and fed to the control block. Inside the RSC control system block, this can be seen in Fig. D9.

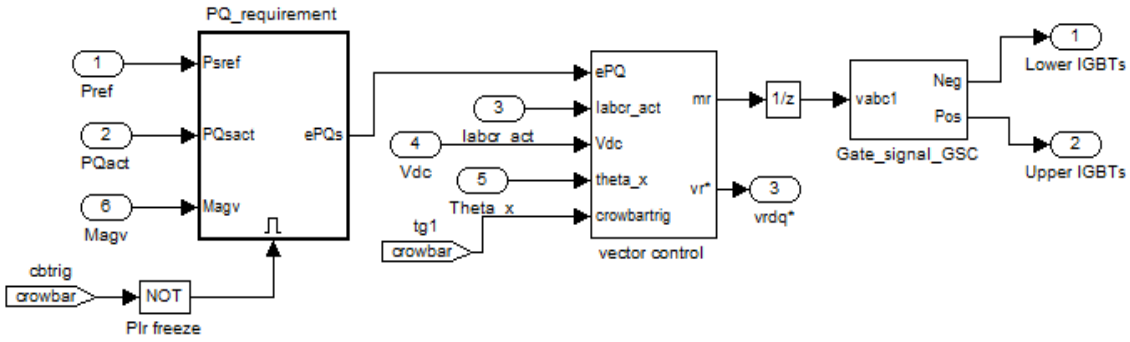

Fig.D9 A block diagram of RSC control system

The RSC control system consists of two cascaded PI controllers. The former is a stator power controller which is used to independently control stator active (P) and reactive (Q) power. While the latter is a current controller, it is used to independently control the d-axis (I_{rd}) and q-axis (I_{rq}) rotor current as shown in Fig.D10.

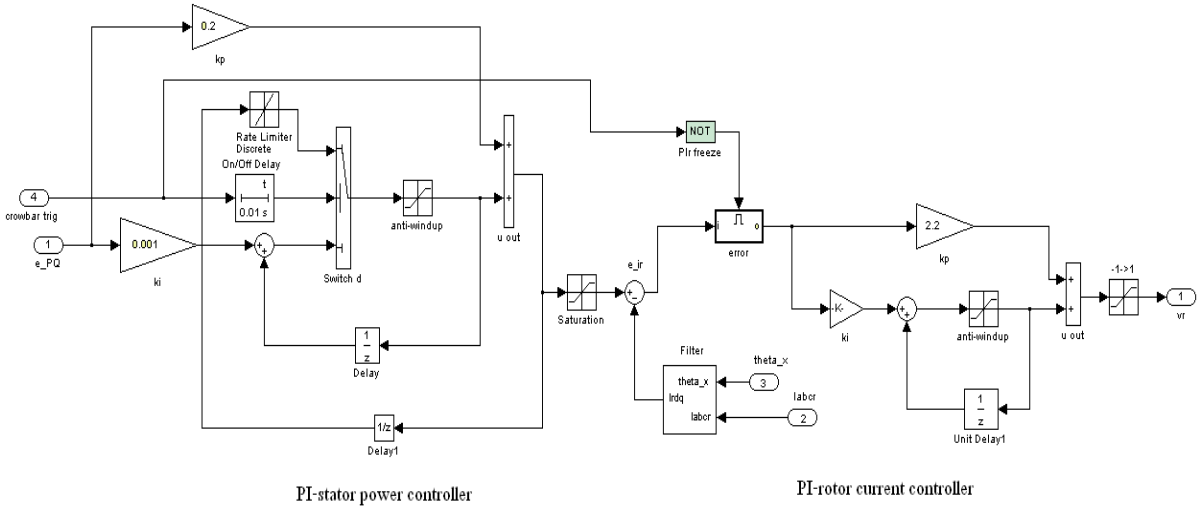

Fig.D10 A block diagram of two cascaded PI –controllers for RSC control system

Finally two cascaded PI-controllers will produce the reference value of the rotor voltage from the stator active and reactive powers error. After that the magnitude of the rotor voltage (vr) is normalised with the value of K1 and V_{dc} (see Fig.D11) and then made it in dq-component again. This voltage in dq-axis components will be transferred from a synchronous to a rotor reference frame before converting to a 3-phase signal. The IGBTs switching signal will be generated using a PWM technique as shown in Fig. D11.

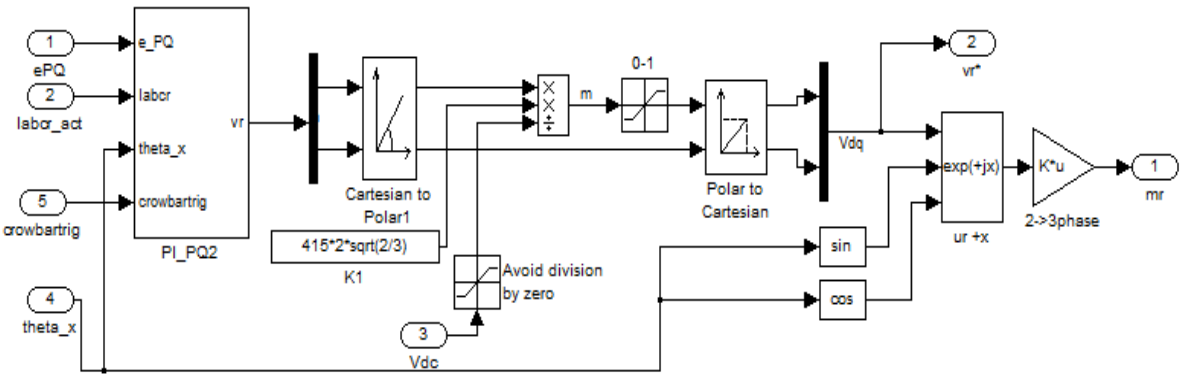

Fig.D11 A block diagram of vector control in RSC control system

During crowbar operation, two PI-controllers are frozen and the RSC control system stops working. As a result the six-IGBTs of the RSC are switched off and the RSC is unable to control active and reactive power, but the grid side converter remains in operation.

5. Grid Side Converter Model (GSC)

Like RSC, each IGBT and anti-parallel diode is simulated by a resistor, inductor and DC-voltage source connected in series with a switch as defined in the SimPowerSystems library. A three-phase PWM grid side converter (GSC) is modelled as shown in Fig.D12.

As described in Chapter 3, the DC-link voltage and grid-side reactive power of DFIG can be independently regulated by controlling the d-axis and q-axis grid side currents through the grid side converter. Hence, to design the proper switching signals of six IGBTS, the grid-side currents, DC-link voltage, rotor angle, stator voltage and grid-side voltage are needed for the input signals of the GSC control system as shown in Fig.D13.

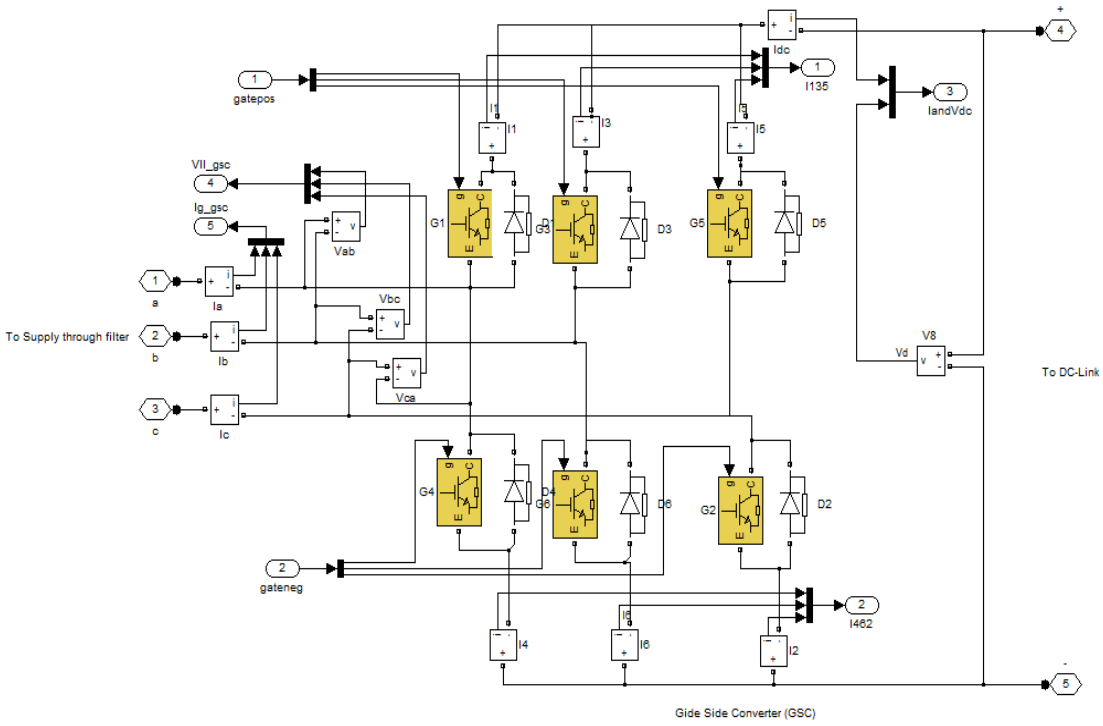

Fig. D12 A block diagram of the GSC model

6. GSC control system

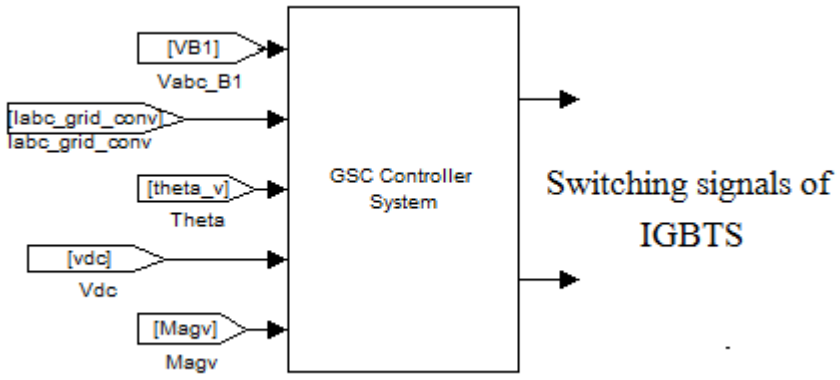

Fig.D13 A block diagram of the GSC control system model

The reference DC-link voltage (V_{dcref}) of 1 pu can be calculated at the nominal DC-link voltage at 750V, while the reference grid-side reactive power is equal to zero during normal condition and then changed to the corresponding value of the grid code requirement during fault condition. Moreover, other values are measured and fed to the control block. Inside the GSC control system block, this can be seen in Fig. D14.

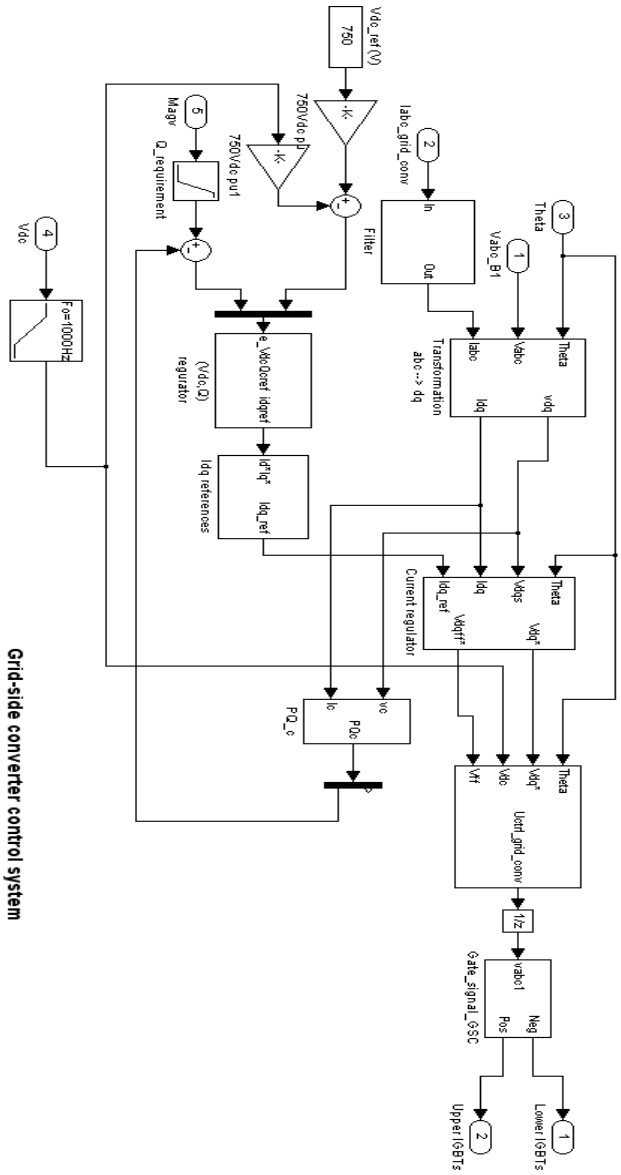

Fig.D14 A block diagram of vector control in GSC control system

There are two cascade PI-controllers in GSC control. The former PI-controller will produce the reference value for the grid-side converter currents from the DC-link voltage and grid-side reactive powers error. After that the error between the reference and measured value of the grid-side converter current is regulated by using the latter PI-controller in order to generate grid-side voltage signal for IGBTs switching.

7. A Crowbar Model

As mentioned in Section D2, during crowbar activation, the rotor resistance of the DFIG (Rr) will be added with crowbar resistance (Rcb) in the DFIG model based on Simulink, resulting in rotor resistance rise in the value of Rr+Rcb'. Also the rotor voltages are set to be zero (short-circuited), i.e. no rotor voltage is supplied from the RSC. At the same time, in a separate model based on SimPowerSystems, the three-phase y-connected crowbar resistor(Rcb'), explained in Section 3.6, is activated by the Breaker Switch as shown in Fig. D15. As a result, only rotor currents from the DFIG model in Section D2 will be fed through current-controlled current source to the crowbar and RSC; based on the SimPowerSystems platform.

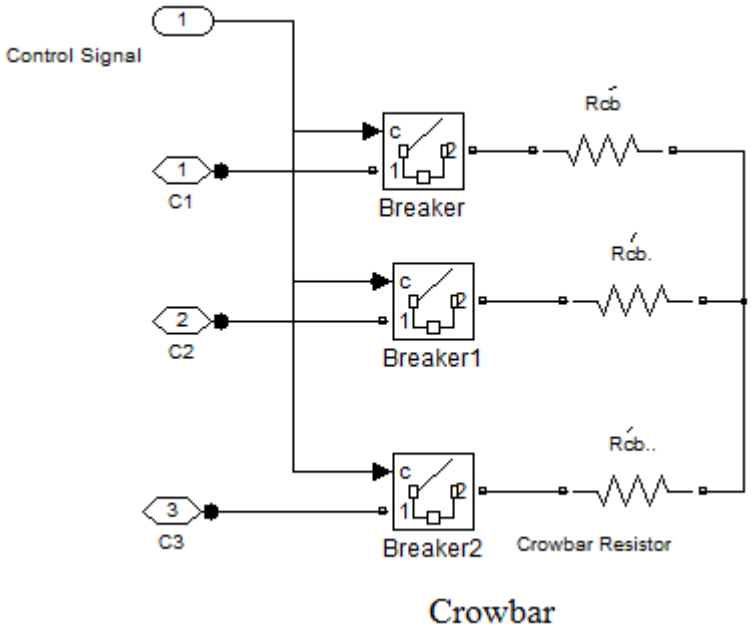

Fig. D15 A three-phase y-connected crowbar

The breaker switch is activated by a trigger signal from the crowbar control system block, as shown in Fig D16. In crowbar activation, whenever the magnitude of the rotor current reaches the threshold value of 2 pu, the crowbar resistor is connected to protect the RSC from rotor over-currents. In the meantime the RSC is stopped to control the active and reactive power of the DFIG, resulting in short-circuiting the rotor side of the DFIG through the crowbar resistance (Rcb').

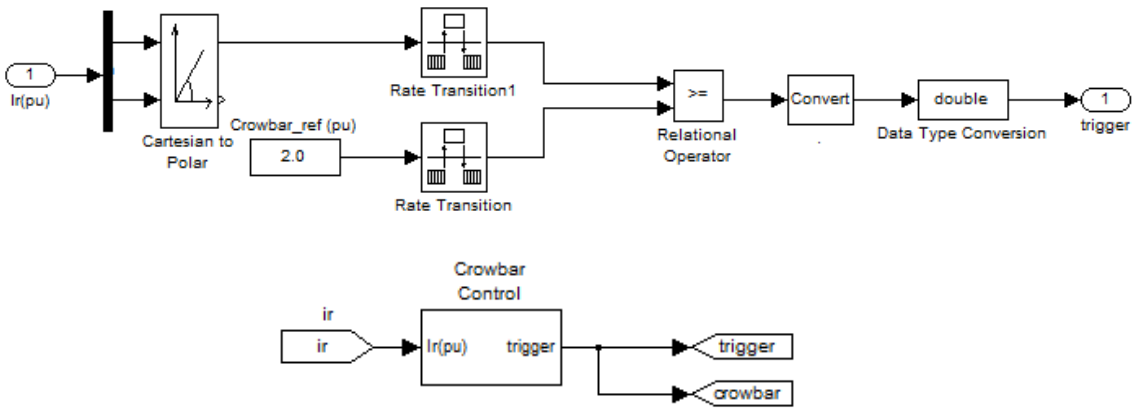

Fig. D16 Crowbar control system

8. DC-break chopper model

As reviewed in Chapter 1, the combined scheme of having a crowbar and DC-break chopper is needed for the best FRT capability of the DFIG. In the DC-break chopper model based on SimPowerSystems platform, a break resistor in series with a controlled switch is used to protect the DC-link capacitor as illustrated in Fig.D17. When DC-link voltage rise reaches the threshold value of 1.08 pu, the DC-break chopper is activated. The DC-break chopper control block is shown in Fig. D18.

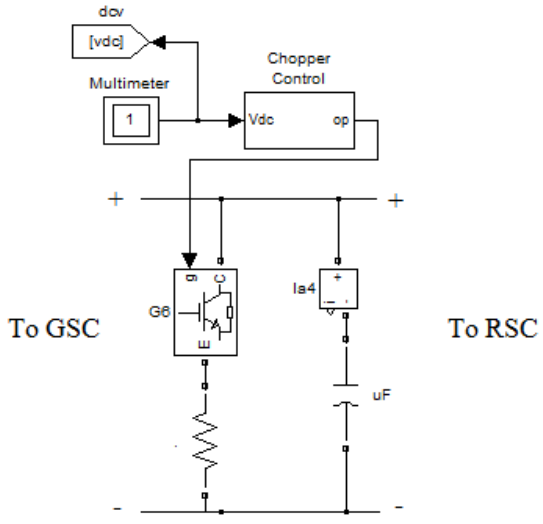

Fig. D17 DC-break chopper

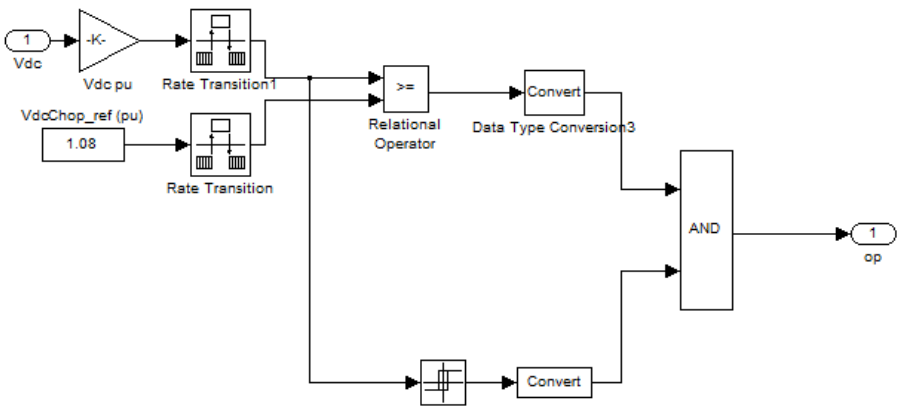

Fig. D18 DC-break chopper control

The brake chopper is automatically set to operate above the upper threshold value of 810V (1.08pu) and to disconnect below the lower threshold level of 795V (1.06pu) regarding the DC link voltage by using a hysteresis control block.

9. Drive train system model

As mentioned in Section 3.1, the wind speed is constant in FRT study and the drive train system of wind turbine is represented as a two-mass model.
Accordingly, the modelled wind speed and active stator power demand are assumed constant in the fault simulations. For the purposes of investigating the DFIG FRT capability, the single generating point of typical wind turbine curves is chosen as a typical normal operating condition in generating power of 0.67 pu at a wind speed of 10 m/s.

The turbine torque (TL) is provided by a PI-speed controller, while the generator torque (Te) is generated by the DFIG for the demands of the two-mass model. The model is composed of turbine mass and generator mass which are connected by a shaft that has a certain stiffness coefficient (Km) and damping constant (Dm) values, as shown in Fig. D19.

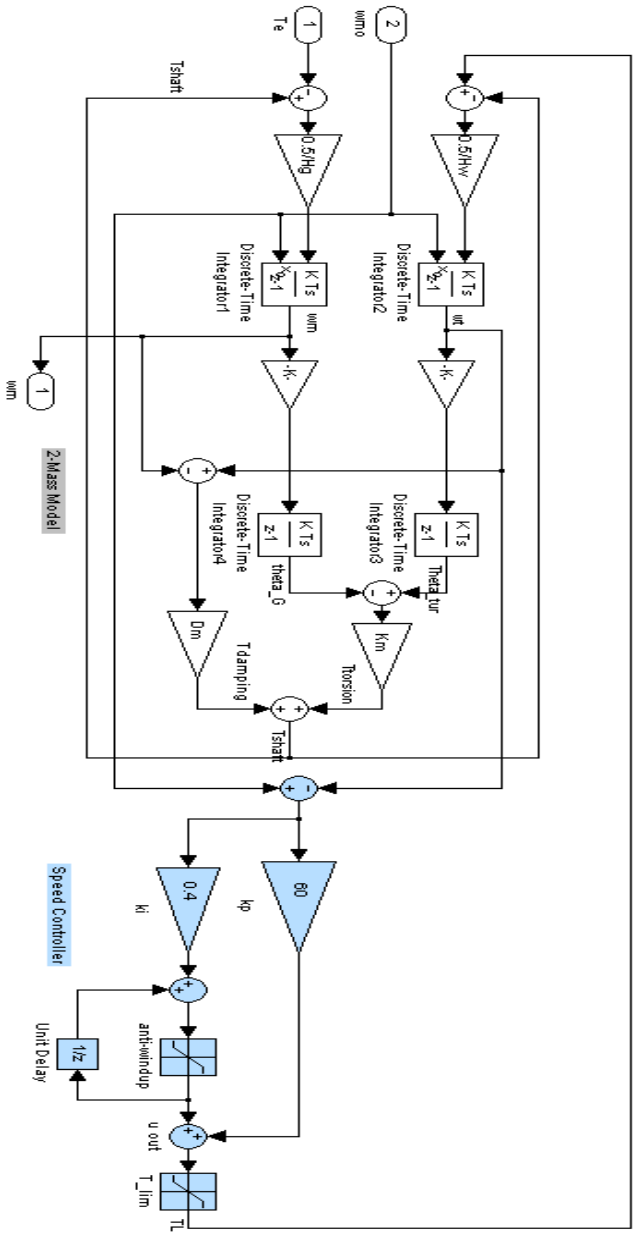

Fig. D19 Drive train system model

References

[1] J. G. Slootweg, H. Polinder, and W. L. Kling, "Dynamic Modelling of a wind Turbine with Doubly Fed Induction Generator," in *IEEE Power Engineering Society Summer Meeting, Vols 1, Conference Proceedings*, vol. 1, 2001, pp. 644-649.

[2] The Global Wind Energy Council, "The Global Wind Report ", 2015.

[3] The REN21 network, "The Renewables 2016 Global Status Report," 2016.

[4] M. Tsili and S. Papathanassiou, "A review of grid code technical requirements for wind farms," *IET Renewable Power Generation.* , vol. 3, pp. 308-332, 2009.

[5] S. Tohidi and M. Behnam, "A Comprehensive Review of Low Voltage Ride Through of Doubly Fed Induction Wind Generators," *Sciencedirect Journal on Renewable and Sustainable Energy Reviews* vol. 57, pp. 412-419, 2016.

[6] P. C. Krause, O. Wasynczuk, and M. S. Hildebrandt, "Reference frame analysis of a slip energy recovery system," *IEEE Transactions on Energy Conversion*, vol. 3, pp. 404-408, 1988.

[7] S. Muller, M. Deicke, and R. W. De Doncker, "Doubly fed induction generator systems for wind turbines," in *IEEE Industry Applications Magazine*, vol. 8, 2002, pp. 26-33.

[8] W. Leonhard, *Control of Electrical Drives*, 3rd ed. Belin: Springer, 2001.

[9] I. Serban, F. Blaabjerg, I. Boldea, and Z. Chen, "A study of the Doubly-Fed Wind Power Generator Under Power System," in *2003 EPE Power Electronics and Applications, 10th European Conference Proceedings*, 2003, pp. 1-10.

[10] R. Pena, J. C. Clare, and G. M. Asher, "A doubly fed induction generator using back-to-back PWM converters supplying an isolated load from a variable speed wind turbine," *Electric Power Applications, IEE Proceedings*, vol. 143, pp. 380-387, 1996.

[11] T. Ackermann, *Wind power in power systems*. Chichester, West Sussex, England ; Hoboken, NJ: John Wiley, 2005.

[12] A. Petersson, S. Lundberg, and T. Thiringer, "A DFIG Wind Turbine Ride-through system.," *Wind Energy*, pp. 251-263, 2005.

[13] J. Serrano-Gonzalez and R. Lacal-Arantegui, "Technological evolution of onshore Wind Tubines -a market-based analysis," *Wind Energy*, 2016.

[14] H. T. Mokui, M. A. S. Masoum, and M. Mohseni, "Review on Australian Grid Codes for Wind Power Integration in Comparison with International Standards," in *AUPEC'14, Perth.* , 2014, pp. 1-11.

[15] M. Tsili, S. Papathanassiou, G. Georgantzis, and G. Antonopoulos, "Grid code requirements for large wind farms: A review of technical regulations and available wind turbine technologies," in *Proc. EWEC'08, Brussels.* , 2008, pp. 1-11.

[16] The EirGrid Grid Code, "Version5.0 October 2013, EirGrid ", 2013.

[17] The Grid Code, "Issue 3, Revision 32, December 2008, National Grid Electricity Transmission plc," 2008.

[18] The Grid Code, "Status1 April 2006, E.ON Netz GmbH, Bayreuth," 2006.

[19] V. Akhmatov, "Analysis of Dynamic Behaviour of Electric Power Systems with Large Amount of Wind Power," PhD Thesis, Technical University of Denmark, 2003.
[20] J. Yang, J. E. Fletcher, and J. O'Reilly, "A Series-Dynamic-Resistor-Based Converter Protection Scheme for Doubly-Fed Induction Generator During Various Fault Conditions," *IEEE Transactions on Energy Conversion*, vol. 25, pp. 314-323, 2010.
[21] J. Yang, D. G. Dorrell, and J. E. Fletcher, "A New Converter Protection Scheme for Doubly-Fed Induction Generators during Disturbances," presented at the 34th IEEE International Conference on Industrial Electronics, 2008.
[22] C. Laxmi, K. S. Latha, and Himani, "Improving the low voltage ride through capability of wind generator system using crowbar and battery energy storage system," *International Journal of Engineering Science Invention*, vol. 2, pp. 14-19, 2013.
[23] S. Li, Y. Sun, T. Wu, L. Y., X. Yu, and J. Zhang, "Analysis of Low Voltage Ride Through Capability in Wind Turbine based on DFIG," presented at International Conference on Electrical and Control Engineering 2010.
[24] M. Wang, W. Xu, H. Jia, and X. Yu, "A New Method for DFIG Fault Ride Through Using Resistance and Capacity Crowbar Circuit," presented at the IEEE International Conference on Industrial Technology, 2013.
[25] M. Bongiorno and T. Thiringer, "A Generic DFIG Model for Voltage Dip Ride-Through Analysis," *IEEE Transactions on Energy Conversion*, vol. 28, pp. 76-85, 2013.
[26] C. Niu and C. Liu, "The Requirements and Technical Analysis of Low Voltage Ride Through for the Doubly-Fed Induction Wind Turbines," *Sciencedirect Journal on Energy Procedia*, vol. 12, pp. 799-807, 2011.
[27] J. Tande, E. Muljadi, O. Carlson, and J. Pierik, "Dynamic models of wind farms for power system studies-status by IEA Wind R&D Annex 21," presented at European Wind Energy Conference&Exhibition (EWEC)2004, London, 2004.
[28] I. Erlich, H. Wrede, and C. Feltes, "Dynamic Behavior of DFIG-Based Wind Turbines during Grid Faults," in *Power Conversion Conference, Nagoya 2007.* , 2007, pp. 1195-1200.
[29] J. B. Ekanayake, L. Holdsworth, X. G. Wu, and N. Jenkins, "Dynamic modeling of doubly fed induction generator wind turbines," *IEEE Transactions on Power Systems*, vol. 18, pp. 803-809, 2003.
[30] P. Ledesma and J. Usaola, "Doubly Fed Induction Generator Model for Transient Stability Analysis," *IEEE Transactions on Energy Conversion*, vol. 20, pp. 388-397, 2005.
[31] L. Holdsworth, X. G. Wu, J. Ekanayake, and N. Jenkins, "Comparison of fixed speed and doubly-fed induction wind turbines during power system disturbances," *IEE Proceeding on Generation, Transmission and Distribution*, vol. 150, pp. 343-352, 2003.
[32] G. Tapia and A. Tapia, "Wind generation optimisation algorithm for a doubly fed induction generator," *IEE Proceedings-Generation, Transmission and Distribution*, vol. 152, pp. 253-263, 2005.
[33] E. Muljadi and C. P. Butterfield, "Pitch-Controlled Variable-Speed Wind Turbine Generation," *IEEE Transactions on Industry Application*, vol. 37, pp. 240-246, 2001.
[34] A. Tapia, G. Tapia, X. Ostolaza, and J. R. Sa'enz, "Modeling and Control of a Wind Turbine Driven Doubly Fed Induction Generator," *IEEE Transactions on Energy Conversion*, vol. 18, pp. 194-204, 2003.

[35] H. Kundsen and J. N. Nielsen, "Introduction to the Modelling of Wind Turbines," in *Wind power in power systems*, T. Ackermann, Ed. Chichester, West Sussex, England ; Hoboken, NJ: John Wiley, 2005, pp. xlvii, 691.
[36] J. Tamura and T. Yamazaki, "Transient Stability Simulation of Power System Including Wind Generator by PSCAD/EMTDC," in *IEEE Porto Power Tech Conference, IEEE 2001.* . Porto, Portugal, 2001.
[37] A. D. Hansen and G. Michalke, "Fault ride-through capability of DFIG wind turbines," *Renewable Energy*, vol. 32, pp. 1594-1610, 2007.
[38] M. A. Poller, "Doubly-fed induction machine models for stability assessment of wind farms," presented at Power Tech Conference Proceedings, 2003 IEEE Bologna, 2003.
[39] G. Pannell, "Grid Fault Ride Through for Wind Turbine Doubly-Fed Induction Generators," EngD Thesis, University of Newcastle upon Tyne, 2008.
[40] Y. A. Kazachkov, J. W. Feltes, and R. Zavadil, "Modeling Wind Farms for Power System Stabilty Studies," *IEEE Transactions on Power Systems*, vol. 20, pp. 1526-1533, 2003.
[41] G. Zhang and J. Furusho, "Speed Control of Two-Inertia System by PI/PID Control," *IEEE Transactions on Industrial Electronics*, vol. 47, pp. 603-609, 2000.
[42] S. K. Salman and A. L. J. Teo, "Windmill Modeling Consideration and Factors Influencing the Stability of a Grid-Connected Wind Power-Based Embedded Generator," *IEEE Transactions on Power Systems*, vol. 18, pp. 793-802, 2003.
[43] J. Marques, H. Pinheiro, H. Grundling, J. Pinheiro, and H. Hey, "A survey on variable-speed wind turbine system," in *Brazilian Conference of electronics of power*, 2003, pp. 732-738.
[44] G. Ramtharan, N. Jenkins, O. Anaya-Lara, and E. Bossanyi, "Influence of Rotor Structural Dynamics Representations on the Electrical Transient Performance of FSIG and DFIG Wind Turbines," *Wind Energy*, pp. 293-301, 2007.
[45] G. Michalke and A. D. Hansen, "Modelling and Control of Variable Speed Wind Turbines for Power System Studies," *Wind Energy*, pp. 1-19, 2009.
[46] J. G. Slootweg and W. L. Kling, "Modeling of large wind farms in power system simulations," in *Power Engineering Society Summer Meeting, IEEE 2002.* , 2002, pp. 503-508.
[47] T. Lei, M. Barnes, and M. Ozakturk, "Doubly-fed induction generator wind turbine modelling for detailed electromagnetic system studies," *IET Renewable Power Generation.* , vol. 7, pp. 180-189, 2013.
[48] S. A. Papathanassiou and M. P. Papadopoulos, "Dynamic Behavior of Variable Speed Wind Turbines under Stochastic Wind," *IEEE Transactions on Energy Conversion*, vol. 14, pp. 1617-1623, 1999.
[49] F. M. Hughes, O. Anaya-Lara, N. Jenkins, and G. Strbac, "A power system stabilizer for DFIG-based wind generation," *IEEE Transactions on Power Systems*, vol. 21, pp. 763-772, 2006.
[50] A. D. Hansen, C. Jauch, P. Sorensen, F. Iov, and F. Blaabjerg, "Dynamic Wind Turbine Models in Power System Simulation Tool," Report 2003.
[51] J. Usaola, P. Ledesma, J. M. Rodriguez, J. L. Fernandez, D. Beato, R. Iturbe, and J. R. Wilhelmi, "Transient stability studies in grids with great wind power penetration. Modelling issues and operation requirements," in *IEEE Power Engineering Society General Meeting,* , vol. 1, 2003, pp. 644-649.
[52] N. Mohan, T. M. Undeland, and W. P. Robbins, *Power Electronics: Converters, Applications and Design*, 2003.

[53] T. Burton, D. Sharpe, N. Jenkins, and E. Bossanyi, *Wind Energy Handbook*: John Wiley & Son Ltd., , 2001.
[54] J. Tande, "Applying Power Quality Characteristics of Wind Turbines for Assessing Impact on Voltage Quality," *Wind Energy*, vol. 5, pp. 37-52, 2002.
[55] G. R. Slemon, "Modelling of Induction Machines for Electric Drives " *IEEE Transactions on Industry Applications* vol. 25, pp. 1126-1131, 1989.
[56] P. Kundur, N. J. Balu, and M. G. Lauby, *Power system stability and control*. New York: McGraw-Hill, 1994.
[57] P. Vas, *Sensorless Vector and Direct Torque Control*: Oxford science publications, 1998.
[58] I. Boldea and S. A. Nasar, *Electric Drives*, Second ed: CRC Press LLC, 1999.
[59] B. K. Bose, "High performance control and estimation in AC drives," in *International conference on Industrial Electronics, Control and Instrumentation*, 1997, pp. 377-385 Vol.2.
[60] D. J. Atkinson, R. A. Lakin, and R. Jones, "A vector-controlled doubly-fed induction generator for a variable-speed wind turbine application," *Trans. Inst. Meas. Contr.*, vol. 19, pp. 2-12, 1997.
[61] B. Hopfensperger, D. J. Atkinson, and R. A. Lakin, "Stator-flux-oriented control of a doubly-fed induction machine with and without position encoder," *IEE Proceedings-Electric Power Applications*, vol. 147, pp. 241-250, 2000.
[62] M. Kayikçi and J. V. Milanovic´, "Assessing Transient Response of DFIG-Based Wind Plants-The Influence of Model Simplifications and Parameters," *IEEE Transactions on Power Systems*, vol. 23, pp. 545-554, 2008.
[63] F. Wu, X. Zhang, K. Godfrey, and P. Ju, "Modeling and Control of Wind turbine with Doubly Fed Induction Generator," presented at IEEE PES Power systems conference and Exposition (PSCE), 2006.
[64] N. P. Quang, A. Dittrich, and A. Thieme, "Doubly-fed induction machine as generator: control algorithms with decoupling of torque and power factor," *Electrical Engineering*, pp. 325-335, 1997.
[65] L. Morel, H. Godfroid, A. Mirzaian, and J. M. Kauffmann, "Doubly- fed induction machine: converter optimisation and field oriented control without position sensor," *Electric Power Applications, IEE Proceedings*, pp. 360-368, 1998.
[66] B. H. Chowdhury and S. Chellapilla, "Double-fed induction generator control for variable speed wind power generation," *Electric Power Systems Research*, vol. 76, pp. 786-800, 2006.
[67] L. SÖder and T. Ackermann, "Wind power in power systems: An Introduction," in *Wind power in power systems*, T. Ackermann, Ed. Chichester, West Sussex, England ; Hoboken, NJ: John Wiley, 2005, pp. xlvii, 691.
[68] C. C. Johnson and R. T. Smith, "Dynamics of Wind Generators on Electric Utility Networks " *IEEE Transactions on Aerospace and Electronic Systems* vol. AES-12, pp. 483-493, 1976.
[69] O. Wasynczuk, D. T. Man, and J. P. Sullivan, "Dynamic Behavior of a Classof Wind Turbine Generators during Random Wind Fluctuations " *IEEE Transactions on Power Apparatus and Systems*, vol. PAS-100, pp. 2837-2845, 1981.
[70] S. B. Crary, "Two-Reaction Theory of Synchronous Machines," *Transactions of the American Institute of Electrical Engineers*, vol. 56, pp. 27-36, 1937.
[71] B. Adkin, "Transient theory of synchronous generators connected to power systems," *Proceedings of the IEE-Part II: Power Engineering*, vol. 98, pp. 510-523, 1951.

[72] Z. M. Salameh and L. F. Kazda, "Commutation Angle Analysis of a Double-Output Induction Generator Using a Detailed d-q Model " *IEEE Transactions on Power Apparatus and Systems*, vol. PAS-104, pp. 512-518, 1985.
[73] P. C. Krause, "The Method of Symmetrical Components Derived by Reference Frame Theory " *IEEE Transactions on Power Apparatus and Systems*, vol. PAS-104, pp. 1492-1499, 1985.
[74] B. K. Bose, "Energy, Environment, and Advences in Power Electronics," *IEEE Transactions on Power Electronics*, vol. 15, pp. 688-701, 2000.
[75] A. Feijo´o, J. Cidra´s, and C. Carrillo, "A third order model for the doubly-fed induction machine," *Electric Power Systems Research*, pp. 121-127, 2000.
[76] J. G. Slootweg, S. W. H. de Hanan, H. Polinder, and W. L. Kling, "Modeling wind Turbines in Power System Dynamics Simulations," in *2001 Ieee Power Engineering Society Summer Meeting, Vols 1, Conference Proceedings*, vol. 1, 2001, pp. 22-26.
[77] J. B. Ekanayake, L. Holdsworth, X. G. Wu, and N. Jenkins, "Comparison of 5th order and 3rd order machine models of doubly fed induction generator(DFIG) wind turbines," *Electric Power Systems Research*, vol. 67, pp. 207-215, 2003.
[78] T. Thiringer and J. Luomi, "Comparison of Reduced-Order Dynamic Models of Induction Machines," *IEEE Transactions on Power Systems*, vol. 16, pp. 119-126, 2001.
[79] M. G. Garcı´a-Gracia, M. P. Comech, J. Salla´ n, and A. Llombar, "Modelling Wind Farms for Grid Distribance Studies," Technical Note 1 February 2008.
[80] T. Petru and T. Thiringer, "Modeling of Wind Turbines for Power System Studies," *IEEE Transactions on Power Systems*, vol. 17, pp. 1132-1139, 2002.
[81] D. Xie, Z. Xu, L. Yang, J. Ostergaard, Y. Xue, and K. P. Wong, "A Comprehensive LVRT Control Strategy for DFIG Wind Turbines With Enhanced Reactive Power Support," *IEEE Transactions on Power Systems*, vol. 28, pp. 3302-3310, 2013.
[82] C. Knowles-Spittle, B. Zahawi, and N. D. MacIsaac, "A doubly fed induction generator using back-to-back PWM converters supplying an isolated load from a variable speed wind turbine," presented at Power Electronics and Variable Speed Drives, IEE Proceedings, 1998.
[83] J. A. Baroudi, V. Dinavahi, and A. M. Knight, "A review of power converter topologies for wind generators," *Renewable Energy*, pp. 2369-2386, 2007.
[84] I. Erlich, J. Kretschmann, S. Mueller-Engelhardt, F. Koch, and J. Fortmann, "Modeling of Wind Turbines based on Doubly-Fed Induction Generators for Power System Stability Studies," presented at Power and Energy Society General Meeting- Conversion and Delivery of Electrical Energy in the 21st Century, 2008.
[85] J. Kretschmann, H. Wrede, S. Mueller-Engelhardt, and I. Erlich, "Enhanced Reduced Order Model of Wind Turbines with DFIG for Power System Stability Studies," in *International Conference on Power and Energy* Putrajaya, Malaysia, 2006, pp. 1195-1200.
[86] S. Yang, Y. Wu, H. Lin, and W. Lee, "Integrated Mechanical and Electrical DFIG Wind Turbine Model Development," *IEEE Transactions on Industry Applications* vol. 50, pp. 2090-2102, 2014.
[87] S. K. Salman, B. Badrzadeh, and J. Penman, "Modelling wind turbine-generators for fault ride-through studies," presented at 39th International Universities Power Engineering Conference, 2004.

[88] B. Xie, B. Fox, and D. Flynn, "Modelling wind turbine-generators for fault ride-through studies," presented at IEEE International Conference on Electric Utility Deregulation, Restructuring and Power Technologies, 2004.
[89] H. A. Mohammadpour and E. Santi, "Modeling and Control of Gate-Controlled Series Capacitor Interfaced With a DFIG-Based Wind Farm," *IEEE Transactions on Industrial Electronics*, vol. 62, pp. 1022-1033, 2015.
[90] T. Lei, M. Barnes, S. Smith, S. Hur, A. Stock, and W. E. Leithead, "Using Improved Power Electronics Modeling and Turbine Control to Improve Wind Turbine Reliability," *IEEE Transactions on Energy Conversion*, vol. 30, pp. 1043-1051, 2015.
[91] "Measurement and assessment of power quality characteristics of grid connected wind turbines : IEC 61400-21," International, Electrotechnical Commission (IEC) wind turbine standard, 1999.
[92] G. Pannell, D. J. Atkinson, and B. Zahawi, "Minimum-Threshold Crowbar for a Fault-Ride-Through Grid-Code-Compliant DFIG Wind Turbine," *IEEE Transactions on Energy Conversion*, vol. 25, pp. 750-759, 2010.
[93] M. Godoy and F. A. Farret, *Alternative Energy Systems: Design and Analysis with Induction Generators*, Second ed: CRC Press and Taylor&Francis Group, 2008.
[94] J. C. Ausin and D. N. Gevers, "Fault Ride-through Capability Test Unit for Wind Turbines," *Wind Energy*, vol. 11, pp. 3-12, 2007.
[95] L. MihePopa, F. Blaabjerg, and I. Boldea, "Wind Turbine Generator Modeling and Simulation Where Rotational Speed is the Controlled Variable," *IEEE Transactions on Industry Application*, vol. 40, pp. 3-10, 2004.
[96] dSPACE GmbH, "dSPACE User's Guide," Digital Signal Processing and Control Engineering, Germany.
[97] J. Morren and S. W. H. de Haan, "Ridethrough of Wind Turbines with Doubly-Fed Induction Generator During a Voltage Dip," *IEEE Transactions on Energy Conversion*, vol. 20, pp. 435-441, 2005.
[98] T. Sun, Z. Chen, and F. Blaabjerg, "Transient Stability of DFIG Wind Turbines at an External Short-circuit Fault," *Wind Energy*, vol. 8, pp. 345-360, 2005.
[99] S. Seman, J. Niiranen, and A. Arkkio, "Ride-Through Analysis of Doubly Fed Induction Wind-Power Generator Under Unsymmetrical Network Disturbances," *IEEE Transactions on Power Systems*, vol. 21, pp. 1782-1789, 2006.
[100] C. Feltes, S. Engelhardt, J. Kretschmann, J. Fortmann, and I. Erlich, "Dynamic performance evaluation of DFIG-based wind trubines regarding new German grid code requirements," in *IEEE Power and Energy Society General Meeting* 2010, pp. 1-8.
[101] W. Chen, D. Xu, N. Zhu, M. Chen, and F. Blaabjerg, "Control of Doubly-Fed Induction Generator to Ride-Through Recurring Grid Faults," *IEEE Transactions on Power Electronics*, vol. 31, pp. 4831-4846, 2016.
[102] D. Campos-Gaona, E. L. Moreno-Goytia, and O. anaya-Lara, "Fault Ride-Through Improvement of DFIG-WT by Integrating a Two-Degrees-of-Freedom Internal Model Control," *IEEE Transactions on Industrial Electronics*, vol. 60, pp. 1133-1145, 2013.
[103] M. Salles, J. R. Cardoso, A. P. Grilo, C. Rahmann, and K. Hameyer, "Control strategies of doubly fed induction generators to support grid voltage," in *Electric Machine and Drives Conference Proceedings, IEEE 2009.* , 2009, pp. 1-6.
[104] J. Vidal, G. Abad, J. Arza, and S. Aurtenechea, "Single-Phase DC Crowbar Topologies for Low Voltage Ride Through Fulfillment of High-Power Doubly

Fed Induction Generator-Based Wind Turbines," *IEEE Transactions on Energy Conversion*, vol. 28, pp. 768-781, 2013.
[105] H. Knudsen and V. Akhmatov, "Induction Generator Models In Dynamic Simulation Tools," in *International Conference on Power Systems Transients* vol. 4. Budapest-Hungary, 1999, pp. 2249-2254.
[106] H. Wen and S. Cai, "Modeling and LVRT Analysis of DFIG Wind Power System," in *IEEE Asia-Pacific Power and Energy Engineering Conference* Brisbane, Queensland, Australia, 2015, pp. 1195-1200.
[107] T. Kawady, C. Feltes, I. Erlich, and A. I. Taalab, "Protection system behavior of DFIG based wind farms for grid-faults with practical considerations," *IEEE Power and Energy Society General Meeting* pp. 1-6, 2010.
[108] H. Wen and S. Cai, "Modeling and LVRT Analysis of DFIG Power System " in *IEEE PES Asia-Pacific Power and Energy Engineering Conference*, 2015, pp. 1195-1200.
[109] O. Anaya-lara, N. Jenkins, J. Ekanayake, P. Cartwright, and M. Hughes, *Wind energy generation modelling and control*. Chichester, West Sussex, United Kingdom: John Wiley & Sons, Ltd., 2009.
[110] J. Mohammadi, S. Afsharnia, S. Vaez-Zadeh, and S. Farhangi, "Improved fault ride through strategy for doubly fed induction generator based wind turbines under both symmetrical and asymmetrical grid faults," *IET on Renewable Power Generation*, vol. 10, pp. 1114-1122, 2016.
[111] J. Serrano-Gonzalez and R. Lacal-Arantegui, "Technological evolution of onshore Wind Turbines-a market-based analysis," *Wind Energy*, 2016.
[112] M. Liserre, R. Cardenas, M. Molinas, and J. Rodriguez, "Overview of Multi-MW Wind Turbines and Wind Parks," *IEEE Transactions on Industrial Electronics*, vol. 58, pp. 1081-1095, 2011.
[113] P. Vas, *Electrical machines and Drives*. Oxford Clarendon Press, 1992.